SYSTEM NOISE ANALYSIS OF THE DUMBBELL TETHERED SATELLITE FOR GRAVITY-GRADIENT MEASUREMENTS

Grant NSG 8063

Final Technical Report
For the period 1 July 1978 to 30 June 1979

Principal Investigator
Dr. Giuseppe Colombo

October 1979

Prepared for
National Aeronautics and Space Administration
George C. Marshall Space Flight Center
Marshall Space Flight Center, Alabama 35812

Smithsonian Institution
Astrophysical Observatory
Cambridge, Massachusetts 02138

The Smithsonian Astrophysical Observatory and the Harvard College Observatory are members of the Center for Astrophysics

The NASA Technical Officer for this grant is Dr. William Johnson, Space Sciences Laboratory, NASA, Marshall Space Flight Center, Alabama 35812.

SYSTEM NOISE ANALYSIS OF THE DUMBBELL TETHERED SATELLITE FOR GRAVITY-GRADIENT MEASUREMENTS

Grant NSG 8063

Final Technical Report
For the period 1 July 1978 to 30 June 1979

Principal Investigator
Dr. Giuseppe Colombo

ACKNOWLEDGMENT

The authors of this report are:

Mr. D. A. Arnold
Dr. G. Colombo
Mr. N. Lanham
Mr. G. Nystrom

TABLE OF CONTENTS

FOREWORD

This is the Final Report on Grant NSG 8063, System Noise Analysis of the Dumbbell Tethered Satellite for Gravity-Gradient Measurements, and covers the period 1 July 1978 to 30 June 1979. For this program, Dr. Giuseppe Colombo served as Principal Investigator, Dr. Michael R. Pearlman as Program Manager, and Mr. David A. Arnold as Analyst.

This technical report fulfills the contractual obligations of the Smithsonian Astrophysical Observatory with respect to the cited grant.

ABSTRACT

This report contains an analysis of the feasibility of using the Dumbbell gravity-gradiometer concept for measuring short-wavelength variations in the earth's gravity gradient to a sensitivity of 0.01 eu. Variations in the gradient are recorded by measuring tension variations in a vertically stabilized satellite consisting of heavy masses connected by a long wire or rod. Tension noise can arise from the excitation of various mechanical oscillations of the system. The principal noise sources that have been identified are fluctuations in atmospheric drag heating and drag force resulting from density variations and winds. Approximate analytical expressions are presented for the tension noise as a function of the system design parameters for various possible configurations. Computer simulations using numerical integration have been performed to study the tension noise for several sample cases. Three designs consistent with Shuttle launch capabilities appear to be capable of achieving the required sensitivity at reasonably low cost.

SYSTEM NOISE ANALYSIS OF THE DUMBBELL TETHERED SATELLITE FOR GRAVITY-GRADIENT MEASUREMENTS

Final Technical Report

Grant NSG 8063

1. INTRODUCTION

The basic principle of the Dumbbell technique for gravity-gradient measurements (Colombo et al., 1976; Kalaghan and Colombo, 1978) is to detect gravity anomalies by measuring the tension change they produce in a long wire of length ℓ with a heavy ballast of mass M at either end. The tension T and the tension change ΔT are proportional to the product $M\ell$. The values of ℓ and M are made large enough so that ΔT is above the threshold of tension measuring devices.

Great care must be taken to reduce system noise introduced from both internal and external sources. The major noise source is the expansion and contraction of the wire owing to small temperature fluctuations, which are introduced through variations in atmospheric drag heating and variable radiative heating from the earth. In addition to this is the direct effect of tension variations caused by drag variations due to density and wind fluctuations along the orbit.

The properties of tension measuring devices require that not only ΔT but also $\Delta T/T$ be above a certain threshold to be measurable. Since the signal ΔT produced by a gravity anomaly decreases with altitude much more rapidly than the total tension T, owing to the central gravitational field of the earth, $\Delta T/T$ depends on orbital height. Another consideration is the risetime and

transfer function of the system. The risetime is determined by the resonant frequency of the longitudinal spring oscillations of Dumbbell. Near the resonant frequency of the system, distortion of the signal occurs and higher frequencies are filtered out. Damping is required for the various natural oscillation modes of the system in order to absorb the energy from both noise sources and previous signal inputs.

2. GRAVITY-ANOMALY SIGNAL

In this section, analytical formulas are derived for calculating the approximate values of the tension change ΔT due to a gravity anomaly and the total tension T for the Dumbbell gravity gradiometer. The calculation of ΔT assumes that an observed gravity anomaly in cm/sec^2 at the earth's surface can be represented analytically by the density of a surface mass layer, which causes a discontinuity in the strength of the gravitational field. The surface layer is then represented by a grid of discrete mass points. The formulas for ΔT and T can be used to calculate the absolute sensitivity ΔT and the fractional sensitivity $\Delta T/T$ required to obtain a given sensitivity. Section 2.1 presents an analytical calculation of the gravity-gradient signal, and Section 2.4 shows the response of the Dumbbell system as it passes over an anomaly.

2.1 Analysis of Expected Signal Level

A small computer program has been written for studying the signature of a gravity anomaly represented by a grid of point masses on the surface of the earth. Both the vertical component and the vertical derivative of the acceleration are computed along a track passing over the anomaly. The vertical derivative is the signal that would be measured by a Dumbbell gravity gradiometer. The acceleration $\ddot{\vec{h}}$ produced by a point anomaly M^* is

$$\ddot{\vec{h}} = -GM^*\vec{h}h^{-3} \quad ,$$

where G is the gravitational constant, $\vec{h}$ is the vector from the anomaly to the gradiometer, and $h = |\vec{h}|$. The vertical component $\ddot{z}$ of the acceleration is

$$\ddot{z} = -GM^*zh^{-3} \quad ,$$

and the vertical derivative of $\ddot{z}$ is

$$\frac{\delta \ddot{z}}{\delta z} = GM^*(3z^2h^{-5}-h^{-3}) \quad .$$

In the case where the satellite is directly overhead, this reduces to

$$\frac{\delta \ddot{z}}{\delta z} = 2GM^*z^{-3} \quad . \tag{1}$$

If an area has a gravity anomaly Δg (cm/sec^2), it can be represented by a surface layer of density σ (g/cm^2) by using the formula

$$G\sigma = \frac{\Delta g}{2\pi} \quad .$$

Multiplying $G\sigma$ by an area dA gives a quantity with units of GM^*, namely

$$GM^* = G\sigma \, dA = \frac{\Delta g}{2\pi} dA \quad .$$

Substituting this expression for GM^* into equation (1), we have

$$\frac{\delta \ddot{z}}{\delta z} = \frac{\Delta g \, dA}{\pi z^3} \quad . \tag{2}$$

In a Dumbbell system consisting of masses M connected by a wire of length ℓ, the tension due to the gravity anomaly is approximately

$$\Delta T = \frac{\delta \ddot{z}}{\delta z} \frac{M\ell}{2} = \frac{\Delta g \, dA}{\pi z^3} \frac{M\ell}{2} \quad . \tag{3}$$

In the cases run with the program, the total mass of the anomaly has been set equal to the integrated surface density of a 100-mgal anomaly (0.100 cm/sec^2)

over a 120-km × 120-km area. This gives a value for GM^* of

$$GM^* = \frac{\Delta g}{2\pi} dA = \frac{0.100}{2\pi} (120 \times 10^5 \text{ cm})^2 = 2.29183 \times 10^{12} \text{ cm}^3 \text{ sec}^{-2} \quad .$$

To study the effect of how the mass causing the anomaly is distributed, the anomaly has been represented in three ways. In the first case, the anomaly is represented by a point mass. This is equivalent to a sphere in the crust whose density differs from the surrounding material. In the second case, the anomaly is represented by a 7 × 7 grid containing 49 points spaced 20 km apart, thereby covering a 120-km × 120-km area. Each point contains one 49th of the total mass. The third case has 40-km spacing between points, so that a 240-km × 240-km area is covered. Keeping the total mass constant, case three is equivalent to a 25-mgal anomaly over a 240-km × 240-km area.

Figures 1 through 4 show the vertical component of the acceleration and the vertical derivative of the acceleration, which is the quantity measured by the Dumbbell gravity gradiometer. The four figures are for satellite altitudes of 120, 200, 220, and 300 km, with the anomaly located on the surface of the earth. The acceleration, which is negative, is plotted down from the zero line and is given in milligals (1 mgal = 10^{-3} cm/sec^2). The derivative of the acceleration, which is mostly positive, is plotted up from the zero line in eotvos units (1 eu = 10^{-9}/sec^2). The horizontal scale is the distance along the orbital path, with the origin directly over the center of the anomaly. The three curves for each quantity correspond to a lumped mass and a 120-km × 120-km and a 240-km × 240-km distribution of mass. The lumped mass always gives the most peaked curve, and the 240-km × 240-km distribution, the flattest curve.

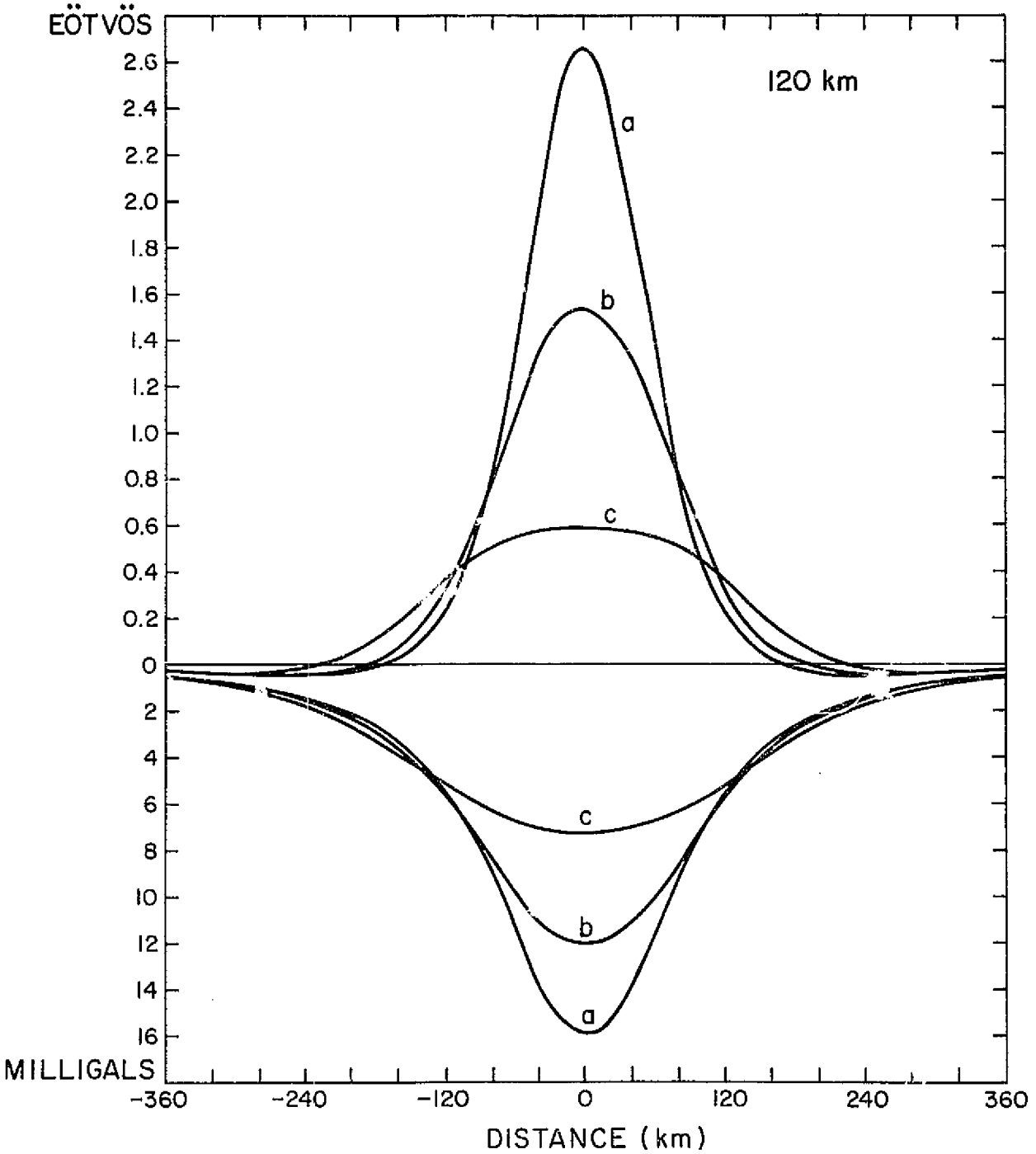

Figure 1. Vertical acceleration (top) and vertical derivative (bottom) of the acceleration along the orbital path due to a) a point mass, b) a 120-km × 120-km distribution of mass, and c) a 240-km × 240-km distribution of mass. In all cases, the total mass equals the integrated mass of a 100-mgal anomaly over a 120-km × 120-km area. Satellite altitude = 120 km.

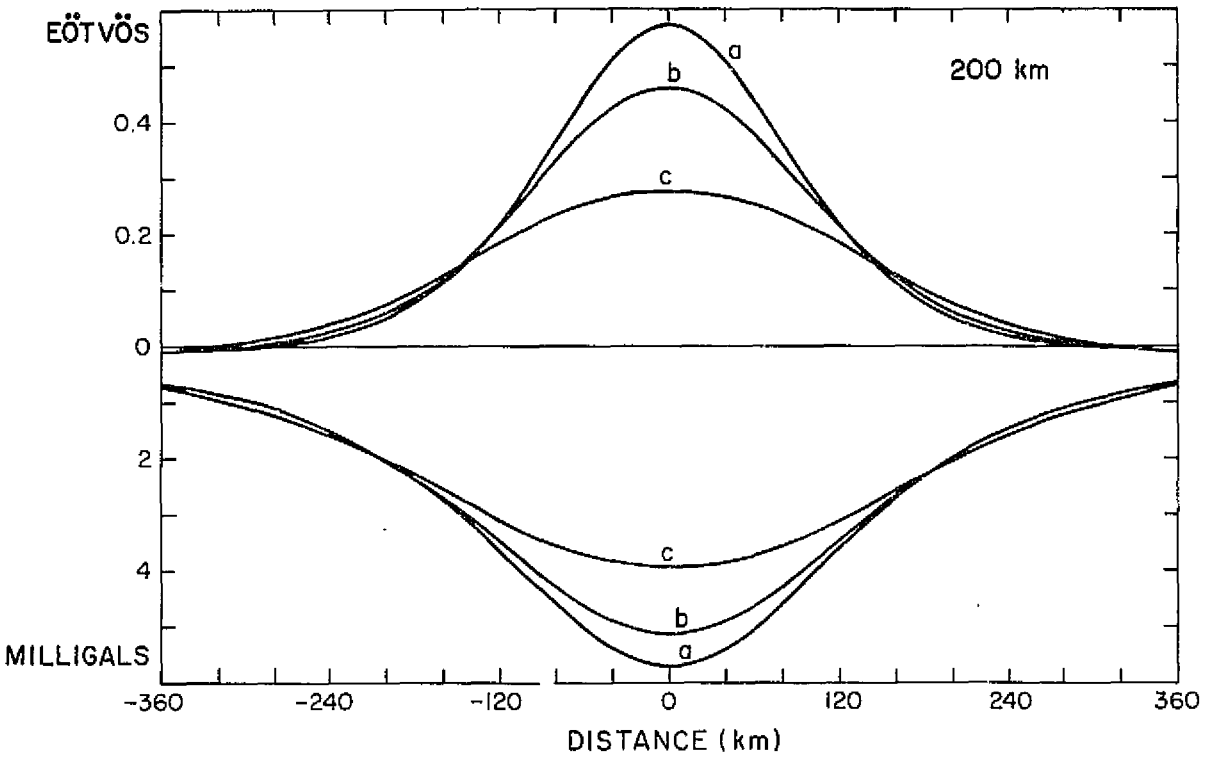

Figure 2. Same as Figure 1 for a satellite altitude of 200 km.

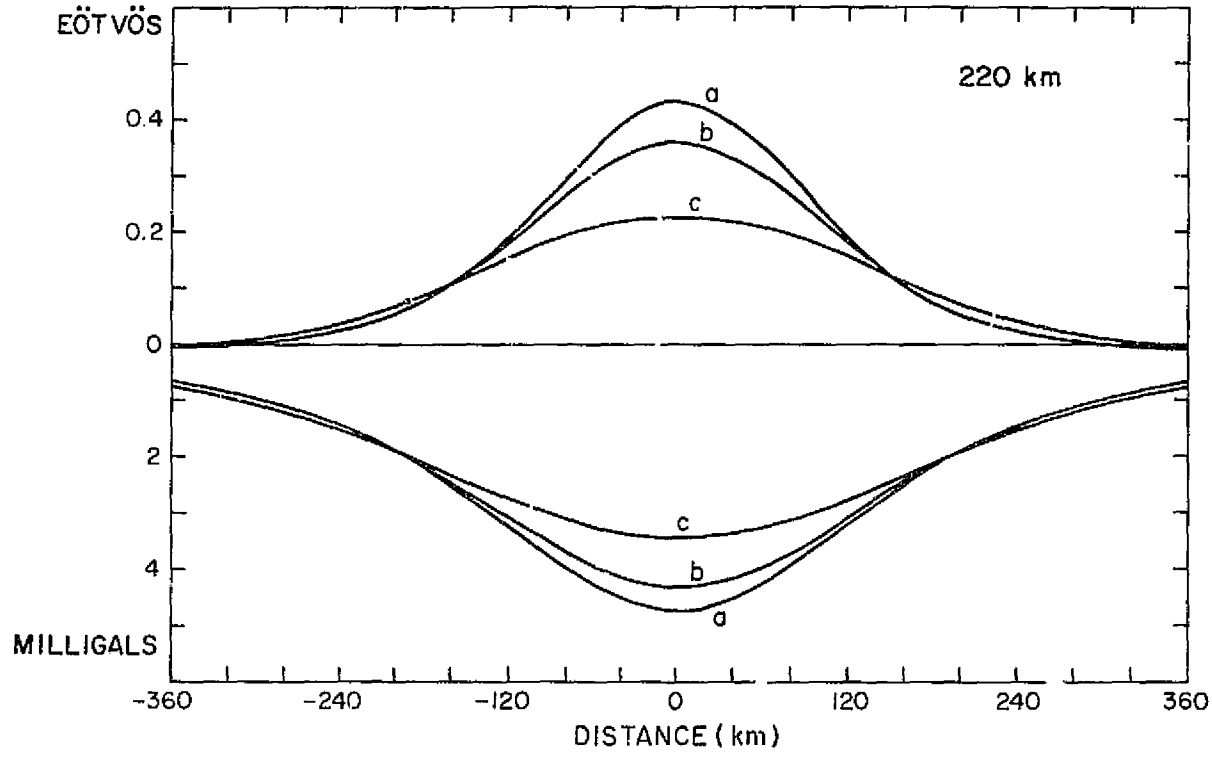

Figure 3. Same as Figure 1 for a satellite altitude of 220 km.

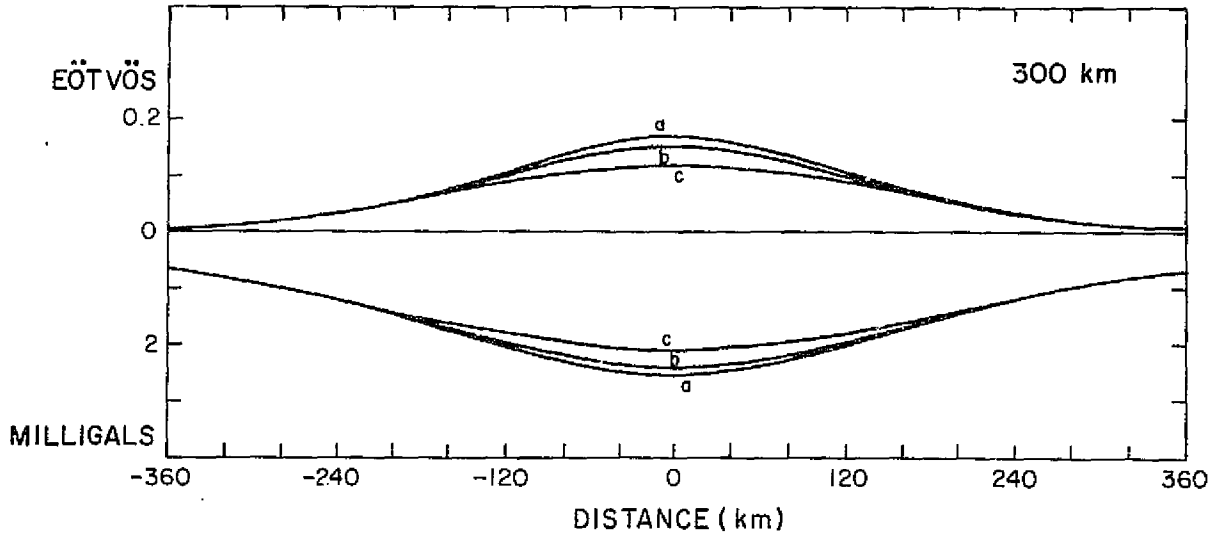

Figure 4. Same as Figure 1 for a satellite altitude of 300 km.

2.2 Wire Tension in a Tethered-Satellite System

An object of mass M in a central gravitational field of strength GM, where M is the mass of the earth and $GM = 3.986013 \times 10^{20}$ cgs, experiences a gravitational force F_g, given by

$$F_g = -\frac{GMM}{a^2} \quad ,$$

where a is the geocentric distance. In a circular orbit, this force is balanced by the centripetal force F_c, given by

$$F_c = \frac{Mv^2}{a}$$

where v is the velocity of the object. In a tethered-satellite system, the center of gravity of the system moves in accordance with the above equations. If the system is vertically stabilized, all parts of the system move with the same angular velocity $\omega = v/a$. The centripetal acceleration at any point is then

$$Ma\omega^2 \quad ,$$

where ω is a constant. The equation $F_g + F_c = 0$ holds only at the center of gravity of the system. Since $|F_g|$ decreases with a and $|F_c|$ increases with a, points not at the center of mass experience a net force away from the center of gravity. The constant ω, obtained by setting $F_g + F_c = 0$ for the center of gravity, is

$$\omega = \sqrt{\frac{GM}{a^3}} \quad .$$

The rate at which the net force F changes with a is obtained by differentiating the quantity $F_g + F_c$, keeping ω constant. We have

$$\frac{\delta F}{\delta a} = \frac{\delta}{\delta a}(F_g + F_c) = \frac{\delta}{\delta a}\left(-\frac{GMM}{a^2} + Ma\omega^2\right) = \frac{2GMM}{a^3} + M\omega^2 \quad .$$

By substituting for ω^2 determined from the center of gravity, the value of the derivative at the center of gravity is

$$\frac{\delta F}{\delta a} = \frac{2GMM}{a^3} + \frac{MGM}{a^3} = \frac{3GMM}{a^3} \quad .$$

The rate of change of the acceleration with respect to a is

$$\frac{\delta \ddot{a}}{\delta a} = \frac{1}{M}\frac{\delta F}{\delta a} = \frac{3GM}{a^3} \quad . \tag{4}$$

As an example, consider a system consisting of two masses weighing 2 metric tons ($= 2 \times 10^6$ g) each connected by a tether of length ℓ = 1 km ($= 10^5$ cm) orbiting at 220 km. The force on the upper mass and therefore the tension in the wire is approximately

$$T = \frac{\delta F}{\delta a}\frac{\ell}{2} = \frac{3GMM}{a^3}\frac{\ell}{2} \quad , \tag{5}$$

which gives

$$T = \frac{3 \times 3.986013 \times 10^{20} \times 2 \times 10^6 \times 10^5}{(6.378 \times 10^8 + 0.220 \times 10^8)^3 \times 2} = 416{,}316 \text{ dynes} \quad .$$

As a second example, consider the same system as above with the mass distributed uniformly along the wire. The force at a distance z_0 from the

center of mass is

$$F(Z_0) = \int_{Z_0}^{\ell/2} \frac{3GM}{a^3} \frac{M}{\ell/2} Z \, dZ = \frac{3GMM}{a^3} \frac{2}{\ell} \frac{Z^2}{2} \Bigg|_{Z_0}^{\ell/2} = \frac{3GMM}{a^3} \frac{2}{\ell} \left(\frac{\ell^2}{8} - \frac{Z_0^2}{4} \right) \quad .$$

The tension at the center of gravity ($Z_0 = 0$) is

$$F(0) = T(0) = \frac{3GMM}{a^3} \frac{\ell}{4} = 208{,}158 \text{ dynes} \quad ,$$

which is half the tension obtained by having all the mass at the ends.

2.3 Tension Measuring Accuracy Required for 0.01-eu Sensitivity

At an altitude of 220 km, the acceleration gradient in a tethered satellite system, from equation (4), is

$$\frac{\delta \ddot{a}}{\delta a} = \frac{3GM}{a^3} \frac{3 \times 3.986013 \times 10^{20}}{(6.378 \times 10^8 + 0.220 \times 10^8)^3} = 4.16 \times 10^{-6} \text{ sec}^{-2} \quad .$$

Since 0.01 eu = 0.01×10^{-9} sec^{-2}, the required precision is about 1 part in 4.16×10^5, or between 2 and 3 parts per million.

In Figure 3 part c, a signal of about 0.23 eu is obtained from a mass distribution that is approximately equivalent to a 25-mgal gravity anomaly over an area 240-km × 240-km. For this case, a measuring sensitivity of 0.01 eu could detect a gravity anomaly on the order of 1 mgal.

2.4 System Response to Gravity Anomalies

The Dumbbell gravity gradiometer must be able to respond to a change in gravity gradient within a time comparable to that required to pass over the source of the signal. In addition to fast response time, the system must

have sufficient damping that the effect of the signal dies out in a time comparable to the length of time the signal lasts. A series of runs has been done with a simple computer program that models two masses M connected by a perfectly elastic wire with a spring and dashpot at one end. The parameters used for the runs are $M = 2 \times 10^6$ g, $\ell = 10^5$ cm, the wire diameter = 0.5 cm, the tether material is ULE (elasticity = 0.7×10^{12} dyne/cm^2), and the altitudes are 50, 120, 160, 220, and 300 km above the gravity anomaly. The gravity anomaly is modeled as a point having an integrated mass of a surface-layer density sufficient to produce a 10-mgal gravity anomaly over a 1 square degree (111 km × 111 km) area. The natural frequency for longitudinal oscillations is about 13.4 sec without a damper. Adding a damper spring with the same spring constant as the wire lengthens the period by $\sqrt{2}$, to about 19 sec. Table 1 lists, as a function of altitude, the equilibrium wire tension, the maximum tension change ΔT directly over the anomaly, the half-amplitude full width of the system response, and the magnitude of the secondary bounce of the system if significant. The response of the system to a sharp signal is an oscillation that decays by about a factor of 2 on each half-cycle. This behavior is particularly evident in the 50-km run, which was included specifically for that purpose, even though it is not a realistic case.

Table 1. System response to a gravity anomaly as a function of altitude.

Altitude (km)	Tension (dynes)	Signal ΔT (dynes)	Width of response signal (sec)	Bounce (dynes)	Orbital velocity (km/sec)
50	450,332	439	6	111	7.87
120	435,934	27.5	13	1	7.83
160	427,981	10.7	19	—	7.81
220	416,410	3.85	27	—	7.77
300	401,622	1.46	39	—	7.73

As an example from the table, we see that at a 160-km altitude, the width of the response signal is 19 sec and the orbital velocity is 7.8 km/sec; the distance traveled along the ground is thus about 148 km. The runs for 160 km and above show satisfactory response to the signal with no significant distortion due to bouncing. We can therefore conclude that the system response will be satisfactory as long as the natural period of the longitudinal oscillations of the system is less than the orbital height divided by the orbital velocity.

Figures 5 through 9 show the tension (in dynes) versus time (in sec) for the five cases in Table 1.

The tension signal ΔT and the total tension T can be calculated from equations (3) and (5), respectively. For the case in Figure 8, we have

$$\Delta T = \frac{\Delta g \, dA}{\pi z^3} \frac{M\ell}{2} = \frac{10 \times 10^{-3} \times (111.3 \times 10^5)^2 \times 2 \times 10^6 \times 10^5}{\pi \times (0.220 \times 10^8)^3 \times 2} = 3.7 \text{ dynes}$$

and

$$T = \frac{3GMM}{a^3} \frac{\ell}{2} = \frac{3 \times 3.986013 \times 10^{20} \times 2 \times 10^6 \times 10^5}{(6.378 \times 10^8 + 0.220 \times 10^8)^3 \times 2} = 416{,}316 \text{ dynes} \quad ,$$

which agree approximately with the results of the actual integration of the orbital dynamics.

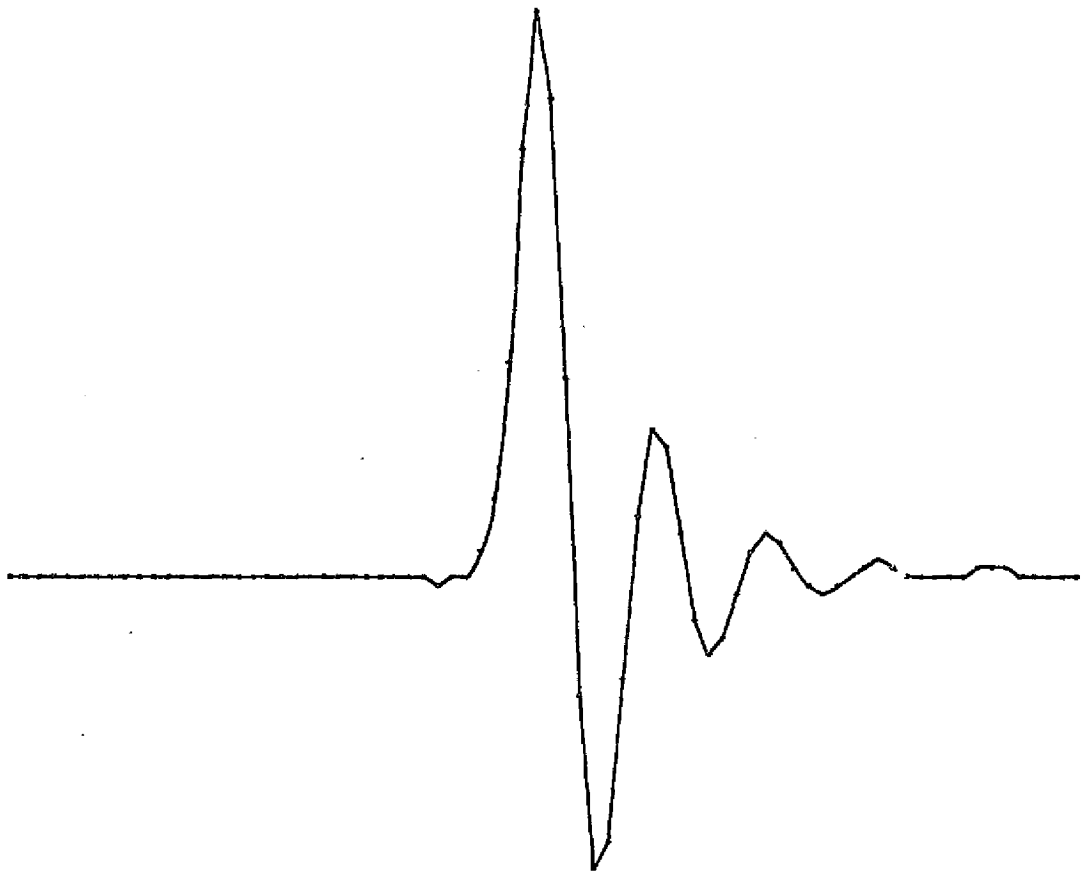

TIME (sec)	TENSION (dynes)
0.	450332.
2.	450332.
4.	450332.
6.	450332.
8.	450332.
10.	450332.
12.	450332.
14.	450332.
16.	450332.
18.	450332.
20.	450332.
22.	450332.
24.	450332.
26.	450332.
28.	450332.
30.	450332.
32.	450332.
34.	450332.
36.	450332.
38.	450332.
40.	450331.
42.	450331.
44.	450331.
46.	450331.
48.	450330.
50.	450330.
52.	450329.
54.	450329.
56.	450328.
58.	450327.
60.	450326.
62.	450326.
64.	450330.
66.	450346.
68.	450393.
70.	450499.
72.	450661.
74.	450771.
76.	450705.
78.	450480.
80.	450235.
82.	450102.
84.	450123.
86.	450246.
88.	450377.
90.	450443.
92.	450428.
94.	450361.
96.	450298.
98.	450269.
100.	450282.
102.	450318.
104.	450351.
106.	450364.
108.	450356.
110.	450337.
112.	450320.
114.	450315.
116.	450330.
118.	450331.
120.	450339.
122.	450341.
124.	450336.
126.	450332.
128.	450328.
130.	450328.
132.	450330.
134.	450333.
136.	450334.
138.	450335.
140.	450334.
142.	450332.
144.	450331.
146.	450331.
148.	450332.
150.	450333.

TIME (sec)	TENSION (dynes)
0.0000000	450332.939585
2.0000000	450332.897233
4.0000000	450332.823737
6.0000000	450332.724415
8.0000000	450332.723415
10.0000000	450332.739681
12.0000000	450332.766648
14.0000000	450332.775443
16.0000000	450332.750951
18.0000000	450332.716089
20.0000000	450332.665612
22.0000000	450332.618694
24.0000000	450332.576324
26.0000000	450332.543225
28.0000000	450332.501286
30.0000000	450332.448891
32.0000000	450332.376919
34.0000000	450332.280622
36.0000000	450332.182337
38.0000000	450332.054584
40.0000000	450331.902081
42.0000000	450331.707637
44.0000000	450331.472382
46.0000000	450331.187273
48.0000000	450330.817928
50.0000000	450330.355152
52.0000000	450329.757422
54.0000000	450329.021453
56.0000000	450328.133214
58.0000000	450327.144884
60.0000000	450326.344320
62.0000000	450326.666232
64.0000000	450330.866131
66.0000000	450346.745987
68.0000000	450393.165434
70.0000000	450499.649079
72.0000000	450661.459153
74.0000000	450771.650807
76.0000000	450705.984163
78.0000000	450480.995185
80.0000000	450235.245003
82.0000000	450102.183361
84.0000000	450123.631061
86.0000000	450246.653425
88.0000000	450377.413474
90.0000000	450443.754518
92.0000000	450428.475695
94.0000000	450361.541803
96.0000000	450298.818205
98.0000000	450269.914549
100.0000000	450282.736564
102.0000000	450318.709314
104.0000000	450351.700078
106.0000000	450364.781997
108.0000000	450356.335556
110.0000000	450337.142299
112.0000000	450320.958739
114.0000000	450315.375539
116.0000000	450330.077798
118.0000000	450331.223327
120.0000000	450339.423921
122.0000000	450341.628121
124.0000000	450336.333164
126.0000000	450332.895320
128.0000000	450328.891190
130.0000000	450328.124498
132.0000000	450330.116834
134.0000000	450333.028489
136.0000000	450334.993300
138.0000000	450335.229085
140.0000000	450334.893027
142.0000000	450332.602364
144.0000000	450331.666656
146.0000000	450331.633388
148.0000000	450332.301554
150.0000000	450333.091749

Figure 5. Tension (dynes) versus time (sec) for a Dumbbell system passing to the integrated mass of a surface-layer density producing a gravity anomaly of 10 mgal over a 111-km × 111-km area. Orbital altitude = 50 km.

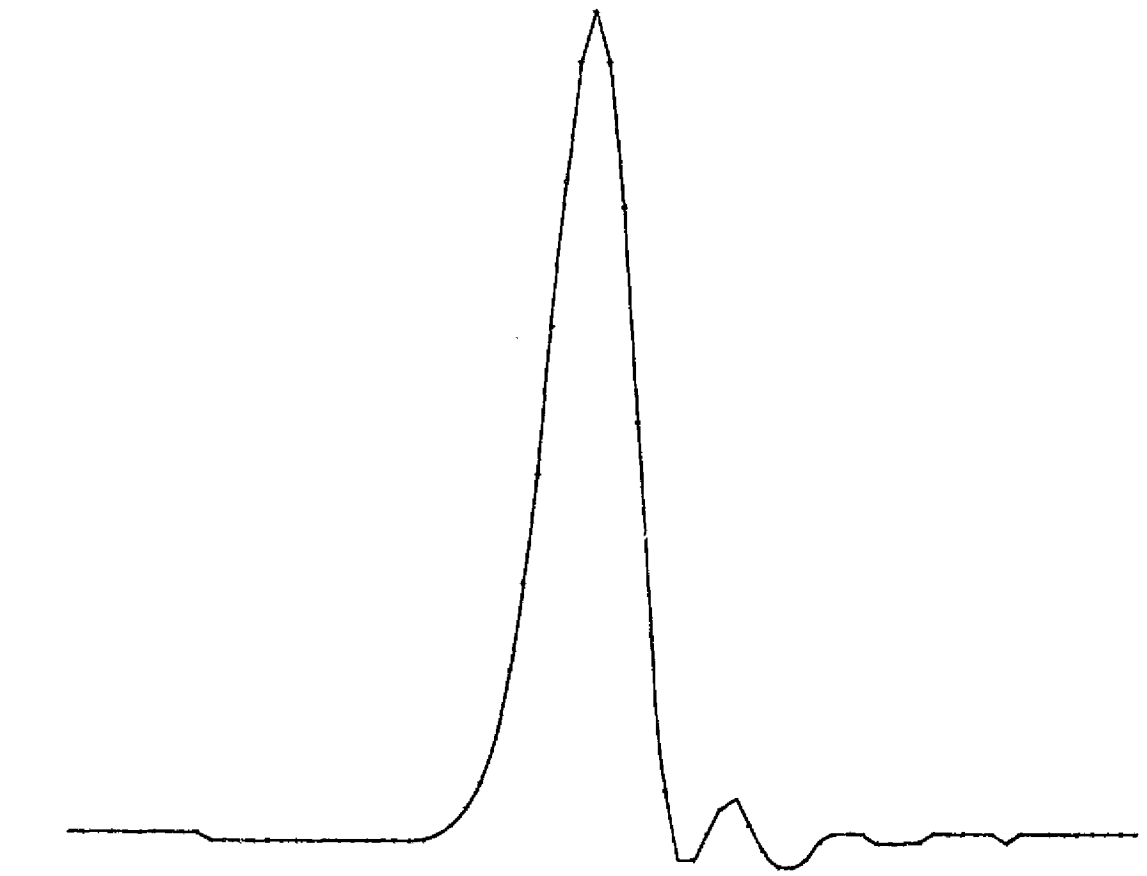

TIME (sec)	TENSION (dynes)
0.0000000	435934.165465
2.0000000	435934.134657
4.0000000	435934.270157
6.0000000	435934.220759
8.0000000	435934.194103
10.000000	435934.209456
12.000000	435934.231692
14.000000	435934.238626
16.000000	435934.237032
18.000000	435934.214564
20.000000	435934.176722
22.000000	435934.142866
24.000000	435934.120984
26.000000	435934.111995
28.000000	435934.103936
30.000000	435934.093180
32.000000	435934.069771
34.000000	435934.040999
36.000000	435934.008269
38.000000	43 1.970878
40.000000	43 1.946302
42.000000	435933.916665
44.000000	435933.941600
46.000000	435933.969424
48.000000	435933.996468
50.000000	435934.026468
52.000000	435934.041146
54.000000	435934.031675
56.000000	435935.266677
58.000000	435936.181590
60.000000	435937.578226
62.000000	435939.643686
64.000000	435942.443841
66.000000	435946.443841
68.000000	435951.141851
70.000000	435956.063200
72.000000	435960.110207
74.000000	435961.854059
76.000000	435960.217903
78.000000	435955.115573
80.000000	435948.814073
82.000000	435940.917884
84.000000	435931.774217
86.000000	435923.401210
88.000000	435933.349014
90.000000	435934.376716
92.000000	435935.261068
94.000000	435935.312077
96.000000	435934.675612
98.000000	435933.797690
100.00000	435933.220081
102.00000	435933.176177
104.00000	435933.543659
106.00000	435934.022902
108.00000	435934.332517
110.00000	435934.374194
112.00000	435934.209971
114.00000	435934.606790
116.00000	435933.897770
118.00000	435933.937145
120.00000	435934.073976
122.00000	435934.211301
124.00000	435934.284090
126.00000	435934.283759
128.00000	435934.239077
130.00000	435934.189548
132.00000	435934.174002
134.00000	435934.198618
136.00000	435934.249762
138.00000	435934.289498
140.00000	435934.310478
142.00000	435934.300623
144.00000	435934.290117
146.00000	435934.278411
148.00000	435934.275681
150.00000	435934.291750

Figure 6. Same as Figure 5 for an orbital altitude of 120 km.

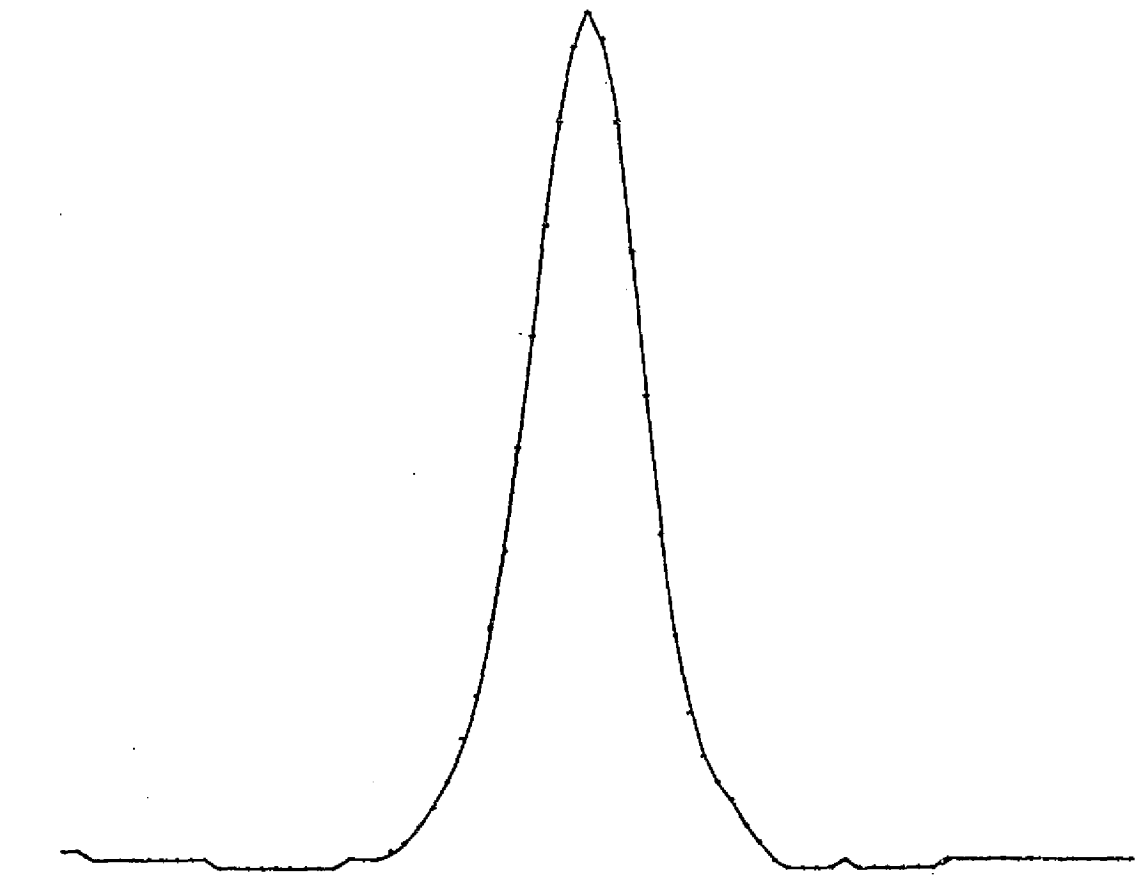

TIME (sec)	TENSION (dynes)
0.0000000	427981.373828
2.0000000	427981.350452
4.0000000	427981.290267
6.0000000	427981.253484
8.0000000	427981.234966
10.000000	427981.239239
12.000000	427981.266974
14.000000	427981.283850
16.000000	427981.282759
18.000000	427981.267094
20.000000	427981.242219
22.000000	427981.219127
24.000000	427981.207663
26.000000	427981.213666
28.000000	427981.212721
30.000000	427981.210408
32.000000	427981.202352
34.000000	427981.201377
36.000000	427981.202322
38.000000	427981.212107
40.000000	427981.233167
42.000000	427981.271681
44.000000	427981.330285
46.000000	427981.418722
48.000000	427981.545506
50.000000	427981.719890
52.000000	427981.962352
54.000000	427982.316042
56.000000	427982.792036
58.000000	427983.411950
60.000000	427984.231201
62.000000	427985.266668
64.000000	427986.497926
66.000000	427987.896297
68.000000	427989.351760
70.000000	427990.698611
72.000000	427991.685400
74.000000	427992.907290
76.000000	427991.757193
78.000000	427990.693151
80.000000	427989.876288
82.000000	427987.223517
84.000000	427985.462600
86.000000	427984.091834
88.000000	427983.145211
90.000000	427982.576371
92.000000	427981.239870
94.000000	427981.997824
96.000000	427981.759428
98.000000	427981.531492
100.00000	427981.313077
102.00000	427981.210457
104.00000	427981.176755
106.00000	427981.186429
108.00000	427981.217559
110.00000	427981.233445
112.00000	427981.227874
114.00000	427981.207406
116.00000	427981.188609
118.00000	427981.179971
120.00000	427981.195752
122.00000	427981.218637
124.00000	427981.236322
126.00000	427981.246323
128.00000	427981.261278
130.00000	427981.274303
132.00000	427981.269877
134.00000	427981.271581
136.00000	427981.274897
138.00000	427981.277894
140.00000	427981.289225
142.00000	427981.296177
144.00000	427981.305879
146.00000	427981.315991
148.00000	427981.317222
150.00000	427981.313340

Figure 7. Same as Figure 5 for an orbital altitude of 160 km.

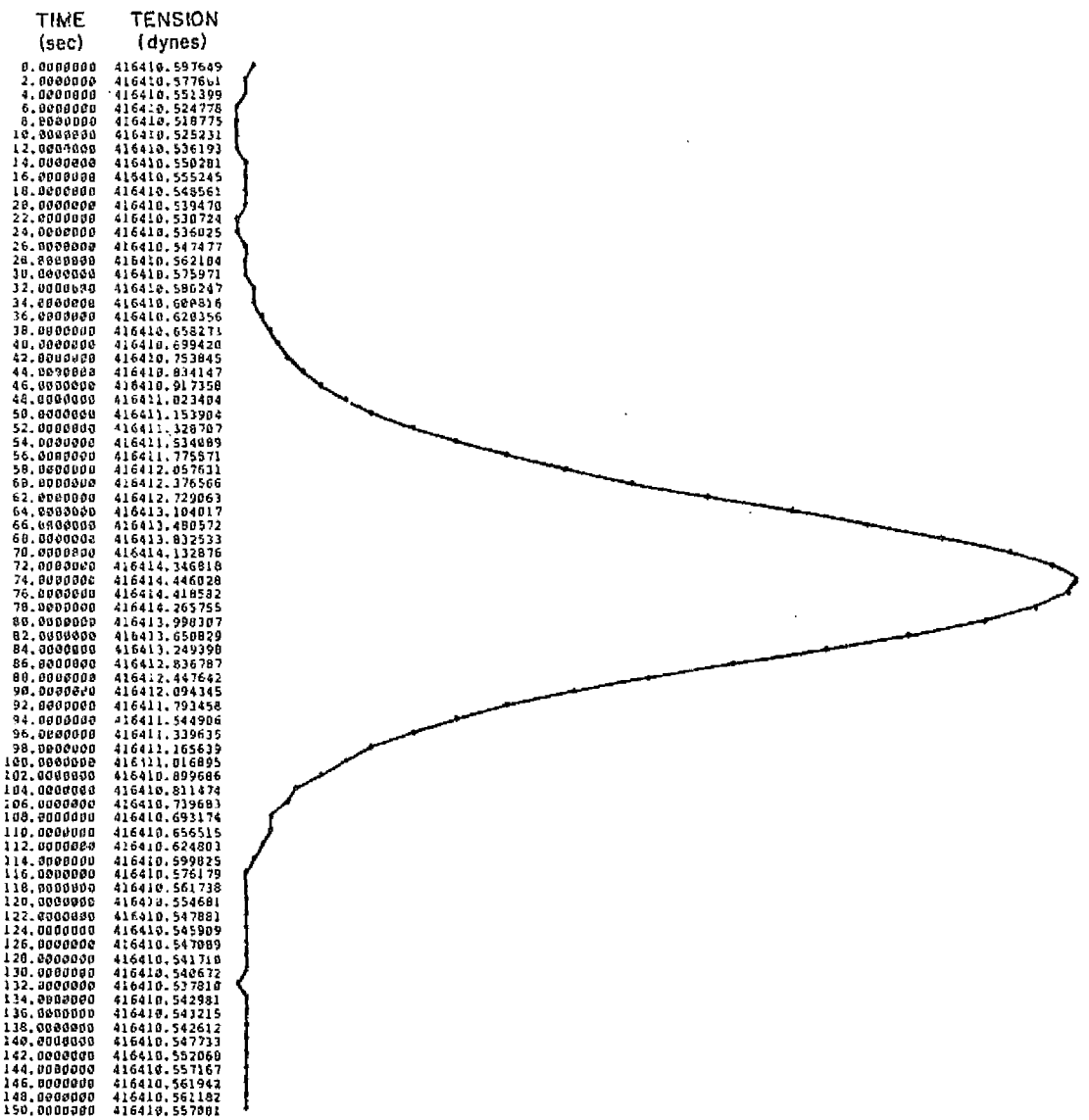

TIME (sec)	TENSION (dynes)
0.0000000	416410.5997649
2.0000000	416410.5776941
4.0000000	416410.551399
6.0000000	416410.524778
8.0000000	416410.518775
10.0000000	416410.525231
12.0000000	416410.536193
14.0000000	416410.550281
16.0000000	416410.555245
18.0000000	416410.548561
20.0000000	416410.539470
22.0000000	416410.530724
24.0000000	416410.536025
26.0000000	416410.547477
28.0000000	416410.562104
30.0000000	416410.575971
32.0000000	416410.586247
34.0000000	416410.600816
36.0000000	416410.620356
38.0000000	416410.658271
40.0000000	416410.699420
42.0000000	416410.753845
44.0000000	416410.834147
46.0000000	416410.917358
48.0000000	416411.023404
50.0000000	416411.153904
52.0000000	416411.328707
54.0000000	416411.534089
56.0000000	416411.775871
58.0000000	416412.057611
60.0000000	416412.376566
62.0000000	416412.729063
64.0000000	416413.104017
66.0000000	416413.480572
68.0000000	416413.832533
70.0000000	416414.132876
72.0000000	416414.346818
74.0000000	416414.446028
76.0000000	416414.418532
78.0000000	416414.265755
80.0000000	416413.990307
82.0000000	416413.650829
84.0000000	416413.249398
86.0000000	416412.836787
88.0000000	416412.447642
90.0000000	416412.094345
92.0000000	416411.793458
94.0000000	416411.544906
96.0000000	416411.339635
98.0000000	416411.165639
100.0000000	416411.016895
102.0000000	416410.899686
104.0000000	416410.811474
106.0000000	416410.739683
108.0000000	416410.693174
110.0000000	416410.656515
112.0000000	416410.624803
114.0000000	416410.599825
116.0000000	416410.576179
118.0000000	416410.561738
120.0000000	416410.554681
122.0000000	416410.547881
124.0000000	416410.545909
126.0000000	416410.547089
128.0000000	416410.541710
130.0000000	416410.540672
132.0000000	416410.537810
134.0000000	416410.542981
136.0000000	416410.543215
138.0000000	416410.542612
140.0000000	416410.547733
142.0000000	416410.552060
144.0000000	416410.557167
146.0000000	416410.561942
148.0000000	416410.561182
150.0000000	416410.557801

Figure 8. Same as Figure 5 for an orbital altitude of 220 km.

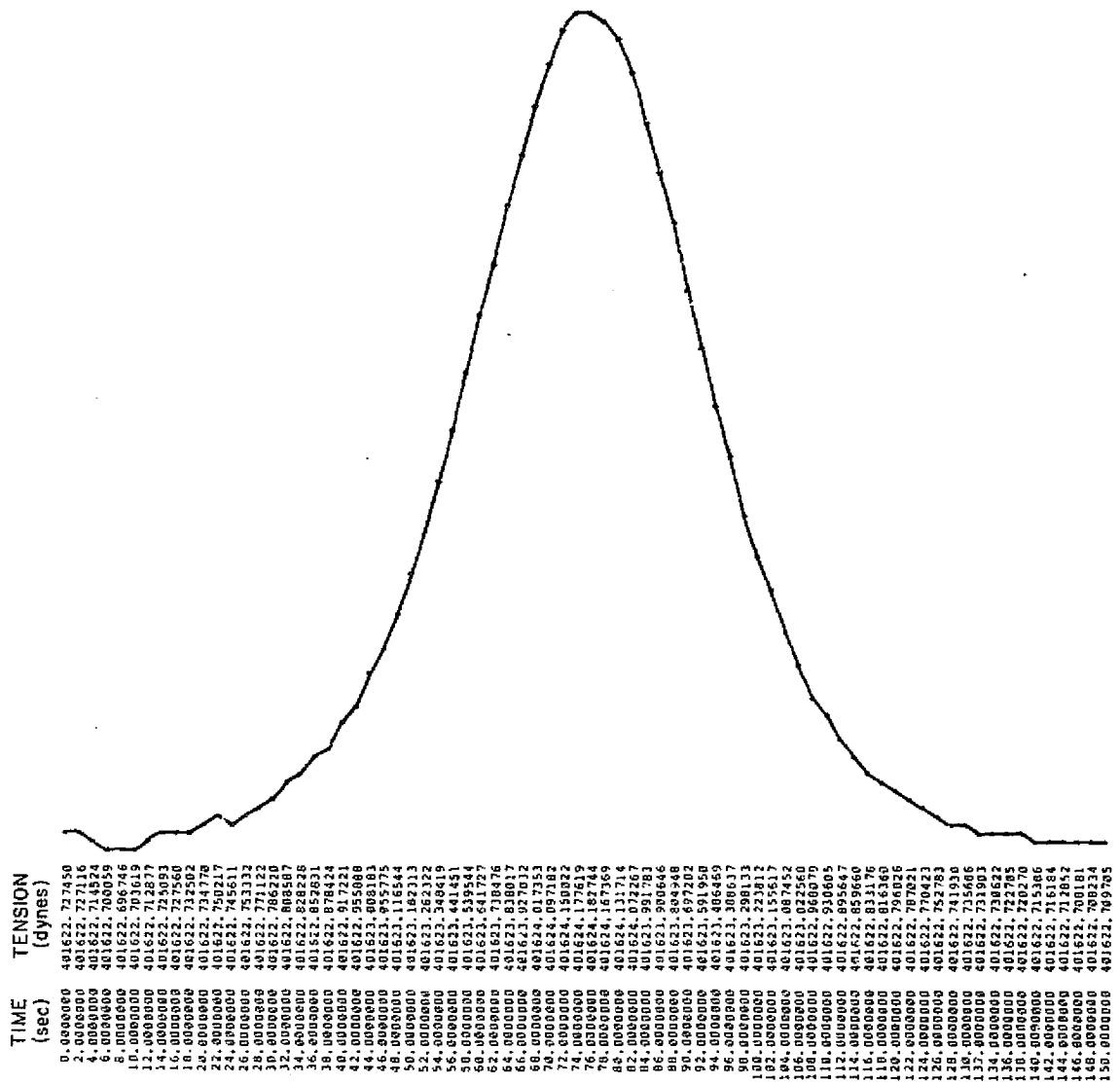

TIME (sec)	TENSION (dynes)
0.0000000	401622.727450
2.0000000	401622.727116
4.0080000	401622.714524
6.0030000	401622.700059
8.0000000	401622.696746
10.0000000	401622.701619
12.0000000	401622.712877
14.0000000	401622.725093
16.0000000	401622.727560
18.0000000	401622.732502
20.0000000	401622.734778
22.0000000	401622.750217
24.0000000	401621.745611
26.0000000	401622.753333
28.0000000	401622.771122
30.0000000	401622.786220
32.0000000	401622.803587
34.0000000	401622.828226
36.0000000	401622.852631
38.0000000	401622.878424
40.0000000	401621.917221
42.0000000	401621.955088
44.0000000	401621.988183
46.0000000	401621.955775
48.0000000	401621.116544
50.0000000	401621.182313
52.0000000	401623.262322
54.0000000	401623.249419
56.0000000	401623.344451
58.0000000	401623.539544
60.0000000	401623.641727
62.0000000	401623.738476
64.0000000	401623.838017
66.0000000	401623.927032
68.0000000	401624.017353
70.0000000	401624.097182
72.0000000	401624.150022
74.0000000	401624.177619
76.0000000	401624.187744
78.0000000	401624.187369
80.0000000	401624.131714
82.0000000	401624.072267
84.0000000	401623.991783
86.0000000	401623.900646
88.0000000	401623.804948
90.0000000	401623.697202
92.0000000	401623.591950
94.0000000	401623.486469
96.0000000	401623.386637
98.0000000	401623.298133
100.0000000	401623.223812
102.0000000	401623.155617
104.0000000	401623.087452
106.0000000	401623.022560
108.0000000	401622.960070
110.0000000	401622.930605
112.0000000	401622.895647
114.0000000	401622.859660
116.0000000	401622.833176
118.0000000	401622.816360
120.0000000	401622.796026
122.0000000	401622.787021
124.0000000	401622.770423
126.0000000	401622.752783
128.0000000	401622.741910
130.0000000	401622.735666
132.0000000	401622.731901
134.0000000	401622.730622
136.0000000	401621.722785
138.0000000	401622.720270
140.0000000	401622.715366
142.0000000	401622.716184
144.0000000	401622.712852
146.0000000	401622.708181
148.0000000	401622.708134
150.0000000	401622.709705

Figure 9. Same as Figure 5 for an orbital altitude of 300 km.

3. SYSTEM NOISE ANALYSIS

Several noise sources have been identified that can interfere with the measurement of the tension signal of a gravity anomaly. The internal noise of the tensiometer is discussed briefly in Section 7.1. The deployment of the system in orbit (Section 4) will introduce various types of oscillations that will die out with time as a result of damping present either naturally or by deliberate design. This section discusses the external noise sources expected to be present during the experiment lifetime. These include electrodynamic forces, long-wavelength gravity features, radiation, and atmospheric drag. Obtaining good resolution of short-wavelength gravity features requires operating at the lowest possible altitude. Since the atmospheric density increases rapidly at low altitudes, the resolution that can be achieved appears to depend primarily on the degree to which the problems of atmospheric drag can be minimized. Data quantity and coverage depend on orbital lifetime as determined by the satellite's initial altitude and the area-to-mass ratio (Section 5). The noise level of the data will increase as the magnitude of variations in atmospheric density and velocity increase. Atmospheric granularity introduces noise directly as a result of variations in drag force and indirectly through variations in drag heating, which cause thermal expansion and contraction of the wire.

3.1 Atmospheric Density Variations

Atmospheric density variations have been measured by several satellites. The information needed to study the effect of density variations on the Dumbbell system is the density as a function of time along the path of the satellite. Presumably, this information is contained in the density data obtained by satellite sensors, but we have been unable to find data presented in this form in the literature. The reports do indicate, however, that the behavior of the atmosphere is variable, with the density sometimes showing a smoothly varying profile and at other times showing pronounced variations.

One report (Rice and Sharp, 1977) suggests that the profiles are smooth about 80% of the time or show variations up to 5%. Variations of 5 to 15% occur about 10 to 15% of the time, and pronounced variations, greater than 15%, occur 5 to 10% of the time.

In the absence of detailed information on the amplitude and wavelength of the density variations to be expected, we have assumed that any wavelength may be encountered, and we have studied the response of the system especially for periods between 10 and 100 sec. We have assumed the amplitude of the variation to be ±10% at 220 km, although the actual variations will probably not be that great most of the time. Unless some means is available to know whether the density is smooth during any set of tension measurements, it may be difficult to tell from the data whether the variations observed are signal or noise. Thus, it would be desirable to have the system designed so that the noise level is within acceptable limits for any density variation that may reasonably be expected. Since the gravity gradient cannot vary with a wavelength shorter than the satellite altitude, variations shorter than this must certainly be noise.

As one means of evaluating the system noise level, it would be useful to have a capability of reading out the tension data at rates faster than the shortest signal expected. Multiple paths over the same ground track also provide a way to investigate the repeatability of measurements. Aside from tidal effects, the gravity field is essentially constant, whereas atmospheric density variations are expected to be random; thus, it should be possible to reduce the effect of noise in the data by averaging the data from passes over the same area. Another possibility is the inclusion of wind- and density-measuring devices, such as the instrumentation carried by the Atmospheric Explorer satellite. Data from these devices could be used as a weighting factor or to compute approximate correction factors for the tension measurements.

At orbital heights, wind velocities on the order of 100 to 150 m/sec have been observed. Since orbital velocities are on the order of 7.8 km/sec, the

variation in the velocity of the atmosphere with respect to the satellite is as much as 2%. Since drag heating effects are proportional to the cube of the velocity and drag force is proportional to the square, winds can account for variations of about 6% in drag heating and 4% in drag force.

3.2 Thermal Analysis

The temperature of the wire used in the Dumbbell satellite can undergo short-period variations as a result of changes in atmospheric drag heating or thermal and albedo radiation from the earth. The resulting changes in natural length of the wire cause variations in tension and excite longitudinal oscillations of the wire. Various approaches and materials have been considered for minimizing this problem. A thermal model of the wire has been developed and used in a computer program that calculates the thermal behavior of the wire by numerical integration. In addition, an approximate analytical solution for the thermal behavior has been derived to facilitate parameter optimization by showing how the thermal variations depend on the design parameters. Sample calculations using the analytical expressions are presented for comparison with the numerical integration results.

Temperature changes cause tension noise by accelerating the end masses. For example, if the temperature changed linearly with time, there would be no effect on the tension since the end masses would be moving at a uniform velocity. The tension change depends on the second derivative of the temperature with respect to time. Tension noise from thermal cycling can be reduced by insulating the wire to prevent rapid temperature changes.

3.2.1 Approaches to the thermal problem

Three approaches have been considered for handling the problem of thermal expansion and contraction of the wire: thermal compensation, thermal insulation, and the use of low-expansion materials. Thermal compensation might be accomplished by the use of two wire materials, one with a positive coefficient and

one with a negative coefficient such as Kevlar. If the wire is made with alternating sections of two different materials, care must be taken that the specific heat, emissivity, and absorptivity of the two materials are such that they undergo the same thermal cycling. If interwoven strands of two materials are used, it is essential that neither material goes slack under different temperature conditions. Since certain low-expansion materials are composite substances that achieve their properties essentially by internal compensation, this approach appears to be sound and will achieve the same objective as thermal compensation.

Thermal insulation can be used in conjunction with low-expansion materials. The time constants for conduction in a small-diameter wire (such as 1 mm) are very fast. Conductive isolation between the load-bearing tether and an insulating jacket appears to be required for effective insulation. We have done preliminary investigations into possible manufacturing techniques for achieving such isolation (see Section 7.2).

3.2.2 Materials properties

Various materials have been considered for use either as insulating materials or for construction of the tether itself. The first five entries in Table 2 are are potential tether materials, presented in order of decreasing expansion coefficient. The lowest expansion material is ULE,* a doped fused silica. It could be drawn into fibers and used to construct a cable with a suitable filler material to bind the fibers together. Cervit, a glass ceramic material with a fairly low expansion, cannot be reworked and would be unsuitable for use as a tether. Kevlar is a very strong material but would require much more thermal shielding than ULE does because of its higher expansion coefficient.

---

*ULE (UltraLow Expansion) is a synthetic amorphous silica glass of titanium silicate and is a trademark of Corning Glass Works, Corning, New York 14830.

Table 2. Materials Properties.

Material	Conductivity (ergs cm^{-1} sec^{-1} $°C^{-1}$) ($\times 10^5$)	Expansion coefficient (cm cm^{-1} $°C^{-1}$) ($\times 10^{-6}$)	Heat capacity (ergs cm^{-3} $°C^{-1}$) ($\times 10^7$)	Elasticity (dynes cm^{-2}) ($\times 10^{12}$)
Steel	—	20	—	2.11
Kevlar	10.3	-2	1.7 to 3.8	1.3
Invar	14.4	0.7	4.2	1.38
Cervit	1.67	0.15	2.2	0.9
ULE	1.31	0.03	1.65	0.7
Foam	0.02	—	—	—
Mylar	0.15	—	1.17	—
Mylar superinsulation	0.0001	—	—	—

The last three entries in the table are insulating materials. Calculating the thermal behavior of a 1-mm-diameter wire with a conductivity of 0.02×10^5 (cgs) gives a time constant on the order of 10 sec. The five potential tether materials listed in the table all have conductivities much larger than 0.02×10^5 (cgs) and would therefore have fast thermal time constants. The last entry in the table is for layers of aluminized mylar. The layers are conductively isolated by spacers or a crinkled construction that provides point contacts for conduction. When conductive isolation is used, the important quantities in determining the effectiveness of a material are the heat capacity and emissivity rather than conductivity. The elasticity of the potential tether materials is given because it enters into the calculation of the risetime of the system. In the diameters contemplated, all the tether materials possess sufficient strength to support the loads that must be carried.

3.2.3 Analytical model of thermal behavior

Since thermal expansion and contraction of the wire is the major noise source that has been identified, a computer program was written to analyze the

thermal behavior of the wire. The wire is modeled as a series of concentric cylinders with conductive or radiative heat transfer or both, between the layers. Azimuthal temperature variations were not included. In practice, the thermal time constants for conduction are so fast that layers having only radiative coupling will be nearly isothermal. The model can represent layers of a homogeneous material if the problem has azimuthal symmetry and will give order-of-magnitude answers for asymmetric problems. Excluding the aximuthal dependence gives conservative results, since the time constants are longer for asymmetric problems. The model includes atmospheric drag heating and solar radiation for the outer layer and thermal radiation from the surface.

The heat input from solar radiation at normal incidence per unit length is $2r\alpha I_{sun}$, where r is the wire radius, α is the solar absorptivity, and I_{sun} is the solar radiation constant. The heat input from atmospheric drag at normal incidence per unit length is $r\rho_a v^3$, where ρ_a is the atmospheric density and v is the velocity of the wire with respect to the atmosphere. The heat radiated from the surface per unit length is $2\pi r\sigma\varepsilon T^4$, where σ is the Stefan-Boltzmann constant ($= 5.6697 \times 10^{-5}$), ε is the emissivity, and T is the temperature. The heat conducted per unit length from the inside to the outside of a cylinder is

$$\frac{2\pi k}{\ell n\,(r_2/r_1)}\,(T_1 - T_2) \quad ,$$

where k is the conductivity of the material and the subscripts 1 and 2 represent the inner and outer surfaces of the cylinder. The net heat radiated per unit area between two infinite parallel surfaces is

$$\frac{\sigma\varepsilon_1\varepsilon_2(T_1^4 - T_2^4)}{\varepsilon_1 + \varepsilon_2 - \varepsilon_1\varepsilon_2} \quad .$$

It is assumed that the thermal absorptivity is the same as the emissivity. For the case of two concentric cylindrical surfaces, the above formula has been

multiplied by the area per unit length of the inner cylinder, giving

$$2\pi r_1 \sigma \frac{\varepsilon_1 \varepsilon_2}{\varepsilon_1 + \varepsilon_2 - \varepsilon_1 \varepsilon_2} (T_1^4 - T_2^4)$$

as the net heat radiated from the inner to the outer surface. If $\varepsilon_2 << \varepsilon_1$, the factor

$$\frac{\varepsilon_1 \varepsilon_2}{\varepsilon_1 + \varepsilon_2 - \varepsilon_1 \varepsilon_2}$$

reduces to ε_2. If $\varepsilon_1 = \varepsilon_2$ and both are much less than unity, the factor reduces to $\varepsilon_2/2$. If the total heat input to a layer due to radiation or conduction, or both, is $\dot{Q}$, the rate of change of temperature is

$$\frac{dT}{dt} = \frac{\dot{Q}}{C_v \pi (r_2^2 - r_1^2)} \quad , \tag{6}$$

where C_v is the heat capacity per unit volume and t is the time.

To simulate the effect of atmospheric granularity, the atmospheric density has been modeled as

$$\rho_a = \rho_0 \left[1 + A \sin \left(\frac{2\pi}{P}\right) t\right] \quad ,$$

where ρ_0 is the average density, A is the fractional variation, and P is the period of the fluctuation. By means of a numerical integrator, we can determine the temperature of each layer as a function of time starting from some initial temperature distribution and using the rate of change of temperature given in equation (6).

3.2.4 Results of thermal analysis

Computer runs have been made to determine the thermal behavior under various conditions of a 1-mm-diameter ULE tether. The wire is assumed to be moving at 7.7 km/sec through a region with an atmospheric density of 2.31×10^{-13} g/cc, which is approximately the density at a typical Shuttle altitude of 220 km. The density is varied sinusoidally with an amplitude of ±10% of the mean value. Variations of the radiational heating of the wire have not been included. The problem of radiative variations is easier to handle than that of drag-heating variations since most of the radiation can be reflected from the surface. Once absorbed at the surface, the effect on the thermal behavior of the wire is the same for either source. If the wire has no insulation, it will be nearly isothermal unless the period of the variations is a small fraction of a second. If the amplitude of the variation in drag heating is kept fixed and the period is varied, the amplitude of the temperature variation of the wire is proportional to the period. For a 20-sec period, the temperature variation is 0.0135°C. Twenty seconds corresponds to 154 km along the ground at 7.7 km/sec.

A second case analyzed is a 1-mm cable consisting of a 0.9-mm load-bearing core and a 0.05-mm-thick jacket conductively isolated from the core. In this case, the heat transfer is radiative and depends on the emissivity of the surfaces exchanging energy. A low emissivity is desirable, and runs have been made assuming an emissivity of 0.05 for one surface and 0.8 for the other. Table 3 gives some sample values of the emissivity factor, which determines the rate of radiative heat transfer.

Table 3. Emissivity factors.

ε_1	ε_2	$\frac{\varepsilon_1\varepsilon_2}{\varepsilon_1 + \varepsilon_2 - \varepsilon_1\varepsilon_2}$
0.8	0.8	0.6666
0.05	0.8	0.0494
0.05	0.05	0.0256

The protective jacket acts as a heat reservoir to contain the variations in thermal input and transmit them only slowly to the core via radiation. Since the conductive time constant of the jacket is a fraction of a second, it functions solely as a heat reservoir, with the gap between it and the core providing a thermal barrier. The effectiveness of the jacket as a heat reservoir is proportional to the product of the specific heat and the mass of the jacket. Table 4 gives the temperature variation of the core for selected periods of drag-heating variations. The variation of the core temperature increases nonlinearly with period because the core has more time to come to thermal equilibrium when the period is longer. In the limit of very long periods, the jacket would have no effect, since the core would always be nearly in equilibrium with the jacket, and the temperature variation of the core would be proportional to the period. The 20- and 200-sec periods correspond to 154 and 1540 km, respectively, along the ground.

Table 4. Temperature variations.

Period (sec)	ΔT (°C)
20	±0.0005
50	±0.0035
100	±0.012
200	±0.0415

A third type of run used two jackets. The core is 0.77 mm, the inner jacket is 0.06 mm, and the outer jacket is 0.05 mm. With a 20-sec period, the temperature variation of the core is ±0.00001°C. This type of multilayer insulating jacket is clearly quite effective in principle. We have not looked into the practical feasibility of such a design.

3.2.5 Approximate analytical solution of thermal behavior

The Dumbbell wire will receive heat input from solar radiation, atmospheric drag heating, and infrared and albedo radiation from the earth. In equilibrium,

the heat input equals the thermal radiation from the surface of the wire. In general, the heat input will vary with orbital conditions, and the temperature of the wire and its jacket will vary continuously with a time lag that depends on the cooling time constants. Long-period temperature variations have negligible effect on the wire tension. In this section, approximate solutions are derived for short-period temperature fluctuations, expected primarily from variations in drag heating. The short-period temperature fluctuations derived below will, in general, be superimposed on the temperature variations of orbital period.

In the small-diameter wires considered for use with Dumbbell, the time constants for conduction across the wire diameter are a fraction of a second. We can therefore obtain an approximate solution for the thermal behavior of the wire by assuming that all parts of the wire in conductive contact are essentially isothermal. We consider here the cases of a bare wire and a wire with an insulating jacket conductively isolated from the core.

The heat energy per second per unit length resulting from atmospheric drag is approximately $r\rho_a v^3$. If the drag heating varies by the factor $1 + A \sin \omega t$, where ω is the frequency, the wire will have a variable heat input $\dot{q}$ given by

$$\dot{q} = r\rho_a v^3 A \sin \omega t \quad .$$

If the temperature fluctuations are small enough that the fluctuations in thermal radiation are negligible, the fluctuation in the wire temperature rate is approximately

$$\dot{T} = \frac{\dot{q}}{H} \quad ,$$

where H ($= C_v \pi r^2$) is the heat capacity per unit length. The expression for $\dot{T}$ is

$$T = \frac{r\rho_a v^3 A \sin \omega t}{C_v \pi r^2} = \frac{\rho_a v^3 A \sin \omega t}{C_v \pi r} \quad ,$$

which we can integrate with respect to time to get

$$T = - \frac{\rho_a v^3 A \cos \omega t}{C_v \pi r \omega} \quad .$$

The amplitude of the temperature fluctuation is then

$$\Delta T = \frac{\rho_a v^3 A}{C_v \pi r \omega} \quad .$$

As an example, for the case of a 2-mm-diameter wire with $\rho_a = 2.3 \times 10^{-13}$ g/cc, v = 7.77 km/sec, A = 10%, $C_v = 1.65 \times 10^7$ ergs cm^{-3} $°C^{-1}$, and $\omega = 0.314$ (20-sec period), we get $\Delta T = 0.00666°C$. Since the temperature fluctuation is inversely proportional to r, we can reduce ΔT by increasing r. The value of r required to obtain a fluctuation ΔT is

$$r = \frac{\rho_a v^3 A}{C_v \rho \omega \Delta T} \quad .$$

So, for these same parameters, we can reduce ΔT to 0.0005°C if r = 1.33 cm. (A temperature fluctuation of 0.0005°C gives an acceptable tension variation with a ULE cable, as we will show in Section 3.3). For r = 0.1 cm, we have $\Delta T = 0.0133°C$, in good agreement with the result obtained by numerical integration (first paragraph of Section 3.2.4).

If the wire is protected by a jacket that is conductively isolated from the core, we can obtain an approximate analytical solution under the assumption that the fluctuation of the heat transfer between the jacket and the core is small compared to the fluctuations of drag heating. The rate of change of the jacket temperature due to drag fluctuations is

$$\dot{T}_2 = \frac{\dot{q}_2}{H_2} \quad ,$$

where $\dot{q}_2 = r_3\rho_a v^3 A \sin \omega t$ and H_2 is the heat capacity of the jacket, given by,

$$H_2 = C_2\pi(r_3^2 - r_2^2) \quad ;$$

r_3 is the outer and r_2 is the inner radius of the jacket. Integrating $\dot{T}_2$ with respect to time gives

$$T_2 = - \frac{r_3\rho_a v^3 A \cos \omega t}{C_2\pi(r_3^2 - r_2^2)\ \omega} \quad .$$

The amplitude of the temperature fluctuation of the jacket is

$$\Delta T_2 = \frac{r_3\rho_a v^3 A}{C_2\pi(r_3^2 - r_2^2)\ \omega} \quad .$$

The radiative heat input from the jacket to the core, $\dot{q}_1$, is

$$\dot{q}_1 = 2\pi r_1\sigma \frac{\varepsilon_1\varepsilon_2}{\varepsilon_1 + \varepsilon_2 - \varepsilon_1\varepsilon_2} (T_2^4 - T_1^4) \quad ,$$

where r_1 is the radius of the core, ε_1 and ε_2 are the emissivities of the core and the inner surface of the jacket, and T_1 and T_2 are the core and jacket temperatures. If we assume that the fluctuation of T_1^4 is small compared to the fluctuation of T_2^4, then the amplitude of the fluctuation in heat input to the core is

$$\Delta\dot{q}_1 = \frac{\delta\dot{q}_1}{\delta T_2} \Delta T_2 = 2\pi r_1\sigma \frac{\varepsilon_1\varepsilon_2}{\varepsilon_1 + \varepsilon_2 - \varepsilon_1\varepsilon_2} 4T_2^3\ \Delta T_2 \quad .$$

The heat input as a function of time has the form

$$\dot{q}_1 = \Delta\dot{q}_1 \sin \omega t \quad ,$$

and the rate of change of core temperature is

$$\dot{T}_1 = \frac{\dot{q}_1}{H_1} = \frac{\Delta\dot{q}_1 \sin \omega t}{H_1} \quad ,$$

where $H_1 = C_1 \pi r_1^2$. Integrating, we obtain

$$T_1 = - \frac{\Delta\dot{q}_1}{H_1 \omega} \cos \omega t \quad .$$

The amplitude of the temperature variation is

$$\Delta T_1 = \frac{2\pi r_1 \sigma \varepsilon_1 \varepsilon_2 4 T_2^3 \Delta T_2}{C_1 \pi r_1^2 \omega (\varepsilon_1 + \varepsilon_2 - \varepsilon_1 \varepsilon_2)} = \frac{8\sigma \varepsilon_1 \varepsilon_2 T_2^3 \Delta T_2}{C_1 r_1 \omega (\varepsilon_1 + \varepsilon_2 - \varepsilon_1 \varepsilon_2)} \quad .$$

We can substitute for ΔT_2 to obtain

$$\Delta T_1 = \frac{8\sigma \varepsilon_1 \varepsilon_2 T_2^3 r_3 \rho_a v^3 A}{C_1 C_2 \pi r_1 \omega^2 (r_3^2 - r_2^2)(\varepsilon_1 + \varepsilon_2 - \varepsilon_1 \varepsilon_2)} \quad . \qquad (7)$$

As an example, consider the case of a 1-mm cable consisting of a core and a jacket with r_1, r_2, and r_3 equal to 0.044, 0.045, and 0.05 cm. For the other parameters, take $T_2 = 448.7°K$, $\rho_a = 2.3 \times 10^{-13}$ g/cc, v = 7.77 km/sec, $C_1 = C_2 = 1.65 \times 10^7$ ergs cm^{-3} $°C^{-1}$, $\varepsilon_1 = 0.05$, $\varepsilon_2 = 0.8$, and $\omega = 0.314$ (20-sec period). The amplitude of the fluctuation of the core temperature is 6×10^{-4} °C, which agrees approximately with the first entry in Table 4, obtained by numerical integration. If the outside diameter of the cable is increased to 4 mm and we use $r_1 = 0.1$ cm, $r_2 = 0.15$ cm, and $r_3 = 0.2$ cm, keeping the other parameters the same, we obtain $\Delta T_1 = 3 \times 10^{-5}$ °C. Increasing the wire diameter simplifies the problem of thermal insulation, as the example shows. Equation (7)

can be used to determine a set of wire parameters that will reduce the temperature fluctuations of the core to the level required for keeping the tension noise below the signal.

3.3 Longitudinal Oscillations

Longitudinal oscillations of the Dumbbell system can be excited by various means, such as the process of deployment, drag-force variations, short-period gravity-gradient variations (which are the signal being measured), and thermal expansion and contraction of the wire. Damping is required to prevent continuous oscillation at the resonant frequency, which would obscure the signals being measured. The resonant frequency of the longitudinal oscillations is an important design consideration, since it determines the risetime of the system.

A physical model of the Dumbbell system, including an end-mass damper, has been implemented in a small computer program that calculates, by numerical integration, the orbital motion of two masses connected by a massless tether. The program also models the natural length of the wire as a function of temperature. The results of the thermal analysis in Section 3.2 are used as input to this program to study the effect of temperature variations on the wire tension. In addition, an approximate analytical expression is derived for the tension noise due to temperature variations. Two limiting cases are considered, depending on whether the frequency of the temperature variations is faster or slower than the resonant frequency of the longitudinal oscillations. These approximations utilize the high- and low-frequency limits of the general solution for the steady-state behavior of a driven harmonic oscillator.

The approximations for a harmonic oscillator are also employed in various other parts of this report for obtaining closed-form solutions valid in certain frequency ranges. The analytical expression for the tension noise shows the dependence on the design parameters and can be used in selecting a set of parameters to achieve the required tension noise level.

3.3.1 System risetime and frequency of the longitudinal oscillations

For a change in the gravity gradient due to a gravity anomaly to be detected, the Dumbbell system must stretch to a new length such that the change in wire tension equals the change in the gravity-gradient force on the system. The risetime for this to be accomplish depends on the natural frequency of the longitudinal oscillations of the system. Consider a system consisting of two weights of mass M connected by a wire of length ℓ. The system can perform longitudinal oscillations with the center of the wire remaining fixed, and the problem is identical to that of a mass on the end of a spring of length $\ell/2$ attached to a fixed support. The restoring force F supplied by the wire is $F = -kx$, where x is the displacement of the mass from equilibrium and k is the spring constant, given by

$$k = E\frac{A}{\ell/2} \quad ,$$

E being the wire's elasticity and A is its cross section. The equation of motion of the system is

$$M\ddot{x} = -kx \quad ,$$

and the frequency ω of the oscillations is

$$\omega = \sqrt{k/M} \quad .$$

For a system consisting of two masses of 2×10^6 g each, connected by a 10^5-cm wire with an elasticity of 0.7×10^{12} dynes/cm^2, a wire thickness of 2 mm is required to give a fast enough risetime. Since $A = \pi r^2$, the frequency ω is

$$\omega = r\sqrt{\frac{2\pi E}{M\ell}} = 0.1\sqrt{\frac{2\pi \times 0.7 \times 10^{12}}{2 \times 10^6 \times 10^5}} = 0.4689 \text{ rad/sec} \qquad (8)$$

and the corresponding period is

$$P = \frac{2\pi}{\omega} = 13.4 \text{ sec.}$$

Since the end masses have spring dampers whose spring constant is comparable to that of the wire, the period of the longitudinal oscillations is increased. If the effective k is reduced by a factor of 2, the period is increased by $\sqrt{2}$. Considering only the wire, the frequency is proportional to the wire radius.

Equation (8) can be used to make sure that a given set of system parameters allows for an adequate risetime for measuring gravity anomalies. Since dampers will lower the frequency, the frequency from equation (8) should be about a factor of $\sqrt{2}$ faster than that required for the overall system. The cross section $A = \pi r^2$ is the cross section of the load-bearing part of the cable only. For a stranded cable, void or filler space should be taken into account.

3.3.2 Analytical model of longitudinal wire oscillations

The temperature variation of the wire obtained from the thermal model is the form

$$T = T_0 \left[1 + B \sin \left(\frac{2\pi}{P} t\right)\right] \quad ,$$

where T_0 is the average temperature, B is the fractional variation of the temperature, and P is the period of the variation. A simple orbital dynamics program has been used to determine the tension variation produced in the Dumbbell wire by a temperature variation of a given amplitude and period.

If the temperature variation has the same frequency as the resonant frequency of Dumbbell, the amplitude of the oscillations will increase indefinitely. This can be prevented by having a damper on the end mass to dissipate

the energy of the oscillations. The Skyhook dynamic simulation computer program (Kalaghan et al., 1978) has a damping force proportional to the rate of change of the length of the wire. The damping constant is usually chosen large enough to provide critical damping and allow rapid numerical integration, since there are no fast wire oscillations to integrate. This damping model could represent hysteresis in the tether; however, the actual hysteresis would presumably be far smaller than the values that have been used simply to obtain fast numerical integration. A model of an end-mass damper has been added to a simple version of the Skyhook program to study the effect of wire temperature variations with a more physically realistic model. This damper consists of a spring and dashpot inserted between the wire and the end mass, as shown in Figure 10.

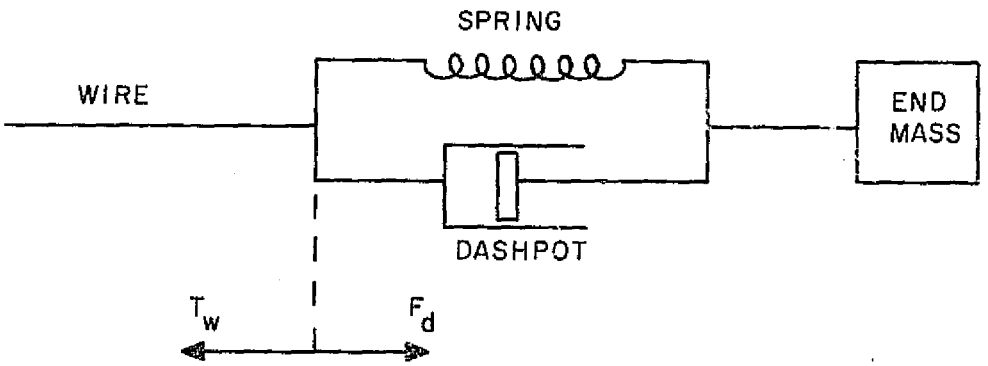

Figure 10. Model of damper inserted between the tether and the end mass.

The force F_d exerted by the damper is equal to the wire tension T_w. The wire tension can be written

$$T_w = k[\ell - \ell_0(T)] \quad ,$$

where $\ell_0(T)$ is the natural length of the wire, given by

$$\ell_0(T) = \ell_0(T_0) + \alpha(T - T_0) \quad ,$$

in which α is the thermal expansion coefficient and T_0 is some reference temperature. The damping force is given by

$$F_d = k_d(\ell_d - \ell_{0d}) + b_d\dot{\ell}_d \quad ,$$

where k_d is the spring constant of the damper, ℓ_d is the actual length of the damper, ℓ_{0d} is the natural length of the damper, and b_d is the damping constant of the dashpot. In the orbital dynamics computer program, the length of the damper ℓ_d must be added to the other variables to be integrated numerically as a function of time. The rate of change of ℓ_d is obtained by solving the equation

$$T_w = F_d \quad ,$$

$$k[\ell - \ell_0(T)] = k_d(\ell_d - \ell_{0d}) + b_d\dot{\ell}_d$$

for $\dot{\ell}_d$, which gives

$$\dot{\ell}_d = \frac{1}{b_d}\left\{k[\ell - \ell_0(T)] - k_d(\ell_d - \ell_{0d})\right\} \quad .$$

The end-mass damper does not appear to be capable of providing the critical damping by which the system returns to equilibrium in minimum time without overshooting. However, if k_d is set equal to k and b_d is set equal to $\sqrt{k/M}$, the amplitude of the oscillations is reduced by about a factor of 2 on each half-cycle. The damper lengthens the natural period of oscillation of the wire, because if reduces the overall spring constant of the system. If $k_d = k$, the period is lengthened by a factor of $\sqrt{2}$.

3.3.3 Results of mechanical analysis

When the period of the temperature variations in the wire is less than the resonant frequency of the Dumbbell system, the end masses do not have time

to adjust their positions to an equilibrium configuration during a cycle. Therefore, the fractional change in tension in the wire is independent of the period of the temperature variations. As the period becomes longer than the resonant period, the fractional change in tension drops off and becomes negligible for long periods because the end masses are in quasi-static equilibrium throughout the cycle of temperature variations. Table 5 shows the fractional tension change when the temperature variation is ±1°C and the resonant frequency of the system is 35 sec.

Table 5. Effect of temperature-variation period on fractional tension change.

Period (sec)	$\frac{\Delta \text{ tension}}{\text{tension}} \times 10^{-4}$
1	4.05
2	4.17
5	3.94
10	3.73
20	4.21
50	2.74
100	0.336
200	0.0875

For a tether with no insulation, the magnitude of the temperature variation in the wire is proportional to the period. Since the fractional change in tension is proportional to the amplitude of the temperature variation, the fractional tension variation is obtained by multiplying the tension in Table 5 by the actual temperature variation. For an uninsulated wire, this results in a kind of resonance curve, where the maximum tension change for a constant-amplitude drag-heating variation occurs at the resonant frequency of the Dumbbell system. Table 6 gives the fractional tension change for an uninsulated tether and a tether with one jacket.

Table 6. Fractional tension change for an uninsulated tether and for a tether with one jacket.

Period (sec)	Uninsulated tether		Insulated tether	
	ΔT (°C)	$\frac{\Delta \text{ tension}}{\text{tension}} \times 10^{-6}$	ΔT (°C)	$\frac{\Delta \text{ tension}}{\text{tension}} \times 10^{6}$
1	0.000675	0.27	—	—
2	0.00135	0.56	—	—
5	0.00337	1.3	—	—
10	0.00675	2.5	—	—
20	0.0135	5.7	0.0005	0.21
50	0.0337	9.2	0.0035	0.96
100	0.0675	2.27	0.0120	0.40
200	0.135	1.18	0.0415	0.36

The design goal is a fractional tension change of a few parts per million. The tether with no insulation does not quite meet this requirement, but the insulated tether is well within the limit.

3.3.4 Driven harmonic oscillator

A number of sections in this report contain approximate analytical solutions for the behavior of the Dumbbell system under various conditions. The approximations depend primarily on whether the driving force is faster or slower than the natural frequency of the system being driven. The equation of motion for a damped harmonic oscillator driven by a force of magnitude F and frequency ω is

$$m\ddot{x} + b\dot{x} + kx = Fe^{i\omega t} \quad ,$$

where m is the mass of the object and b is the damping coefficient. A solution of the form

$$x = Ce^{i\omega t}$$

gives

$$C(-m\omega^2 + i\omega b + k) = F \quad ,$$

where C is the amplitude of the oscillation. If there is no driving force, the frequency of the natural oscillation is

$$\omega = \frac{ib \pm \sqrt{b^2 + 4mk}}{2m} \quad .$$

With no damping, the natural frequency is $\omega = \sqrt{k/m}$; for critical damping, $|b| = 2\sqrt{mk}$. The amplitude of the oscillation with a driving force is

$$C = \frac{F}{k - m\omega^2 + i\omega b} \quad .$$

When the driving force is at the resonant frequency, $k - m\omega^2 = 0$, and the amplitude is largest. Without damping, the amplitude increases indefinitely with time. If the frequency is low compared to the natural frequency, the amplitude is $C = F/k$; in other words, the restoring force is in equilibrium with the driving force. This assumes either that the natural frequency has not been excited at any time in the past or that any natural oscillation has died out owing to the presence of some damping in the system. If the driving frequency is fast compared to the natural frequency, the amplitude is $A = -F/m\omega^2$, which is small in this case because of the factor ω^2.

The derivations in various sections of this report use the approximation that the system is in equilibrium for low frequencies and stationary for high frequencies.

3.3.5 Tension variations due to end-mass acceleration

The end masses in the Dumbbell system can be accelerated as a result of temperature variations in the wire or transverse oscillations of the wire.

We can write approximate analytical solutions for the tension noise in two limiting cases. If the period of the variations is long compared to the resonant frequency of the longitudinal oscillations of the system, the wire acts nearly as a rigid rod and the motion of the end masses is approximately equal to the change in natural length of the wire or the change in distance between the ends of the wire. If the oscillations are fast compared to the response time of the system, the end masses do not have time to move and the tension noise is that due to the stretching of the wire.

If the end mass M is forced to oscillate so that the position y as a function of time is

$$y = \Delta y \sin \omega t \quad ,$$

then the tension force as a function of time is

$$F = m\ddot{y} = -M\omega^2 \Delta y \sin \omega t$$

and the amplitude of the tension noise is $\Delta F = M\omega^2 \Delta y$. For example, if each end mass is 10^6g, $\ell = 2 \times 10^5$ cm, and $\alpha = 3 \times 10^{-8}/°C$, then the amplitude of the motion for a 1°C temperature fluctuation is

$$\Delta y = \frac{\ell\alpha}{2} \Delta T = 3 \times 10^{-3} \text{ cm} \quad .$$

The tension noise for a 200-sec-period variation is

$$\Delta F = 10^6 \times \left(\frac{2\pi}{200}\right)^2 \times 3 \times 10^{-3} = 3 \text{ dynes} \quad ,$$

and the fractional tension noise for T = 416,000 dynes is

$$\frac{\Delta F}{T} = \frac{3}{416{,}000} = 7 \times 10^{-6} \quad ,$$

in approximate agreement with the last entry in Table 5, obtained by numerical integration.

If the frequency of the change in wire length is faster than the resonant frequency, the tension noise is $F = k\,\Delta y$. The spring constant k for the wire is

$$k = \frac{EA}{\ell} \quad .$$

Setting $E = 0.7 \times 10^{12}$ dynes/cm^2, $A = \pi(0.05)^2$ cm^2, and $\ell = 2 \times 10^5$ cm, we have $k = 2.75 \times 10^4$ dynes/cm. With $\alpha = 3 \times 10^{-8}$/°C and $\Delta T = 1$°C, the change in natural length of the wire is

$$\Delta y = \alpha \ell\, \Delta T = 6 \times 10^{-3} \text{ cm} \quad .$$

The tension change is

$$\Delta F = k\,\Delta y = 165 \text{ dynes} \quad ,$$

and the fractional tension noise is

$$\frac{\Delta F}{T} = \frac{165}{416{,}000} = 4 \times 10^{-4} \quad ,$$

in good agreement with the first five entries of Table 5, which are below the resonant frequency.

In summary, we can use the formula

$$\Delta F = M\omega^2\,\Delta y \tag{9}$$

to obtain the tension noise when the end mass M is executing a motion of amplitude Δy at a frequency ω that is small compared to the resonant frequency. When ω is larger than the resonant frequency, we can use

$$\Delta F = k\,\Delta y \quad , \tag{10}$$

where k is the spring constant of the whole wire and Δy is the change in natural length of the wire (thermal expansion and contraction) or the change in arc length of the wire (transverse wire oscillations).

3.4 Transverse Oscillations and Drag

This section discusses the tension noise introduced by variations in atmospheric drag force. Since the area-to-mass ratio of the Dumbbell wire is much larger than that of the end masses, the wire will be curved back by the drag force. If the drag force varies along the orbital path, the amount of curvature will vary and a force will be exerted on the end masses as a result of the change in distance between the ends of the wire.

Three effects of drag are considered here, in order of increasing significance with respect to tension noise: the change in average tension from the constant part of the drag, tension noise from higher modes of transverse oscillation of the wire, and tension noise from the excitation of the fundamental transverse oscillation mode by drag-force variations. The change in average tension affects the measurement of the absolute value of the total gravity gradient but does not interfere with measuring the short-wavelength gravity-gradient variations. The excitation of higher transverse oscillation modes can occur as a result of nonuniform drag along the wire. The excitation force is weak, and large oscillations develop only under resonant conditions. The excitation of the fundamental transverse mode is the most significant effect.

Computer runs using numerical integration have been performed to study the fundamental and higher transverse oscillation modes. The program models the wire as a series of discrete masses having the lumped properties of a section of the wire (Kalaghan et al., 1978). For studying the fundamental mode, a single point is used to represent the wire. The accuracy of this approximation is compared to an analytical calculation of the wire configuration resulting from drag force (see Section 3.4.1). The derivation (which contains nothing new) indicates the approximations and limits of validity of the analytical expression.

In addition to the computer runs, an approximate analytical expression is derived for the tension noise arising from the excitation of the fundamental mode. This can be used to calculate the noise as a function of the system parameters. Sample calculations are compared with the numerical-integration results. Practical considerations limit the extent to which the tension noise can be minimized by varying the system parameters for a configuration consisting of two masses connected by a flexible wire. Such a system would probably be limited to operation at altitudes where drag effects are not too severe. For this reason, two additional configurations designed to help cope with the problems of drag are also considered. One includes ballast masses along the wire, and the other uses a rigid rod to resist the bending effects of drag. Analytical expressions are presented for the tension noise in each case, and sample calculations are compared with the results of numerical integration of the system dynamics.

3.4.1 Wire curvature due to drag

When drag acts on a wire connecting two masses, each section is given an acceleration that depends on its area-to-mass ratio. Assuming that the area-to-mass ratio of the wire is large compared to that of the end masses, we can neglect the effect of the acceleration of the end masses. Other assumptions are that the tension in the wire is constant, the curvature of the wire is small, and the drag force is prependicular to the wire. In equilibrium, the drag force on each element of wire must equal the restoring force due to wire curvature.

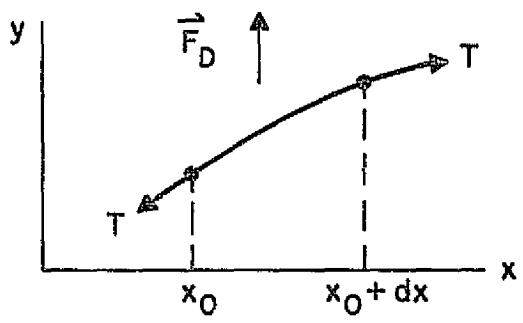

Figure 11. Equilibrium drag force on a wire element.

In Figure 11, we see that the transverse force F_T due to wire tension is

$$F_T = -T \frac{dy(x_0)}{dx} + T \frac{dy(x_0 + \Delta x)}{dx} = T \frac{d^2y}{dx^2} dx \quad .$$

The drag force on each section is

$$F_D = 2r\rho_a v^2 \, dx \quad .$$

Since

$$F_T + F_D = 0$$

in equilibrium, we can substitute for F_T and F_D and get

$$T \frac{d^2y}{dx^2} dx + 2r\rho_a v^2 \, dx = 0 \quad ,$$

$$\frac{d^2y}{dx^2} = - \frac{2r\rho_a v^2}{T} \quad .$$

For simplicity, let the origin of the coordinates be at the center of the wire, so that y and dy/dx are zero at the origin (see Figure 12).

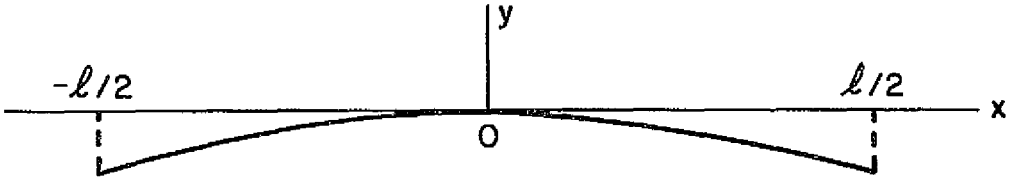

Figure 12. Coordinate system for wire configuration.

Integrating twice to get the wire configuration, we have

$$\frac{dy}{dx} = -\frac{2r\rho_a v^2}{T} x \tag{11}$$

and

$$y = -\frac{r\rho_a v^2}{T} x^2 \quad . \tag{12}$$

To evaluate the displacement of the end masses due to changes in wire curvature, we need the arc lengths of the curve from $x = -\ell/2$ to $x = \ell/2$. This is given by

$$S = 2\int_0^{\ell/2} ds = 2\int_0^{\ell/2} \sqrt{dx^2 + dy^2} = 2\int_0^{\ell/2} \sqrt{1 + \left(\frac{dy}{dx}\right)^2}\, dx \quad .$$

Assuming that dy/dx is a small quantity, the integral is approximately

$$S \approx 2\int_0^{\ell/2} \left[1 + \frac{1}{2}\left(\frac{dy}{dx}\right)^2\right] dx \quad .$$

Substituting dy/dx from equation (11), we have

$$S = 2\int_0^{\ell/2} \left[1 + \frac{1}{2}\left(\frac{2r\rho_a v^2}{T}\right)^2 x^2\right] dx = \left[2x + \frac{1}{3}\left(\frac{2r\rho_a v^2}{T}\right)^2 x^3\right]\Bigg|_0^{\ell/2}$$

$$= \ell + \frac{1}{3}\left(\frac{2r\rho_a v^2}{T}\right)^2 \left(\frac{\ell}{2}\right)^3 \quad .$$

If the wire configuration changes due to a change in atmospheric density, the change in arc length is

$$dS = \frac{\partial S}{\partial \rho_a} d\rho_a = \frac{2}{3} \left(\frac{2r\rho_a v^2}{T}\right) \left(\frac{\ell}{2}\right)^3 \left(\frac{2rd\rho_a v^2}{T}\right) \quad .$$

If we write $d\rho_a$ as $\alpha\rho_a$, where α is the fractional variation of the drag force, the expression becomes

$$dS = \frac{2\alpha}{3} \left(\frac{2r\rho_a v^2}{T}\right)^2 \left(\frac{\ell}{2}\right)^3 = \frac{\alpha}{3} \left(\frac{r\rho_a v^2}{T}\right)^2 \ell^3 \quad . \tag{13}$$

In the Skyhook dynamic simulation computer program, when a single mass point is used to represent the lumped properties of the wire, the cross section for drag is computed as the total cross section divided by the number of wire sections, which in this case is two. In Figure 13, the lumped properties of the wire are represented by the mass m. The drag force F

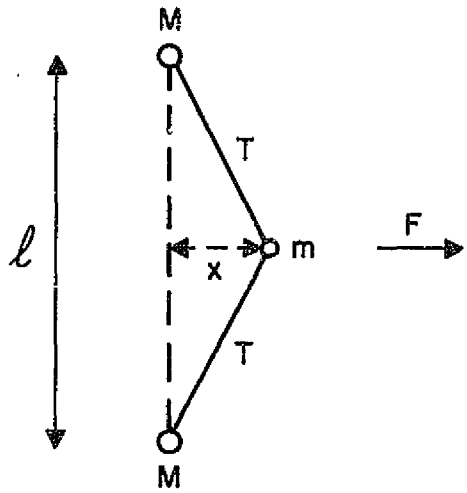

Figure 13. Equilibrium displacement of wire midpoint by atmospheric drag.

displaces the mass m by a distance x such that in equilibrium,

$$F = 2T \frac{x}{\ell/2} = \frac{4Tx}{\ell} \quad , \tag{14}$$

or

$$x = \frac{\ell}{4T} F \quad . \tag{15}$$

By convention, the drag force on m is

$$F = 2r\rho_a v^2 \frac{\ell}{2} = r\rho_a v^2 \ell \quad , \tag{16}$$

and thus the displacement of the midpoint of the wire is

$$x = \frac{\ell}{4T} r\rho_a v^2 \ell = \frac{r\rho_a v^2 \ell^2}{4T} \quad . \tag{17}$$

The accuracy of this convention can be compared to the results of the analytical solution. From equation (12), the magnitude of the displacement of the middle of the wire relative to the ends is

$$\frac{r\rho_a v^2}{T} \left(\frac{\ell}{2}\right)^2 = \frac{r\rho_a v^2 \ell^2}{4T} \quad ,$$

in agreement with equation (17).

The distance S between the ends of the wire in the lumped-mass case is

$$S = 2\sqrt{\left(\frac{\ell}{2}\right)^2 - x^2} = \ell\sqrt{1 - \left(\frac{2x}{\ell}\right)^2} \approx \ell\left[1 - \frac{1}{2}\left(\frac{2x}{\ell}\right)^2\right] \quad .$$

If the drag force changes, the change dS in distance between the ends of the wire is

$$dS = \ell\left[-\left(\frac{2x}{\ell}\right)\left(\frac{2}{\ell}\right)\frac{\partial x}{\partial \rho_a}\right] d\rho_a = -\frac{4x}{\ell}\frac{\partial x}{\partial \rho_a} d\rho_a \quad .$$

Differentiating equation (17) with respect to ρ_a gives

$$\frac{\partial x}{\partial \rho_a} = \frac{r v^2 \ell^2}{4T} = \frac{x}{\rho_a} \quad ,$$

and thus

$$dS = -\frac{4x}{\ell} \frac{x}{\rho_a} d\rho_a = -\frac{4x^2}{\ell} \frac{d\rho_a}{\rho_a} \quad .$$

If $d\rho_a = \alpha \rho_a$, then, from equation (17), we have

$$dS = -\frac{4\alpha x^2}{\ell} = -\frac{4\alpha}{\ell} \left(\frac{r\rho_a v^2 \ell^2}{4T}\right)^2 = -\frac{\alpha}{4} \left(\frac{r\rho_a v^2}{T}\right)^2 \ell^3 \quad . \qquad (18)$$

Equation (18) differs from equation (13) by having a factor of 4 in the denominator instead of 3, so that the lumped-mass approximation underestimates the change in displacement of the ends by the factor 3/4. (The minus sign results from computing the change in distance between the ends for a fixed wire length rather than computing the stretching of the wire with fixed end points, as is done in the analytical treatment.) Since the amount of computer time increases sharply with the number of mass points, most runs were done with two points representing the end masses and one point representing the wire.

3.4.2 Effect of drag on total equilibrium wire tension

In equilibrium, the tension force that the wire exerts on each end mass has a vertical component T_G resulting from gravity-gradient and centripetal forces and a horizontal component T_D due to drag. Since the drag force is shared equally by the two end masses, T_D is half the total drag force on the wire. The total tension T is the vector sum of the two components, and the magnitude of T is

$$T = \sqrt{T_G^2 + T_D^2} = T_G \sqrt{1 + \left(\frac{T_D}{T_G}\right)^2} \approx T_G \left[1 + \frac{1}{2}\left(\frac{T_D}{T_G}\right)^2\right] = T_G + \frac{T_D^2}{2T_G} \quad .$$

For example, if $\ell = 10^5$ cm and the wire diameter is 0.5 cm, $T_D = 2130$ dynes and $T_G = 416{,}400$ dynes. The change ΔT in T due to T_D is

$$\Delta T = T_D \left(\frac{T_D}{2T_G}\right) = 2130 \times 2.557 \times 10^{-3} = 5.45 \text{ dynes} \quad ,$$

and the fractional tension error is

$$\frac{\Delta T}{T} = \frac{1}{2}\left(\frac{T_D}{T_G}\right)^2 = 13 \times 10^{-6} \quad .$$

This tension error affects the absolute value of the gravity-gradient measurement but will not interfere with measuring the variations in the gravity gradient due to gravity anomalies.

If the ballast is distributed along the wire, the effect of drag is different. Suppose, for example, that the ballast consists of N equal masses distributed uniformly along the wire. Let us assume that the area-to-mass ratio of each section is designed to be uniform, so that the ballast masses stay in a straight configuration. Near the center of the system, the tension will be half as great as the tension produced by the same total mass concentrated at the ends of the wire. Compared to the system with two end masses, the tension due to the gravity gradient with N masses is $T_G/2$ and the tension due to drag is T_D/N for a wire section in the middle. The fractional tension error becomes

$$\frac{\Delta T}{T} = \frac{1}{2}\left(\frac{T_D/N}{T_G/2}\right)^2 = \frac{2}{N^2}\left(\frac{T_D}{T_G}\right)^2 \quad .$$

The effect of drag on the total tension can be reduced by $4/N^2$ with this technique.

3.4.3 Normal modes of transverse wire oscillations

This section reviews the analytical expressions for the transverse oscillation modes of a string fixed at both ends. The formulas can be used to calculate the frequencies of the normal oscillation modes. The frequency of the fundamental mode calculated analytically is compared to the frequency of the lumped-mass approximation used in the Skyhook dynamic simulation computer program.

In a system consisting of a long wire with heavy end masses, the normal modes for transverse wire oscillations are given by (Morse, 1948)

$$y = A_n \sin\left(\frac{\pi n x}{\ell}\right) \cos\left(\frac{\pi n c}{\ell} t\right) \quad ,$$

where A_n is amplitude of the n^{th} mode and n is a positive integer. The velocity of wave propagation c is $\sqrt{T/\varepsilon}$, where T is the tension and ε is the mass per unit length of the wire. The frequency of the transverse oscillation is

$$\omega = \frac{\pi n c}{\ell} = \frac{\pi n}{\ell}\sqrt{\frac{T}{\varepsilon}} \quad . \tag{19}$$

In the Skyhook dynamic simulation computer program, the wire is represented by discrete masses having the lumped properties of the section of the wire that they represent. If the wire is divided into N sections, each of the N - 1 masses representing a section of the wire has 1/N of the total mass and total cross section of the wire. A single point halfway between the ends is used to represent the properties of the wire (see Figure 13). If the mass m is displaced from its equilibrium position by a distance x, the restoring force is (reversing the sign in equation (14)),

$$-\frac{4Tx}{\ell} \quad .$$

The equation of motion of the mass is

$$m\ddot{x} = -\frac{4Tx}{\ell} \quad ,$$

and the frequency of the transverse oscillation of m is

$$\omega = \sqrt{\frac{4T}{m\ell}} = 2\sqrt{\frac{T}{m\ell}} \quad . \tag{20}$$

By convention, the Skyhook program computes the mass m by the formula

$$m = \frac{\ell\varepsilon}{2} \quad .$$

Substituting this into equation (20) gives

$$\omega = 2\sqrt{\frac{2T}{\ell\varepsilon\ell}} = \frac{2\sqrt{2}}{\ell}\sqrt{\frac{T}{\varepsilon}} = \frac{2.828}{\ell}\sqrt{\frac{T}{\varepsilon}} \quad .$$

This value is 0.9 times the frequency of the fundamental frequency computed from equation (19), which has a factor of π. The agreement is sufficient for the purpose of system noise analysis.

3.4.4 Resonant excitation of higher modes of transverse wire oscillations

Transverse oscillations of the Dumbbell wire can exist initially as a result of deployment or can develop during the course of the system lifetime as a result of drag-force variations on the wire. These oscillations can be controlled by the use of dampers on the wire. The frequencies of the normal modes given in Section 3.4.3 are proportional to the integers. If the frequency of the drag-force variation is the same as that of the fundamental period or any of the higher harmonics, there will be a resonant excitation of transverse wire oscillations. In the absence of dampers on the wire, the amplitude of the oscillations and the resulting tension variations will increase with time as long as the force variations are applied. Because the drag force decreases with altitude, higher harmonics can be excited by drag variations since the force on the lower part of the wire is greater than that on the upper part.

Simulations have been done to see the rate at which higher harmonics are excited by drag. For example, when the periods of the first three harmonics are 320, 160, and 106 sec and the drag varies with a 160-sec period, a drag variation of 10% at 220 km produces a tension variation of ±20 dynes in two cycles. The total tension is 372,000 dynes. At 106 sec, a tension noise of ±20 dynes is reached in three cycles. The excitation of transverse modes other than the fundamental can be minimized by changing the mass-to-area ratio along the wire to match the decrease in atmospheric density with altitude. In this way, the wire receives a nearly uniform acceleration at each point, but since the scale height varies with altitude, the correction is only approximate. In the case of a wire with heavy masses at each end, we cannot prevent the excitation of the fundamental transverse mode, although the frequency can be designed to be outside the bandwidth of interest, which is roughly between 20 and 100 sec.

3.4.5 Tension noise due to drag-force variations

Computer simulations have been used to study the tension noise resulting from drag excitation of the fundamental transverse oscillation mode of a wire connecting two heavy end masses. The atmospheric density is assumed to vary with time according to the expression

$$\rho_a = \rho_0(A_0 + A_1 \sin \frac{2\pi t}{P}) \quad ,$$

where ρ_a is the density as a function of time, ρ_0 is the mean value of the density, A_0 is a constant, A_1 is the fractional variation, and P is the period of the variations. If the Dumbbell system begins with the wire straight, atmospheric drag forces the wire back and an oscillation is set up whose frequency is that of the fundamental transverse mode.

Figures 14, 15, and 16 show the results of a simulation using a wire 2 km long and 2 mm thick, with a density of 1.5 g/cc; masses of 2 metric tons each are at the ends of the wire, which is orbiting at 220-km altitude. The

TIME (sec)	TENSION (dynes)
0.0000000	833010.607000
2.0000000	833021.073000
4.0000000	833058.430000
6.0000000	833138.172000
8.0000000	833246.291000
10.0000000	833376.800000
12.0000000	833491.401000
14.0000000	833613.418000
16.0000000	833706.951000
18.0000000	833791.714000
20.0000000	833864.695000
22.0000000	833928.423000
24.0000000	833967.894000
26.0000000	833951.935000
28.0000000	833869.314000
30.0000000	833705.402000
32.0000000	833451.762000
34.0000000	833156.511000
36.0000000	832851.387000
38.0000000	832584.264000
40.0000000	832373.597000
42.0000000	832211.625000
44.0000000	832072.777000
46.0000000	831927.004000
48.0000000	831754.412000
50.0000000	831565.668000
52.0000000	831392.731000
54.0000000	831286.906000
56.0000000	831297.147000
58.0000000	831429.843000
60.0000000	831674.556000
62.0000000	831982.014000
64.0000000	832300.379000
66.0000000	832572.795000
68.0000000	832796.247000
70.0000000	832970.850000
72.0000000	833127.860000
74.0000000	833289.940000
76.0000000	833473.060000
78.0000000	833664.297000
80.0000000	833834.840000
82.0000000	833948.276000
84.0000000	833989.476000
86.0000000	833950.650000
88.0000000	833849.334000
90.0000000	833714.902000
92.0000000	833572.552000
94.0000000	833439.764000
96.0000000	833320.618000
98.0000000	833217.114000
100.0000000	833124.943000
102.0000000	833046.015000
104.0000000	832991.091000
106.0000000	832973.619000
108.0000000	832995.096000
110.0000000	833054.675000
112.0000000	833144.410000

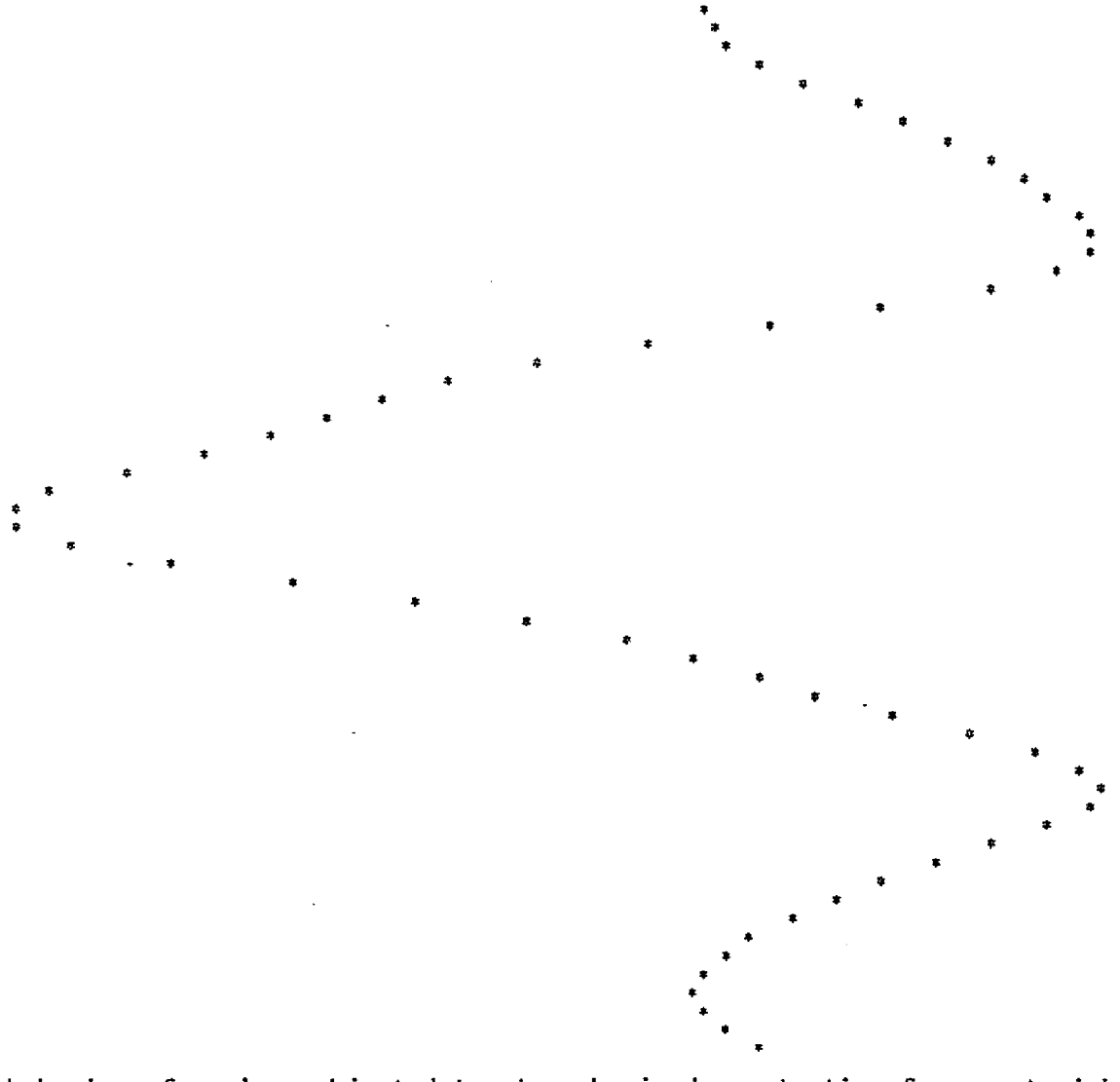

Figure 14. Transient behavior of a wire subjected to atmospheric drag starting from a straight configuration. Wire tension (dynes) versus time (sec).

TIME (sec)	IN-PLANE DISPLACEMENT (cm)
0.0000000	0.000000
2.0000000	0.746101
4.0000000	4.027926
6.0000000	8.863609
8.0000000	12.206401
10.0000000	18.909707
12.0000000	26.814639
14.0000000	35.719756
16.0000000	45.447512
18.0000000	55.860527
20.0000000	66.862498
22.0000000	78.381264
24.0000000	90.336292
26.0000000	102.610211
28.0000000	115.029395
30.0000000	127.366556
32.0000000	139.464581
34.0000000	150.770710
36.0000000	161.373344
38.0000000	171.023129
40.0000000	179.636122
42.0000000	187.174191
44.0000000	193.614813
46.0000000	198.919035
48.0000000	203.012323
50.0000000	205.785979
52.0000000	207.118616
54.0000000	206.908640
56.0000000	205.107846
58.0000000	201.741916
60.0000000	196.909260
62.0000000	190.760943
64.0000000	183.465656
66.0000000	175.177355
68.0000000	166.012260
70.0000000	156.048076
72.0000000	145.341729
74.0000000	133.961480
76.0000000	122.016288
78.0000000	109.674933
80.0000000	97.163173
82.0000000	84.741508
84.0000000	72.668596
86.0000000	61.167122
88.0000000	50.400083
90.0000000	40.468687
92.0000000	31.430435
94.0000000	23.329856
96.0000000	16.230655
98.0000000	10.233252
100.0000000	5.474048
102.0000000	2.103772
104.0000000	0.253846
106.0000000	0.001641
108.0000000	1.351117
110.0000000	4.231534
112.0000000	8.519280

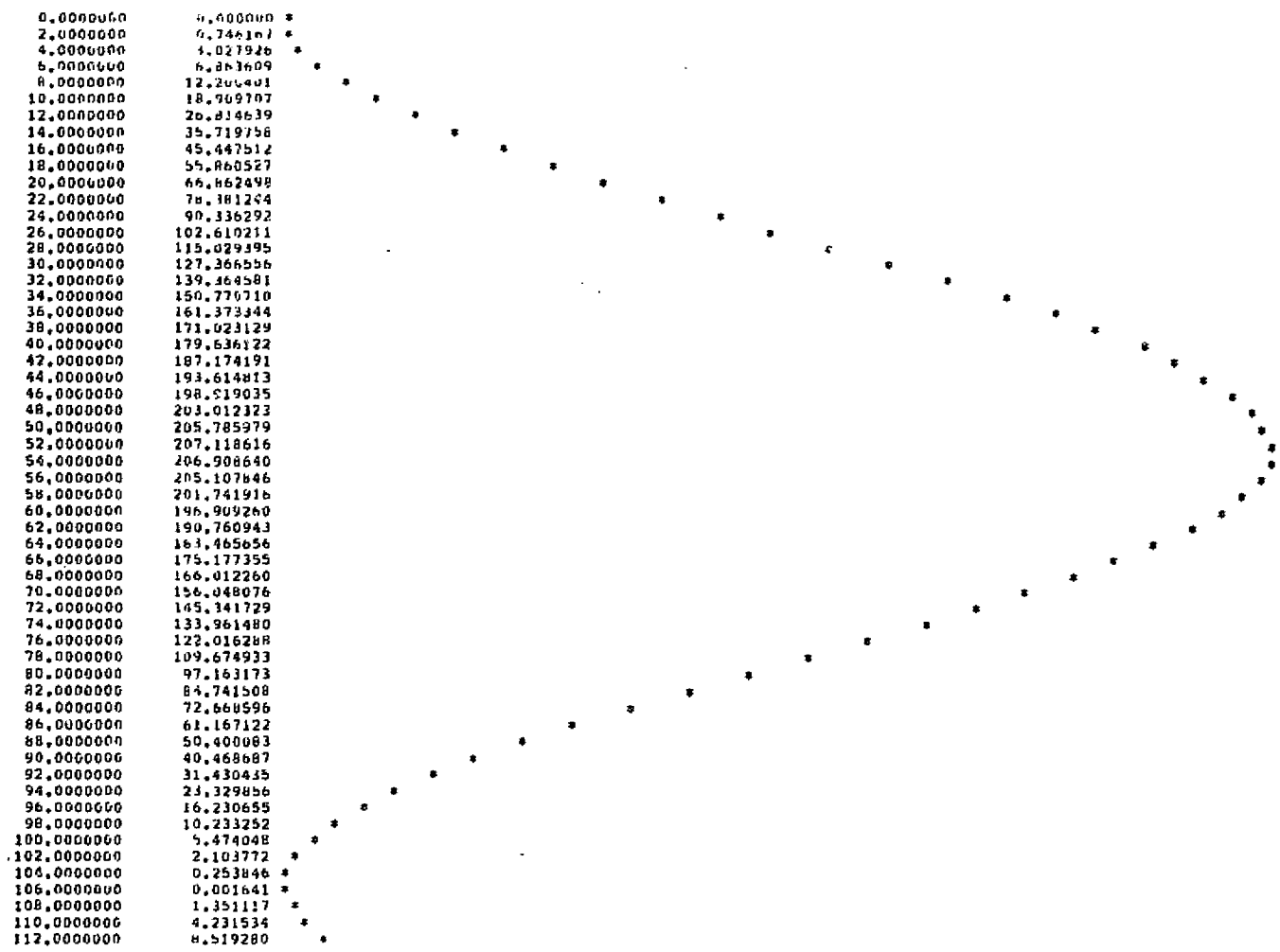

Figure 15. Transient behavior of a wire subjected to atmospheric drag starting from a straight configuration. In-plane displacement (cm) of the center mass point representing the wire versus time (sec).

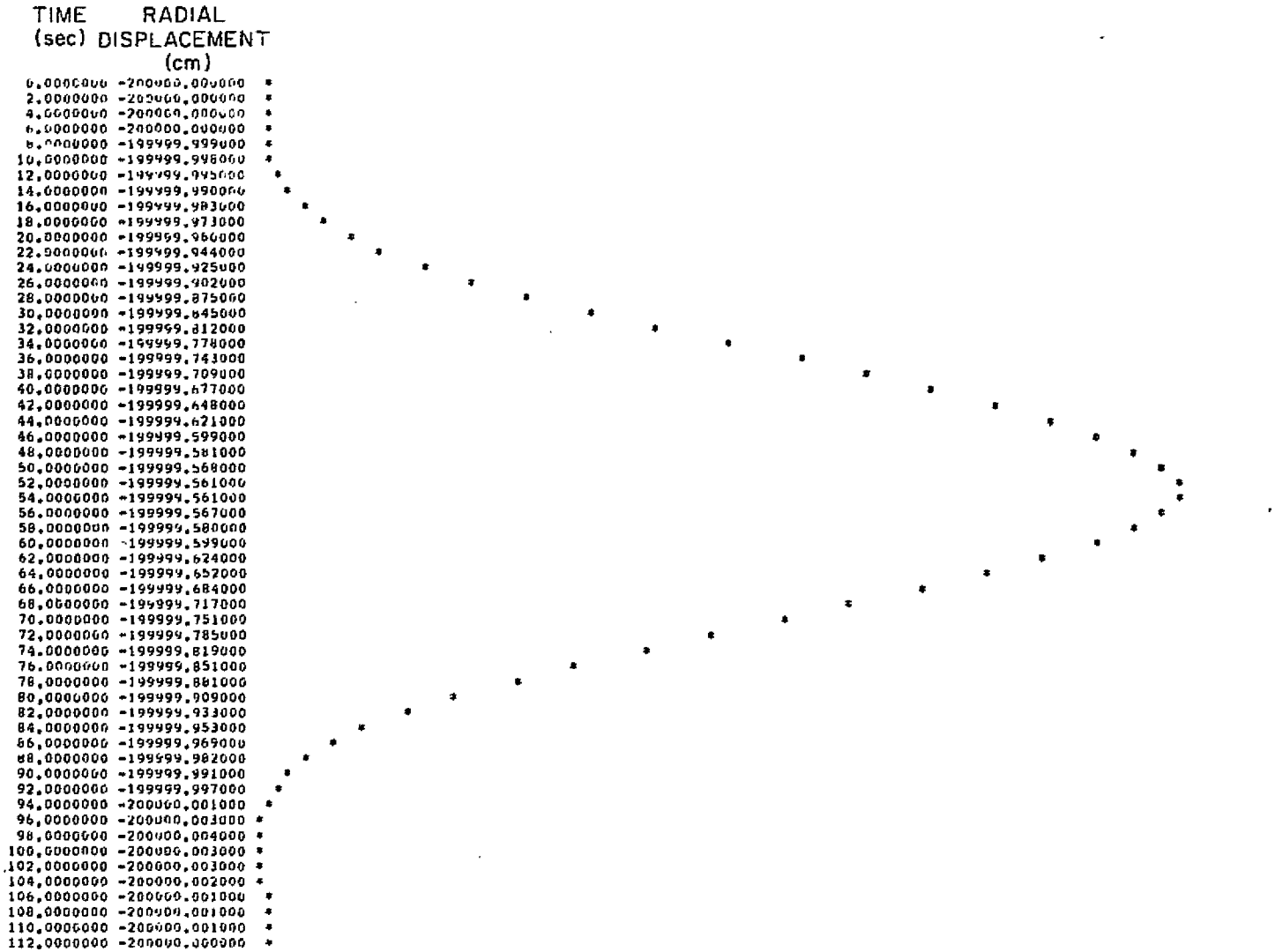

Figure 16. Transient behavior of a wire subjected to atmospheric drag starting from a straight configuration. Vertical position (cm) of the bottom mass with respect to the top versus time (sec).

middle of the wire moves back 207 cm in 53 sec and returns to the straight position in 105 sec. The displacement of the center of the wire causes the end masses to be pulled back and forth, resulting in tension variations. The equilibrium tension is 833,000 dynes, and the variations in tension are +957 and -1724 dynes. A 20-sec 10% atmospheric density fluctuation was also included in the run, but its effect is not visible on the plot compared with the large tension variation due to the transient behavior of the system.

Some runs were done with the wire straight and with only the variable part of the drag included ($A_0 = 0$). For P = 20 sec, the tension noise is negligible. For P = 105 sec (the fundamental frequency), the tension noise increases with t and reaches ±200 dynes, out of a total of 833,000 dynes, in 200 sec. Resonant excitation of the fundamental frequency can be prevented by having a damper on the wire. However, the excitation within one cycle would still be substantial.

The resonant frequency of 105 sec for this case is very close to the bandwidth of interest (approximately 20 to 100 sec, which corresponds to horizontal wavelengths of 150 to 770 km along the ground). The fundamental period can be lengthened by increasing the mass of the wire and thereby moving the frequency away from the bandwidth of interest. Runs done with the wire density set to 6 g/cc and the wire diameter increased to 4 mm do not show resonant excitation for P = 100 sec. The low noise for P = 20 sec, unfortunately, is not representative of the actual system noise to be expected, because only the variation of the drag was included. When the wire is straight, slight motions of the wire back and forth do not produce significant motion in the end masses, because the distance between the ends of the wire changes as the cosine of the angle of the bending of the wire.

To be able to see the effect of atmospheric density variations in the presence of transient wire oscillations, pairs of runs were done with and without the drag variations. Subtracting the tension in the baseline run from the tension with the drag variations included makes it possible to see the effect of the variations. With a 1-km wire, 5 mm thick, having an

average density of 5 g/cc and 2-ton masses at either end, the noise due to atmospheric density fluctuations increases as the drag bows the wire back (see Figures 17 and 18). The tension noise becomes about ±20 dynes when the wire displacement has reached 125 cm, at about 80 or 90 sec into the run. The noise is about the same for 20-sec and 50-sec drag variations, and the total tension is 416,000 dynes.

Additional runs were done with the wire initially displaced to the approximate equilibrium position (125 cm) to eliminate most of the transient motion (see Figure 19). Drag fluctuations with P = 20 and 100 sec show a nearly constant tension noise of about ±23 dynes.

All the runs described above involved integrating the motion of three masses, two at the ends of the wire representing the ballast masses and one half-way between the ends representing the lumped properties of the wire. A pair of runs with four points representing the wire and two end masses gave essentially the same results for the tension noise due to drag-force variations.

If the area-to-mass ratio for each point whose motion is being integrated is the same, drag-force variations will have no effect. A pair of runs was done integrating the motion of six 700-kg masses having a cross section of 1 m^2. The length of the system was 1 km and the tensions between the pieces were 145749, 233194, 262338, 233185, and 145737 dynes. There was no observable tension noise resulting from a 20-sec 10% atmospheric drag variation.

3.4.6 Approximate analytical solution for drag-force tension noise

In a Dumbbell system consisting of a long wire with two heavy end masses, tension noise will result from drag-force variations. The particular case shown in Figures 14 through 18 indicates that the tension noise is above the sensitivity required for the system. In order to study the dependence of the tension noise on the orbital, atmospheric, and system design parameters, an approximate analytical expression has been derived that is valid in the

TIME (sec)	TENSION DIFFERENCE (dynes)
0.0000000	0.000000
2.0000000	-0.127000
4.0000000	-0.353000
6.0000000	-0.459000
8.0000000	-0.717000
10.0000000	-0.220000
12.0000000	-0.327000
14.0000000	-0.395000
16.0000000	-0.573000
18.0000000	-0.339000
20.0000000	0.398000
22.0000000	1.427000
24.0000000	2.554000
26.0000000	3.344000
28.0000000	3.207000
30.0000000	1.772000
32.0000000	-0.437000
34.0000000	-2.612000
36.0000000	-3.817000
38.0000000	-2.960000
40.0000000	-0.110000
42.0000000	3.746000
44.0000000	7.304000
46.0000000	8.888000
48.0000000	7.289000
50.0000000	2.812000
52.0000000	-3.188000
54.0000000	-8.376000
56.0000000	-10.354000
58.0000000	-7.886000
60.0000000	-1.616000
62.0000000	6.687000
64.0000000	13.043000
66.0000000	14.907000
68.0000000	11.098000
70.0000000	2.328000
72.0000000	-8.353000
74.0000000	-16.927000
76.0000000	-19.394000
78.0000000	-14.471000
80.0000000	-3.573000
82.0000000	9.411000
84.0000000	19.184000
86.0000000	21.533000
88.0000000	14.933000
90.0000000	1.102000
92.0000000	-14.653000
94.0000000	-26.335000
96.0000000	-28.898000
98.0000000	-21.107000

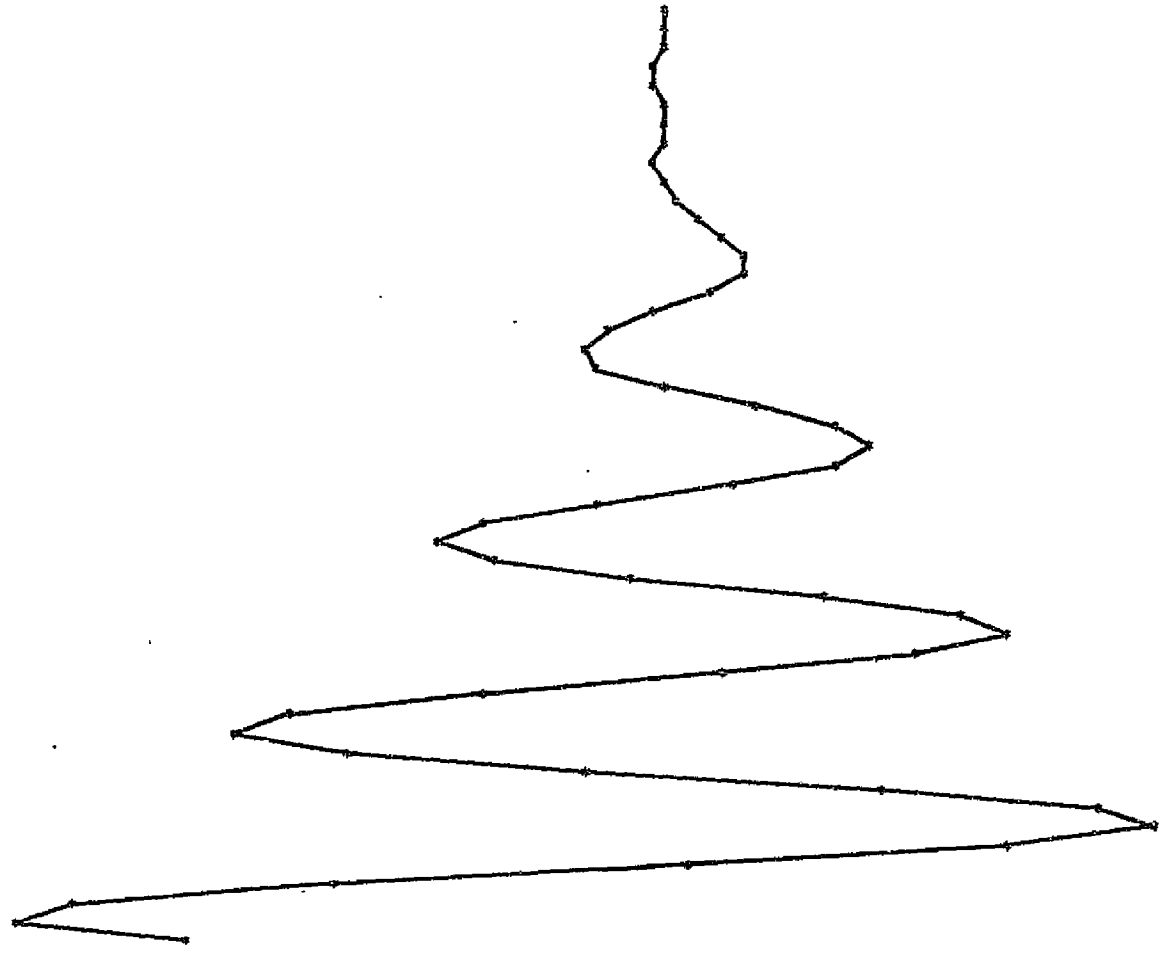

Figure 17. Effect of wire curvature on tension noise arising from atmospheric granularity. Difference between tension with a 20-sec period atmospheric density fluctuation and tension for a baseline run with no density fluctuation. Time is in sec, and tension difference is in dynes.

TIME (sec)	IN-PLANE DISPLACEMENT (cm)
0.0000000	0.000000
2.0000000	0.085715
4.0000000	0.342748
6.0000000	0.770750
8.0000000	1.369137
10.0000000	2.137091
12.0000000	3.073561
14.0000000	4.177267
16.0000000	5.446696
18.0000000	6.880110
20.0000000	8.475543
22.0000000	10.230810
24.0000000	12.143504
26.0000000	14.211002
28.0000000	16.430469
30.0000000	18.798861
32.0000000	21.312931
34.0000000	23.969228
36.0000000	26.764109
38.0000000	29.693741
40.0000000	32.754102
42.0000000	35.940994
44.0000000	39.250044
46.0000000	42.676711
48.0000000	46.216292
50.0000000	49.863938
52.0000000	53.614619
54.0000000	57.463211
56.0000000	61.404424
58.0000000	65.432849
60.0000000	69.542957
62.0000000	73.729108
64.0000000	77.985555
66.0000000	82.306458
68.0000000	86.685886
70.0000000	91.117830
72.0000000	95.596208
74.0000000	100.114875
76.0000000	104.667633
78.0000000	109.248233
80.0000000	113.850394
82.0000000	118.467801
84.0000000	123.094124
86.0000000	127.723016
88.0000000	132.348132
90.0000000	136.963131
92.0000000	141.561686
94.0000000	146.137495
96.0000000	150.684287
98.0000000	155.195834
100.0000000	159.665956
102.0000000	164.088530
104.0000000	168.457501
106.0000000	172.766888
108.0000000	177.010793
110.0000000	181.183408
112.0000000	185.279027
114.0000000	189.292047
116.0000000	193.216981

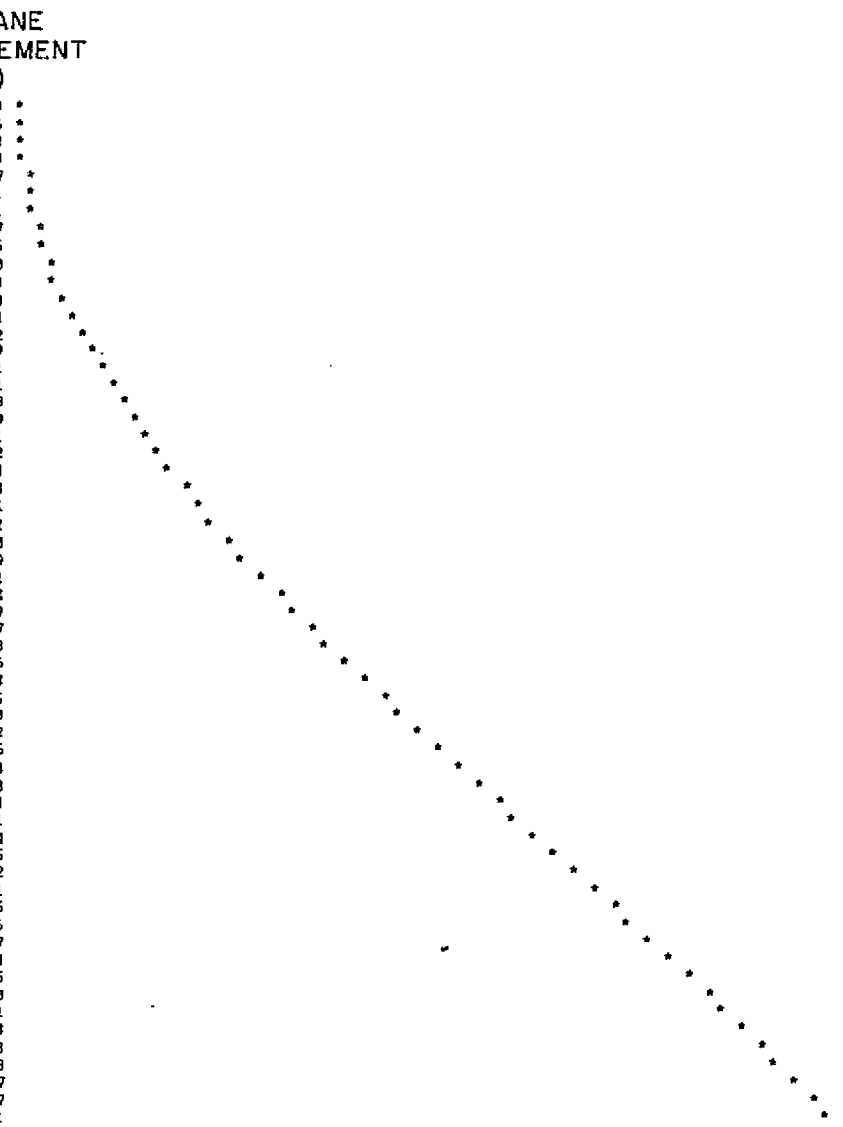

Figure 18. Effect of wire curvature on tension noise arising from atmospheric granularity. In-plane displacement (cm) of the center mass representing the wire versus time (sec).

TIME (sec)	TENSION DIFFERENCE (dynes)
0.0000000	0.000000
2.0000000	11.598000
4.0000000	20.501000
6.0000000	20.701000
8.0000000	12.479000
10.0000000	-1.013000
12.0000000	-14.457000
14.0000000	-22.797000
16.0000000	-22.784000
18.0000000	-14.461000
20.0000000	-1.032000
22.0000000	12.284000
24.0000000	20.453000
26.0000000	20.345000
28.0000000	12.063000
30.0000000	-1.328000
32.0000000	-14.896000
34.0000000	-23.083000
36.0000000	-23.102000
38.0000000	-14.778000
40.0000000	-1.333000
42.0000000	12.688000
44.0000000	20.304000
46.0000000	20.248000
48.0000000	12.103000
50.0000000	-1.462000
52.0000000	-14.875000
54.0000000	-23.221000
56.0000000	-23.173000
58.0000000	-14.893000
60.0000000	-1.276000
62.0000000	12.590000
64.0000000	20.512000
66.0000000	20.366000
68.0000000	11.974000
70.0000000	-1.363000
72.0000000	-14.886000
74.0000000	-23.223000
76.0000000	-23.026000
78.0000000	-14.710000
80.0000000	-1.304000
82.0000000	12.214000
84.0000000	20.451000
86.0000000	20.471000
88.0000000	12.237000
90.0000000	-1.171000
92.0000000	-14.679000
94.0000000	-22.750000
96.0000000	-22.868000
98.0000000	-14.450000

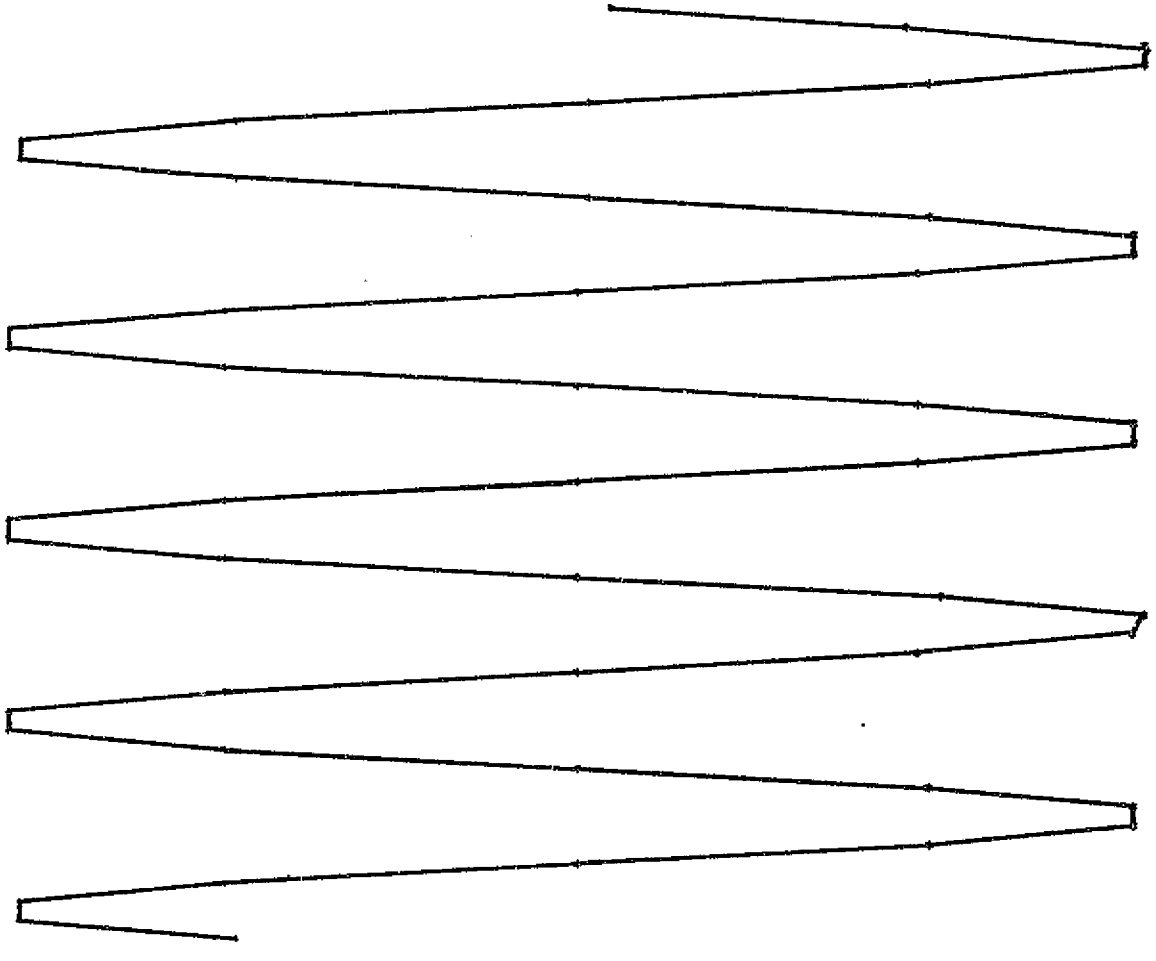

Figure 19. Difference between tension with a 20-sec period atmospheric density fluctuation and a baseline run with no density fluctuation. The center mass representing the wire has a nearly constant in-plane displacement of 125 cm.

wavelength range of the gravity anomalies to be measured. This expression can be used to determine a set of parameters that will achieve the required noise level.

Because the area-to-mass ratio of the wire is large compared to that of the end masses, atmospheric drag forces the Dumbbell wire into a bowed configuration. If the drag force varies, the amount of bowing fluctuates about the equilibrium configuration. If the period of the fundamental transverse oscillation of the wire is designed to be long compared to the period of the gravity-gradient signals of interest, then drag fluctuations within the bandwidth of the system will excite transverse oscillations at a frequency well below the resonant frequency. In this situation, the actual displacement of the wire will be small compared to that required to establish equilibrium between the drag force and the restoring force resulting from curvature in the wire. The movement of the wire is that due to inertial acceleration by the drag-force variations. As the wire oscillates, the distance between the ends of the wire changes, since the curvature of the wire is changing, and the end masses are displaced back and forth.

If the end masses undergo a periodic acceleration of amplitude $\Delta\ddot{y}$, the force causing that oscillation is of amplitude $M\,\Delta\ddot{y}$, where M is the mass of the ballast. This force is the tension noise resulting from drag-force variations. We assume that the response time of the end masses is fast compared to the frequency of the drag variations, so the masses move with the wire. If the wire changes its length or configuration at a frequency faster than the risetime of the system, the tension change will be that due to elastic stretching of the wire, since the end masses do not have time to respond and remain essentially stationary.

In equilibrium, the drag force displaces the mass m, representing the lumped properties of the wire (see Figure 13), by the distance x, given in equation (15). If the force changes by an amount ΔF, the mass m will be accelerated from its equilibrium position and the mass M will undergo an acceleration $\ddot{y}$, where

$$\ddot{y} = \ddot{x}\,\frac{x}{\ell/2} = \frac{2\ddot{x}x}{\ell} \quad .$$

Similarly, the velocity $\dot{y}$ of mass M is $\dot{y} = 2\dot{x}x/\ell$.

For typical parameters, the work done by the drag variation ΔF goes almost entirely into the kinetic energy of m, and thus we can neglect M in the equation of motion. For example, if the velocity of m is $\dot{x}$, and $x = 125$ cm, $\ell = 10^5$ cm, $m = 50 \times 10^3$ g, and $M = 2 \times 10^6$ g, the ratio of the kinetic energy of the mass M to that of m is

$$\frac{(1/2)M(2\dot{x}x/\ell)^2}{(1/2)m\dot{x}^2} = \frac{4M(x/\ell)^2}{m} = 2.5 \times 10^{-4} \quad .$$

Therefore, the equation of motion of the system due to force ΔF is approximately

$$\Delta F = m\ddot{x} \quad .$$

The acceleration of m is $\Delta F/m$, and the acceleration of M is $\ddot{y} = 2\Delta F\, x/m\ell$. The tension noise is

$$\Delta T = M\ddot{y} = \frac{2M\ \Delta F\ x}{m\ell} \quad , \tag{21}$$

and the relative tension noise is

$$\frac{\Delta T}{T} = \frac{2M\ \Delta F\ x}{m\ell T} \quad .$$

To see how the relative noise depends on the design parameters of the system, we can rewrite equation (21) as follows. Using $x = F\ell/4T$, from equation (15), and setting $\Delta F = \alpha F$, where α is the fractional variation of the drag force, we get

$$\frac{\Delta T}{T} = \frac{2M\alpha F F\ell}{4TmlT} = \frac{\alpha MF^2}{2mT^2} \quad . \tag{22}$$

If the density of the wire is ρ_w, the mass m of half the wire is $m = \pi r^2 \rho_w \ell/2$. The tension in the wire given by equation (5), is

$$T = \frac{3GMm}{a^3}\frac{\ell}{2} \quad . \tag{23}$$

The velocity v for a circular orbit of radius a is

$$v = \sqrt{GM/a} \quad ,$$

so the expression for the drag force in equation (16) becomes

$$F = r\rho_a \frac{GM}{a}\ell \quad . \tag{24}$$

Substituting these expressions into equation (22), we have

$$\frac{\Delta T}{T} = \frac{\alpha M r^2 \rho_a^2 (GM/a)^2 \ell^2}{2\pi r^2 \rho_w (\ell/2)(3GMm\ell/2a^3)^2} = \frac{4\alpha\rho_a^2 a^4}{9\pi\rho_w M\ell} \tag{25}$$

The analytical derivation above can be compared with the results obtained by numerical integration in Section 3.4.5. The simulation of Figure 19 was run with T = 416,400 dynes, M = 2×10^6 g, x = 125 cm, m = 49×10^3 g, and $\ell = 10^5$ cm, with a 5-mm-diameter wire of average density 5 g/cc at an orbital altitude of 220 km. The drag force of 2130 dynes was varied by 10%, giving ΔF = 213 dynes. Using equation (21), we get $\Delta T = 2M\,\Delta F\, x/m\ell$ = 21.7 dynes which agrees approximately with the tension noise of 23 dynes in Figure 19.

From equation (25), we see that the noise can be reduced to an acceptable level by some combination of increasing ρ_w, ℓ, or M or by going to an altitude where ρ_a is sufficiently reduced. The dependence of noise on a^4 results from the decrease in wire tension as the radius of the orbit increases.

Since ρ_a decreases with altitude much more rapidly than the factor a^4, the tension noise can be significantly reduced by going to a higher altitude. The factor α probably depends on altitude also, so α and ρ_a^2 should be evaluated together.

3.4.7 Drag-force noise with a small number of ballast masses

In Section 3.4.2, we considered what effect adding ballast masses along the wire would have on the change in total tension resulting from atmospheric drag on the wire. Here, we consider the effect of ballast masses on the tension noise arising from short-period drag-force variations.

The expression derived below is an approximate solution for the case where the frequency of the drag-force variations is fast compared to the natural frequency of the transverse wire oscillations but slow compared to the risetime of the system determined by the natural frequency for longitudinal oscillations. For simplicity, we assume that the ballast masses are heavy enough to create nodes in the wire but not heavy enough to increase the tension significantly, which we assume to be constant.

In equilibrium, the drag force F on each section of wire equals the horizontal components of the tension vectors, so we have, from Figure 20,

$$F = 2T \frac{x}{\ell/2N} = \frac{4TxN}{\ell} \quad . \tag{26}$$

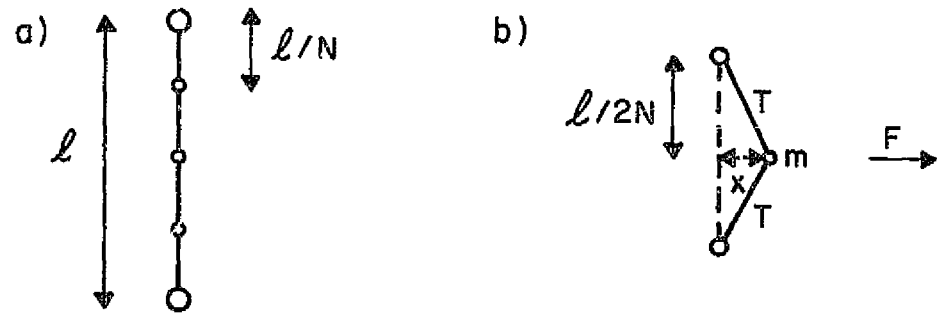

Figure 20. Dumbbell wire with a small number of ballast masses. a) System configuration. b) Equilibrium displacement of a section of the wire.

If a force $\Delta F = \alpha F$ is applied, the equation of motion of the mass m is

$$\alpha F = m\ddot{x} \quad . \tag{27}$$

The acceleration $\ddot{x}$ will cause an acceleration in the vertical direction at each end of the section of wire, given by

$$\ddot{y}_N = \ddot{x}\,\frac{x}{\ell/2N} = \frac{2Nx\ddot{x}}{\ell} \quad .$$

Since the center of the whole system remains fixed, the acceleration produced on the end mass is

$$\ddot{y} = N\ddot{y}_N = \frac{2N^2 x\ddot{x}}{\ell} \quad , \tag{28}$$

and the tension noise produced is $\Delta T = M\ddot{y}$. The relative tension noise is

$$\frac{\Delta T}{T} = \frac{M\ddot{y}}{T} \quad .$$

To see the dependence on the basic parameters of the system, we must substitute the expressions $\ddot{y}$ and T. Solving equations (26) and (27) for x and $\ddot{x}$, we have

$$x = \frac{F\ell}{4TN} \quad , \tag{29a}$$

$$\ddot{x} = \frac{\alpha F}{m} \quad , \tag{29b}$$

which can be substituted into equation (28) to give

$$\ddot{y} = 2N^2\,\frac{F\ell}{4TN}\,\frac{\alpha F}{m\ell} = \frac{\alpha N F^2}{2Tm} \quad ,$$

so that

$$\frac{\Delta T}{T} = \frac{\alpha M N F^2}{2T^2 m} \quad .$$

Since F is the total drag force F_T divided by N and m is the total wire mass m_T divided by N, we have

$$\frac{\Delta T}{T} = \frac{\alpha M N F_T^2/N^2}{2T^2 m_T/N} = \frac{\alpha M F_T^2}{2T^2 m_T} \quad . \tag{30}$$

This is exactly the same expression as equation (22), which was obtained for the tension noise without ballast masses on the wire. Therefore, the noise is independent of the number of ballast masses in this approximation and is given by equation (25),

$$\frac{\Delta T}{T} = \frac{4\alpha \rho_a^2 a^4}{9\pi \rho_w M \ell} \quad .$$

A simulation has been run with a mass of 10^6 g at the center of the wire, so that N = 2. The other parameters are the same as those in Section 3.4.6 with two end masses, namely, M = 2×10^6 g, x = 125 cm, $\ell = 10^5$ cm, and T = 416,400 dynes. The mass m of each wire segment is 24.5×10^3 g and the tension noise is about ±22.5 dynes, as in the case with no ballast in the center of the wire. Since the factor N cancels in equation (30), the effect of short-period drag variations cannot be reduced by adding ballast masses along the wire. This result holds in the frequency range where the drag variations are faster than the natural frequency for the transverse oscillation of each section of wire. In this bandwidth, the effect of drag fluctuations is inertial acceleration of the wire mass, and the wire does not have time to assume an equilibrium configuration.

3.4.8 Drag-force noise with a large number of ballast masses

At the end of Section 3.4.2, we noted that dividing the wire into N equal sections reduced the effect of drag on the equilibrium wire tension, but in Section 3.4.7, we found that adding ballast masses did not reduce the effect of short-period drag fluctuations. The difference in these results arises from the fact that the first case is an equilibrium condition while the second is a dynamic situation. Let us now consider the case where the wire segments are made sufficiently short that their response time is fast enough for them to stay approximately in equilibrium with the drag fluctuations. We wish to see how the tension noise depends on the number of ballast masses as a means of reducing drag noise.

An approximate analytical solution is derived for the tension noise when a large number of ballast masses are distributed along the wire, as shows in Figure 21. Considered as a continuum, the distributed ballast gives

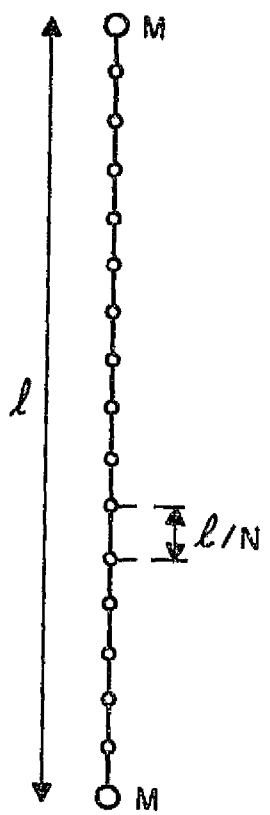

Figure 21. Dumbbell wire with a large number of ballast masses.

the wire as a whole a high effective mass-to-area ratio and lengthens the period for transverse wire oscillations. The tension noise from drag-force variations in such a system would result from oscillations of the short sections of wire between the ballast masses. We assume that the ballast masses are heavy compared to the connecting pieces of wire, thus creating nodes that are nearly stationary. The tension in each section of wire will be at least as large as that produced by the end masses M. If the total mass of the lumps is comparable to the mass M, the tension can be significantly increased, especially at the middle of the wire. For simplicity in the present calculation, we assume a constant tension equal to that produced by the masses at the ends.

The short sections of wire of length ℓ/N are displaced by a distance x, as shown in Figure 20 b, by the drag force F. In equilibrium, the drag force is given by equation (26). With a large number of ballast masses, the period of the fundamental transverse wire oscillation will be short. If we assume that the period of the driving force is long compared to the natural period of the oscillations, the wire will have time to move to a new position that is nearly in equilibrium with the instantaneous value of the drag force. Oscillations at the natural frequency are assumed to be at a high frequency outside the bandwidth of interest, and they can be minimized by damping.

Under these conditions, if a force ΔF is applied to the wire, the additional displacement of the wire is obtained by replacing F and x with ΔF and Δx in equation (26) and solving for Δx to obtain

$$\Delta x = \frac{\ell \, \Delta F}{4TN} \quad . \tag{31}$$

From Figure 20, we see that the distance between the ends of the section of wire will be decreased by

$$\Delta y_N = 2\Delta x \, \frac{x}{(\ell/2N)} = \frac{4Nx \, \Delta x}{\ell} \quad .$$

This assumes that the risetime of the system for longitudinal motion is fast compared to the period of the drag-force variations, so that the system has time to respond. Since there are N equal sections, the length of the whole system will decrease by N Δy, and each end mass will be displaced by a distance

$$\Delta y = \frac{1}{2} N \Delta y_N = \frac{2N^2 x \Delta x}{\ell} \quad . \tag{32}$$

If the end masses oscillate with an amplitude Δy and frequency ω, the tension noise according to equation (9) will be

$$\Delta T = \Delta F = M\omega^2 \Delta y \quad . \tag{33}$$

We can express Δy in terms of the basic system parameters to see the dependence of the noise on the choice of parameters. If we set $\Delta F = \alpha F$ in equation (31) to obtain

$$\Delta x = \frac{\ell \alpha F}{4TN}$$

and substitute this plus equation (29a) into equation (32), we have

$$\Delta y = \frac{2N^2 \alpha (\ell F/4TN)^2}{\ell} = \frac{\alpha \ell F^2}{8T^2} \quad . \tag{34}$$

The drag force F on each section is obtained by dividing equation (24) by N:

$$F = \frac{r\rho_a (GM/a)\ell}{N} \quad . \tag{35}$$

The fractional tension noise, given by dividing equation (33) by T and substituting equation (34) for Δy, is

$$\frac{\Delta T}{T} = \frac{M\omega^2 \Delta y}{T} = \frac{M\omega^2 \alpha \ell F^2}{8T^3} \quad . \tag{36}$$

Substituting equation (23) for T and equation (35) for F gives

$$\frac{\Delta T}{T} = \frac{M\omega^2 \alpha \ell r^2 \rho_a^2 (GM/a)^2 \ell^2 / N^2}{8(3GM\ell/2a^3)^3} = \frac{\omega^2 \alpha r^2 \rho_a^2 a^7}{27GMM^2N^2} \quad . \tag{37}$$

For example, if we take $\omega = 0.314$ (20-sec period), $\alpha = 0.1$, $r = 0.25$ cm, $\rho_a = 1.6 \times 10^{-13}$ g/cc, $a = 6.598 \times 10^8$ cm (220-km altitude), $M = 2 \times 10^6$ g, $N = 100$, and $GM = 3.986 \times 10^{20}$ (cgs), we have $\Delta T/T = 2 \times 10^{-6}$, which is an acceptable noise level.

Equation (37) is valid only when the transverse frequency of the wire segments is faster than the frequency of the drag variations. The frequency of the transverse oscillations of each wire is proportional to N. We can show this, starting from equation (19) and setting n = 1 to give the frequency of the fundamental, which is

$$\omega = \frac{\pi}{\ell}\sqrt{\frac{T}{\epsilon}} \quad .$$

If the wire is split up into N sections by ballast masses so that the length of each section is ℓ/N, the frequency as a function of N becomes

$$\omega_N = \frac{N\pi}{\ell}\sqrt{\frac{T}{\epsilon}} \quad .$$

Equation (37) for $\Delta T/T$ contains the factor ω^2, which indicates that the tension noise rises sharply with the frequency of the drag-force fluctuations. If the driving frequency ω becomes greater than the longitudinal risetime of the system, the assumption that the end masses move with the wire breaks down. The tension noise in this case results from elastic stretching of the wire. The spring constant for half the wire is

$$k = \frac{EA_0}{\ell/2} = \frac{2EA_0}{\ell} \quad ,$$

where $A_0 = \pi r_0^2$ and r_0 is the radius of the core. The tension noise is $\Delta T = k\,\Delta y$, where Δy is the stretching of half the wire, and the fractional tension noise is

$$\frac{\Delta T}{T} = \frac{k\,\Delta y}{T} \quad . \tag{38}$$

The expression $\Delta y/T$ appears in equation (36) multiplied by $M\omega^2$. Therefore, we can evaluate equation (38) by multiplying the right side of equation (37) by $k/M\omega^2$ to obtain

$$\frac{\Delta T}{T} = \frac{\alpha r^2 \rho_a^2 a^7 k}{27\,GMM^3N^2} \quad \text{(high frequency)} \quad . \tag{39}$$

For example, using the same case calculated for equation (37), together with $E = 0.7 \times 10^{12}$ dynes/cm^2, $r_0 = 0.1$ cm, $\ell = 10^5$ cm, $k = 4.4 \times 10^5$ dynes/cm, and $k/M^2 = 2.24$, we get a fractional tension noise at high frequency of 4.46×10^{-6}. The variable r in equation (39), on which the drag force depends, should not be confused with the core radius r_0, which determines the wire stiffness.

In the Skyhook computer program, the amount of space and time required to integrate the motion of the system rises sharply as the number of masses increases. For this reason, no attempt has been made to verify the calculations for N = 100. However, a computer run has been done for N = 2 and a drag variation of 60 sec. The other parameters for the run were v = 7.29 km/sec, $M = 2 \times 10^6$ g, a drag cross section of half of each wire segment of $A = 1.25 \times 10^4$ cm^2, (drag force) F = 1063 dynes, $\ell = 10^5$ cm, and T = 416,410 dynes. Using equation (15), we get an equilibrium displacement of each wire midpoint:

$$x = \frac{\ell F}{4TN} = \frac{10^5 \times 1063}{4 \times 416{,}410 \times 2} = 31.9 \text{ cm} \quad .$$

The amplitude of the end-mass motion with $\alpha = 0.1$, from equation (32), is

$$\Delta y = \frac{2 \times 2^2 \times 31.9 \times 3.19}{10^5} = 8.14 \times 10^{-3}$$

With $\omega = 2\pi/60 = 0.1047$, the tension noise calculated analytically from equation (33) is

$$\Delta T = M\omega^2 \Delta y = 2 \times 10^6 \times (0.1047)^2 \times 8.17 \times 10^{-3} = 179 \text{ dynes} \quad .$$

We could have used equation (39) directly, but the above calculation allows a more precise comparison with the computer simulation, which takes into account factors like corotation of the atmosphere.

Since the formula (37) assumes that the driving force is slower than the natural frequency of the transverse oscillations, the masses representing the lumped-wire properties were set to 337.5 g, which gives a transverse period of 20 sec (equation (39) is independent of the wire mass). The Skyhook program has no model in it for transverse wire dampers. An initial attempt to run this case failed because the wire was oscillating at the natural frequency and giving a large tension noise (about ±500 dynes) with a period of 20 sec. A crude damping model was added to the program by putting in a force proportional to the velocity of the wire mass relative to its equilibrium position with no drag. With this model, the tension noise was ±168 dynes with a 60-sec period, in approximate agreement with the noise level calculated analytically. Equation (39) shows that the tension noise from drag-force fluctuations is reduced by the factor N^2 when the system has a large number of ballast masses along the wire.

3.4.9 Short Dumbbell system

Preliminary information regarding performance data on tension measuring devices indicates that the dynamic range required for tension measurements can be substantially exceeded with full-scale signals much less than the

1-lb signals considered so far. For example, it appears that 0.5 parts in 10^7 can be achieved on a total signal of 0.1 lb. This means that the minimum detectable signal is 0.002 dyne, rather than 1 dyne, as previously assumed. Since the tension is proportional to the mass times the length of the system, a reduction of at least two orders of magnitude could be achieved in mass or length, or in a combination of both. Because system lifetime is a limiting factor in the choice of parameters, and the drag cross section of the wire is the major contributor, the high measuring sensitivity of the tensiometer could best be utilized to decrease the length of the system. Looking at equation (25) for the drag-force variations, we see that the noise is inversely proportional to the product $M\ell$; thus, decreasing this product by two orders of magnitude increases the noise by the same factor. Equation (39), for noise with a large number of ballast masses, is independent of length. If $N = 100$ and $\ell = 10$ m, the wire segments would be 10 cm long. Equations (25) and (39) are both derived under the assumption of negligible bending stiffness for the wire, with the only restoring force to keep the wire straight being the tension. In a very short system, the cross section of the wire for drag is not a problem. For example, if the length of the system is 10 m and we allow 1 m^2 for the cross section, the support could be as much as 10 cm in width. In the case of a rod instead of a flexible string, the restoring force is the stiffness rather than the tension. As the diameter of the rod increases, the temperature fluctuations due to drag-heating fluctuations are reduced because of the larger thermal mass of the rod. The rod can still be insulated with a jacket to reduce the temperature fluctuations further. Because the rod is both short and thick, the system risetime is very fast. The frequencies of both the longitudinal and the transverse oscillations of the rod are fast, and damping devices should be simple to construct. Given that the area-to-mass ratio of the system can be kept low, the orbital lifetime is larger. Such a system appears to be capable of providing a high signal-to-noise ratio at low altitudes with reasonable lifetime. Analysis of this system requires including models for the stiffness of the rod.

3.5 Pendulum Oscillations of the Dumbbell System

The periods of the pendular oscillations of the Dumbbell are

$$P_O = \frac{\pi}{\omega_o}$$

for the out-of-plane oscillation and

$$P_I = \frac{2\pi}{\sqrt{3}\omega_o} = 1.15P_O$$

for the in-plane oscillation, where ω_o is the orbital frequency. Since these periods are long, they do not present a problem for measuring short-period gravity-gradient variations. Such oscillations do affect the absolute value of the gravity gradient, however, by changing the orientation of the system. A correction for this effect can be made by measuring the attitude of the system.

Pendulum oscillations also affect the drag force on the tether. Since the drag force is parallel to the velocity of the atmosphere with respect to the wire, drag can have a component along the wire, which has the effect of increasing the tension at one end and decreasing it at the other. Tension variations due to this effect can be removed by measuring the tension at both ends of the wire.

The oscillations of the system are induced primarily by the oblateness of the earth, which changes the direction of the gravity force. Orbital eccentricity also produces oscillations. The oscillations produced by differential drag at low altitudes can be reduced by tailoring the area-to-mass ratio of the system to the variation of atmospheric density with altitude, so that the acceleration from drag is the same on all parts of the system. This can be done only approximately, though, because the scale height varies with altitude. The same technique can be used to minimize the excitation of higher modes of the transverse oscillations of the wire.

3.6 Rotation of the End Masses

A set of computer simulations has been done to investigate the possibility of passive triaxial stabilization of the end masses of the Dumbbell system. In the configuration shown in Figure 22, a total mass of 2 metric tons is at each end of a 1-km wire that is 2 mm in diameter. Mass A is a 100-kg

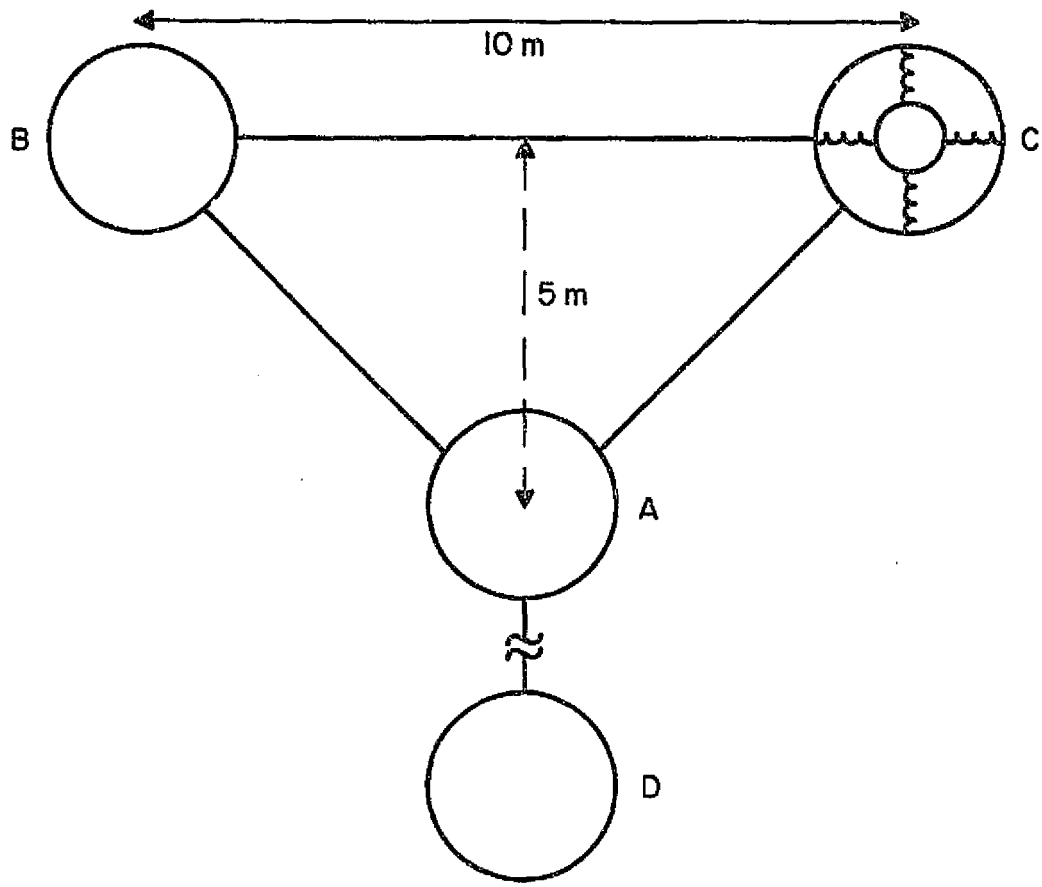

Figure 22. End-mass configuration.

instrument package, mass B a 950-kg ballast, mass C a 475-kg shell with a 475-kg three-axis spring damper inside, and mass D a 2000-kg ballast that would, in practice, be a structure like masses A, B, and C. Masses A, B, and C form a triangular structure lying in the orbital plane. Computer runs have been made with the configuration as shown (integrating the motion of

five masses) and with C as a single ballast identical to B (integration of four masses with no spring damper).

To test the rotational stability of the system, the four-mass configuration (no damper) was run with the following initial conditions: The triangular structure was given a small initial angular momentum parallel to the wire direction by assigning out-of-plane velocities of 0.2 cm/sec and -0.2 cm/sec for masses B and C. the initial conditions were otherwise those for a circular orbit in the xy plane (the equatorial plane). Masses B and C reached a maximum out-of-plane separation of 335 cm in a quarter of an orbit, and after half an orbit, the displacements returned to zero. The initial out-of-plane velocities given to B and C have the effect of putting those masses into orbits having a slight inclination with respect to the orbital plane of the center of mass. Since the orbital planes of B and C and the center of mass all intersect in the x axis, the end masses return to the orbital plane of the center of mass twice per orbit. The configuration is stable against rotation as long as the initial angular velocity about the wire direction is smaller than the orbital angular velocity, so that the ballast masses do not rotate past ±90° from the orbital plane.

A complication in achieving rotational stabilization is that the orbital plane of the center of mass precesses if the orbit is not exactly equatorial or polar, because of the effect of the earth's oblateness. To study this effect, the system was run for two orbits at an inclination of 45°. The out-of-plane separation increased by about 0.1 cm per orbit. This change in the plane of the triangular end-mass configuration with respect to the orbital plane is about 2% of the change of the orbital plane in inertial space due to the earth's oblateness. It appears that the end-mass configuration stays in the plane of the orbit as it precesses, at least to first order. The small discrepancy observed is probably due to the fact that the end mass is not at the center of mass of the Dumbbell and is therefore acted on slightly differently by the earth's oblateness.

Finally, the configuration shown in Figure 22 was run for two orbits with the damper mass included and the orbital plane inclined 45° from the equator. Masses B and C were given initial out-of-plane velocities of 0.2 cm/sec. The maximum out-of-plane separation decreased from 335 cm on the first orbit to 334 cm on the second orbit. This decrease is an order of magnitude larger than the out-of-plane displacement induced by the earth's oblateness. The motion of the damper mass with respect to the shell containing it was about 20 cm in the in-plane direction and 8 cm in the out-of-plane direction. It appears that the reason the damping is effective is that the shell of the damper is constrained to move in a circle about the center of the triangle, whereas the damper mass tries to move in a direction perpendicular to the orbital plane. The constants used for the stiffness of the damper springs and the damping coefficient of the fluid in the damper cavity are 0.3 dynes/cm and 560 dynes cm^{-1} sec^{-1}, respectively.

Since the development of out-of-plane oscillations of the ballast masses is very slow, and a slight rotation of the end masses is probably not detrimental, the damper system described above (with its extremely small damping coefficient and spring stiffness) may not be required. An active system for occasional control of end-mass rotation would not result in the loss of a significant number of data (due to tension noise introduced by the maneuvering). An active system may be required for initial stabilization of the system.

3.7 Electrodynamic Forces

A satellite moving at velocity $\vec{v}$ with respect to the earth's magnetic field $\vec{B}$ has an electric force acting on it given by $\vec{E} = \vec{v} \times \vec{B}$. This electric force will redistribute the electrons in the satellite if they are free to move and will thereby build up an electrostatic potential difference whose maximum value will be $\vec{v} \times \vec{B} \cdot \vec{\ell}$, where $\vec{\ell}$ is the length of the satellite. In the case of a long tether in space, a substantial voltage can develop if the tether is an electrical conductor. If there are electrically conducting surfaces with a potential difference with respect to the plasma, these

surfaces will attract charged particles from the ionospheric plasma, thereby setting up a current loop through the satellite. The current through the satellite will result in a force $\vec{I} \times \vec{B}\, d\ell$ on each segment of the current path.

Consider the case of a long metallic tether moving through the ionosphere. If the satellite moves in an easterly direction, electrons will be forced to the bottom of the wire, creating a negative potential with respect to the plasma and leaving the top at a positive potential. Ions will be collected along the part of the wire that is negative, and electrons will be collected at the top of the wire. The collection of charge from the plasma continuously neutralizes the charges on the wire, and the $\vec{v} \times \vec{B}$ force continually moves electrons from the upper part of the wire to the bottom, replenishing the charge concentrations at the ends of the wire and maintaining a current along the wire. The potential difference that develops along the wire and the value of the current through the wire depend on the efficiency of the charge collection relative to the conductance of the wire. If the wire has a high conductance, the electrostatic potential will be nearly $\vec{v} \times \vec{B} \cdot \vec{\ell}$. As the resistance of the wire increases, the ions and electrons in the plasma neutralize the charges built up toward the ends of the wire faster than they can be replenished by the current in the wire. In the limit of a nonconducting wire, there is no potential difference and no current. If the wire is a conductor but is covered by an insulator so that no charge is collected along the wire, a potential difference will build up along the tether but no current will exist (other than the transient current required to create the charge concentrations that produce the electrostatic potential difference). If the ends of a metal wire with a dielectric shield are electrically connected to a package with exposed conducting surfaces, then charges collected by these surfaces will flow through the wire. If there is no electrical connection between the wire and the package, there will be no current.

In the case of Dumbbell, electrodynamic forces can be avoided by not having long exposed metal surfaces and by not permitting electrical contact between any long metallic pieces and exposed conducting surfaces. Since

orbital velocities are about 7.7 km/sec and the magnetic field is about 0.3 gauss, the potential difference that can develop along a conductor is 0.23 volts/m.

3.8 Parameter Optimization

Three system configurations have been considered that appear to be capable of providing gravity-gradient measurements with a resolution of 0.01 eu. The first two are designed for a tensiometer requiring a minimum signal of 1 dyne, and the third assumes a minimum detectable signal of 0.01 dyne.

The first configuration consists of two heavy ballast masses on the order of 2 metric tons each connected by a tether whose length is on the order of 1 km. Factors that must be taken into account in the design include system risetime, temperature variations of the wire, and transverse oscillations of the wire due to drag fluctuations. Approximate analytical expressions have been derived for estimating each of these quantities as a function of the design parameters for the system. Adequate risetime requires that the load-bearing core of the tether have a cross section equivalent to that of a 2-mm solid wire (the core will probably consist of multiple strands). A thermal jacket conductively isolated from the core should easily provide the required thermal insulation for a core of this diameter.

The limiting factor in the sensitivity of this design appears to be transverse wire oscillations induced by drag variations. Estimates of the noise level are somewhat uncertain owing to the lack of detailed information on the atmospheric granularity to be expected. The noise from drag-force variations can be calculated from equation (25),

$$\frac{\Delta T}{T} \quad \frac{4\alpha\rho_a^2 a^4}{9\pi\rho_w M\ell} \quad .$$

The noise can be reduced by going to higher altitudes (around 300 km), as a result of lower atmospheric density ρ_a at higher altitudes. Limitations on increasing the mass are cost and payload capability of the Shuttle. Increasing

the length decreases the lifetime, unless the mass is also increased, although the lifetime is not too great a problem at higher altitudes. The average wire density can be increased by constructing the jacket from a heavy material. For example, a 1-mm-thick wire-wound jacket of density 7.5 g/cc around a 2-mm-diameter core of density 1.5 g/cc gives an average wire density of ρ_w = 5 g/cc. The period of the fundamental transverse wire oscillation should be kept as long as possible (300 sec or more).

The second configuration has about the same length and total mass as the first, except that a large number of ballast masses (at least 100) are distributed along the wire. The risetime and thermal considerations are the same as for the first case. The noise from transverse oscillations of the wire segments due to drag variations from equation (37), is

$$\frac{\Delta T}{T} = \frac{\omega^2 \alpha r^2 \rho_a^2 a^7}{27 G M^2 N^2} \quad .$$

The wire should have a thin jacket in this case to reduce the factor r^2. Increasing the mass is more effective here than in the first configuration, because the noise decreases as M^2. The only limitation on increasing N is the complexity of construction and deployment. The system could be packaged to take advantage of the gravity gradient for deployment.

The third system has about the same total mass as the first two but is on the order of 10 m long; a rigid rod replaces the wire. The system does not appear to be limited by risetime, thermal variations, or drag-force tension noise.

4. DEPLOYMENT OF THE DUMBBELL SYSTEM FROM THE SHUTTLE

To simplify the deployment of the Dumbbell system, we can take advantage of the gravity gradient, and we suggest three such possibilities below.

The first possibility is to inject a compact package into orbit and deploy it at a distance from the Shuttle. We assume that the initial Dumbbell orbit is circular at a 320-km altitude. The shuttle could be in an eccentric orbit with perigee at 220 km and apogee at 320 km. For circularization, the package would require an injection velocity, Δv in the direction of motion of the order of 30 m/sec. For a 300-km circular orbit, Δv would be smaller.

After injection, the payload has to be deployed. In the gravity-gradient field, there are two possible stable equilibrium configurations of the Dumbbell system, requiring a relatively complex deployment system. Attitude sensors and logics for properly timed activation of the spring mechanism will be needed in order to impress the required relative velocity of separation to the two components of the system. Moreover, it will be necessary to remove the angular momentum (at least to a certain extent) in order to avoid a critical configuration at the beginning of the deployment phase.

Alternatively, the deployment can be done from the Shuttle. Assuming the payload package to be located on one of the pallets, either the upper or the lower component can be deployed directly from the pallet by activation of a single spring until the total length of the tether has been fully deployed; this technique is the same as that of the tethered subsatellite deployment. The second component can be released from the pallet with a very low relative velocity. Actually, the Shuttle can be thrusted away after low-velocity separation. This method provides a very gentle delivery of the system, and the orientation of the payload can be controlled before release. However, the system can be delivered only into the same orbit as the Shuttle, so if the Dumbbell orbit is to be circular, the Shuttle orbit would have to be circularized.

The third possibility is to use a tethered teleoperator for delivery and control of the package, if such a facility is available on the Shuttle. In this way, the package can be delivered and stabilized at the end of a 10-km-long teleoperator, thus increasing the gravity-gradient forces and making deployment activation and control easier.

As an example of this last possibility, assume that the Shuttle is in a slightly eccentric orbit with semimajor axis a and eccentricity e. We can release the gravity gradiometer at the apogee of the Shuttle orbit at the end of a tether that is vertically oriented upward with a length of ea/3. In particular, if $a(1 - 3) = 6378 + 200$ km and $a(1 + e) = 6378 + 320$ km, the tether will be 20 km long and the system will be gently injected at an altitude of 340 km into a circular orbit. Another example, using $a(1 - 3) = 6378 + 195$ km and $a(1 + 3) = 6378 + 285$ km, gives a tether length of 15 km. Thus, the procedure will achieve injection at a 300-km altitude.

5. ORBITAL LIFETIME

The principal constraint in maximizing the signal and minimizing the noise is the orbital lifetime, as determined by the area-to-mass ratio of the satellite and the orbital altitude. The thermal noise and risetime problems could be solved easily by using a thicker wire, but this would increase the atmospheric drag and shorten the lifetime. The fractional and absolute magnitudes of the signal are better at lower altitudes, but the time spent in a given altitude range is less because of the higher air density. Figure 23 shows the orbital height versus time for a satellite with an area-to-mass ratio of 0.02 cm^2/g starting at almost 300 km. This area-to-mass ratio corresponds to a system consisting of a wire 1 km long and 2 mm thick with a mass at each end weighing 1 metric ton and having a cross section of 1 m^2. The time spent between 220 and 150 km is about 10 days. At 16 revolutions per day, 10 days gives 320 equator crossings with an average separation of 125 km. At 300 km, the sensitivity is less than half of that at 220 km, but the time spent at higher altitudes is much greater. It would be desirable to launch the Dumbbell at a higher altitude, such as 300 km, since it will eventually decay to low altitudes anyway and useful data and operating experience could be gained at the higher altitude.

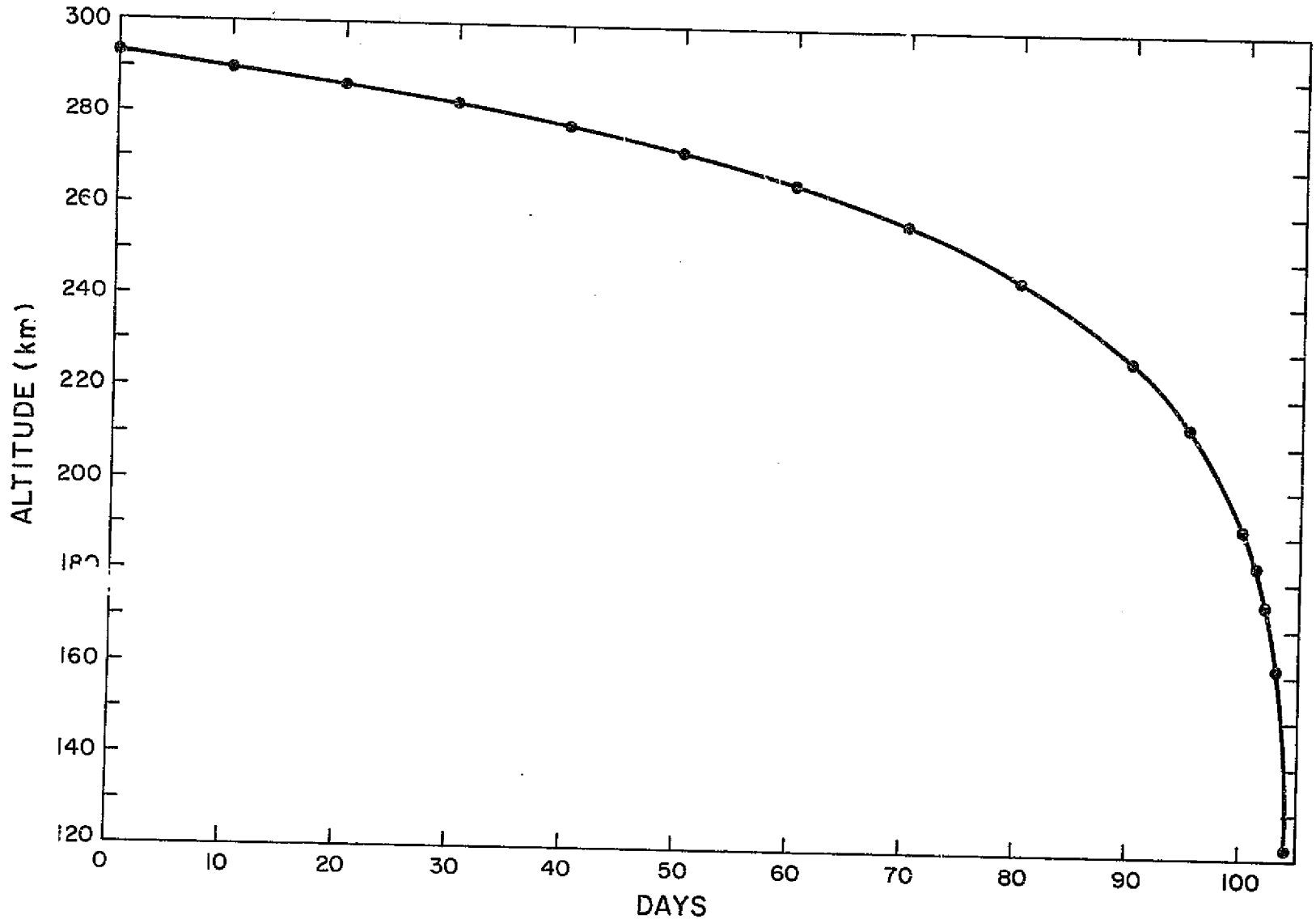

Figure 23. Days in orbit of a satellite as a function of orbital height.

6. POSSIBLE SHUTTLE EXPERIMENTS

The noise level aboard the Shuttle due to maneuvering and motions within it is expected to be high compared to the sensitivity required for gravity-gradient measurements. However, this would not invalidate a Shuttle experiment for the purpose of an engineering evaluation of the design and operation of the systems to be used on Dumbbell, although the data might be too noisy for geophysical analyses. At the same time, the noise from the Shuttle could be reduced by a combination of filtering and calibration. In the system shown in Figure 24, the lines from the Shuttle to filter mass C and

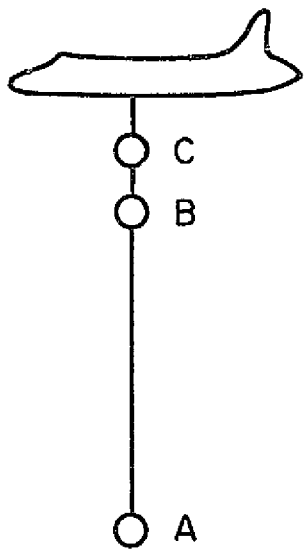

Figure 24. Shuttle-Dumbbell configuration with an isolating filter.

from C to B are designed to have a very slow risetime (a few hundred seconds or more). Since the frequency is $\sqrt{k/M}$, the risetime can be made slow by choosing a very small spring stiffness k. Short-period accelerations (less than 100 sec) of the Shuttle cause only small motions of mass C because the mass is being driven below its resonant frequency. Similarly, the motions of B are small compared to the motions of C because B is being driven well below resonance. By placing a tensiometer at the upper end of mass B,

measurements of the tension between B and C can be used to record any tension fluctuations that are transmitted through the two-stage filter between the Shuttle and mass B. The system from A to B is the Dumbbell experiment. Tensiometers on either A or B can measure the tension from the gravity gradient. The tension will be larger than that produced in a free flyer since it will include the tension in the line connected to the upper part of B. This will reduce the fractional sensitivity somewhat, but the effect will not be too large so long as the distance from the Shuttle to B is not large compared to the distance from A to B. If the tension between B and C changes by ΔT_B in a time long compared to the risetime of the Dumbbell system, the change in the tension ΔT_A between A and B is ΔT_B times the mass ratio $M_A/(M_A + M_B)$. This relation can be used to correct gravity-gradient measurements for the effect of tension noise from the Shuttle.

The tension noise transmitted through the filter can be computed approximately, as follows. Suppose the Shuttle oscillates in the vertical direction according to the equation

$$y_S = \Delta y_S \sin \omega t \quad . \tag{40}$$

If we assume that the motion of C is small compared to the motion of the Shuttle and that the spring constant of the line connecting C to the Shuttle is k_1, then C will be subjected to a force given by

$$\Delta T_C = k_1 \Delta y_S \sin \omega t = M_C \ddot{y}_C \quad . \tag{41}$$

Integrating equation (41) twice with respect to time, the motion of C is

$$y_C = - \frac{k_1 \Delta y_S}{M_C \omega^2} \sin \omega t \equiv \Delta y_C \sin \omega t \quad . \tag{42}$$

Assuming that the motion of the Dumbbell system (including A and B) is small compared to the motion of C and that the spring constant of the line joining B and C is k_2, the force on B is

$$\Delta T_B = k_2 \Delta y_C \sin \omega t = (M_A + M_B)\ddot{y}_B \quad . \tag{43}$$

Integrating equation (43) twice, we have

$$y_B = -\frac{k_2 \Delta y_C}{(M_A + M_B)\omega^2} \sin \omega t \equiv \Delta y_B \sin \omega t \quad . \tag{44}$$

Substituting the expression for Δy_C from equation (42) into equation (44) gives

$$\Delta y_B = -\frac{k_2}{(M_A + M_B)\omega^2} \frac{(-k_1 \Delta y_S)}{M_C\omega^2} = \Delta y_S \frac{k_1 k_2}{(M_A + M_B)M_C\omega^4} \quad . \tag{45}$$

Since the amplitude Δy_A of the motion of A is approximately the same as Δy_B, the tension noise produced in the line from A to B obtained by differentiating equation (44) twice and substituting equation (45) for Δy_B is

$$\Delta T_A = M_A\ddot{y}_B = -M_A \Delta y_B \omega^2 \sin \omega t = -\Delta y_S \frac{M_A k_1 k_2}{(M_A + M_B)M_C\omega^2} \sin \omega t \quad . \tag{46}$$

The tension noise on B obtained by substituting Δy_C from equation (42) into equation (43) is

$$\Delta T_B = -\Delta y_S \frac{k_1 k_2}{M_C\omega^2} \sin \omega t \quad , \tag{47}$$

so we can correct the tension measurements in the line from A to B for the effect of tension noise measured from B to C by noting that equations (46) and (47) are related by the equation

$$\Delta T_A = \Delta T_B \frac{M_A}{M_A + M_B} \quad . \tag{48}$$

If mass A is connected directly to the Shuttle and subjected to an oscillation given by equation (40), where ω is small compared to the natural oscillation frequency of mass A at the end of the wire, the tension noise resulting from the oscillation of M_A obtained by differentiating equation (40) twice would be

$$\Delta T = M_A \ddot{y}_S = -M_Z \Delta y_S \omega^2 \sin \omega t \quad . \tag{49}$$

Dividing the tension noise ΔT_A from equation (46) with the filter by the tension noise ΔT in equation (49) without the filter, we get the ratio R, given by the equation

$$R = \frac{k_2}{M_A + M_B} \frac{k_1}{M_C} \frac{1}{\omega^4} \quad . \tag{50}$$

By defining

$$\omega_{AB} \equiv \sqrt{\frac{k_2}{M_A + M_B}}$$

and

$$\omega_C \equiv \sqrt{\frac{k_1}{M_C}} \quad ,$$

equation (50) for R becomes

$$R = \frac{\omega_{AB}^2 \omega_C^2}{\omega^4} = \left(\frac{\omega_{AB}}{\omega}\right)^2 \left(\frac{\omega_C}{\omega}\right)^2 \quad .$$

The quantity ω_C is the natural oscillation frequency of M_C at the end of spring k_1, and ω_{AB} is the natural frequency of $M_A + M_B$ at the end of spring k_2. If we call ω_f the frequency of one of the filters, we see that noise of frequency ω is reduced by $(\omega_f/\omega)^2$ each time it passes through a filter. In this way, the noise from the Shuttle can be reduced to an acceptable level by passing it through a series of filters whose natural frequency ω_f is low compared to the frequency ω being filtered.

7. ENGINEERING CONSIDERATIONS

7.1 Survey of Tension Measuring Devices

In designing the Dumbbell configuration, limits with respect to present-day instrumentation were taken into consideration. The sensitivity required of the configuration is to measure changes in the gravity gradient of 0.01 eu, which translates to a few parts per million (2 to 3 parts in 10^6) in tension at Shuttle altitudes (220 km).

When fully deployed, the Dumbbell can be simulated by a 1-lb weight attached to a line approximately 1 km in length with a core diameter of 2 mm. This is equivalent to a force of approximately 400,000 dynes, which will cause the tether to stretch approximately 1 cm. Therefore, the instrumentation could measure either the changes in the tension or the actual stretching of the tether itself due to applied forces. Our first choice is to measure the tension in the line because the configuration of the Dumbbell is likely to change during the feasibility study. Every effort will be made to reduce the length of the tether in order to increase the lifetime of the experiment.

As a result, we are increasing the absolute sensitivity required of the sensor to maintain a few parts per million for a reduction in tether length.

The expected variation in the force on the line can have a periodicity from 10 to 100 sec. Therefore, sampling the data once per second will yield adequate information regarding tension variations. It would also be convenient to reduce the sampling rate when the tether is operating in the standby mode or when fewer data are needed.

Thus, preliminary specifications for a sensor suitable for feasibility trials in the laboratory can be given, as follows:

Full-scale range	
Tension:	0 to 400,000 dynes.
Length:	0 to 1 cm.
Measurement accuracy:	2 to 3 parts in 10^6
Data output	
Analog voltages:	0 to 10 volts DC
Analog impedance:	5 kΩ maximum.
Digital voltages and impedance:	TTL.
Data sampling rate:	1.0/10 sec minimum, 1.0/sec maximum.
Other requirements:	"Safety stops" must be provided to prevent damage to the sensor if the full-scale range is exceeded. The sensor will be mechanically coupled to the tether and must be capable of attachment and removal by remote control.
Input voltage and power:	For laboratory testing, power consumption in the sensor is not critical; inputs of +28 volts DC or ±15 volts DC are preferred. In space, the experiment will run continuously for 3 months; thus, the electronics should be designed for minimum power consumption.

Measurement techniques have been investigated, and two suitable methods have been selected: a null balance (servo) type of accelerometer to measure the tension and a laser interferometer to measure the stretching of the tether. A market search showed that suitable sensors using these techniques are available and could be adapted for the experiment and eventually packaged and qualified for operation in space. The most promising such sensor by far is the null balance (servo) accelerometer made by Systron-Donner Corporation (Inertial Division) in Concord, California. It and a Hewlett-Packard laser interferometer are described below.

7.1.1 Null balance servo accelerometer

The basic operation of the servo accelerometer as described here is taken from Morris (1976). The Systron-Donner Model 4841 accelerometer is based on the captured-pendulum principle, wherein the pendulum is held

almost precisely at its null or aligned position by an analog servo capture loop; this is shown diagrammatically in Figure 25. As indicated, the pendulum

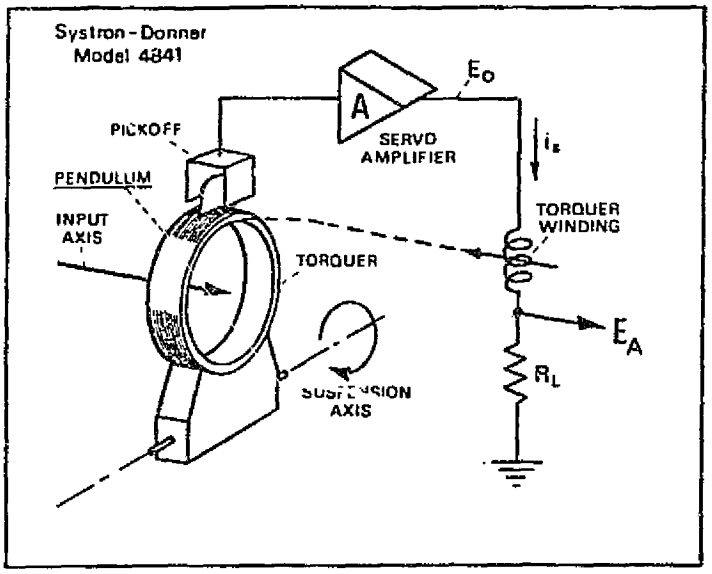

Figure 25. Operational block diagram of the Model 4841 accelerometer.

comprises primarily the torquer itself on a lever arm, constrained to rotate about an axis precisely defined by the suspension. At the end of the pendulum, a pickoff plate is mounted, whose position is sensed by the dual-balanced pickoff system, which converts the pendulum position error to a high-level DC voltage.

The pickoff drives the servo amplifier, forcing current through the combined torquer winding and load (sampling) resistor, so that a current is produced that is linearly proportional to the deflection of the pendulum away from its ideal or null position. This produces the basic high-performance position servo system, which constrains the pendulum motion to very minute angles, reaching less than 1 arcsec at maximum input acceleration. Thus, the pendulum is held tightly by the servo to a position that precisely defines the sensing axis of the accelerometer in the direction perpendicular to the plane containing both the axis of rotation and the pendulum axis.

Input acceleration acts on the pendulum to produce a proportional torque that tends to rotate the pendulum, causing the servo to produce a precisely matching torque in its action of holding the pendulum fixed. This, in turn, requires a current flow in the precision torquer; the current flow is directly proportional to the torque produced and hence provides a direct indication of the input acceleration. The output current i_s, forced to flow in the load or sampling resistor, yields a signal output voltage that is also directly proportional to the input acceleration. In some systems, the output voltage is used directly, while in others, it is converted to digital form for compatibility with the using circuitry. Figure 26 is a

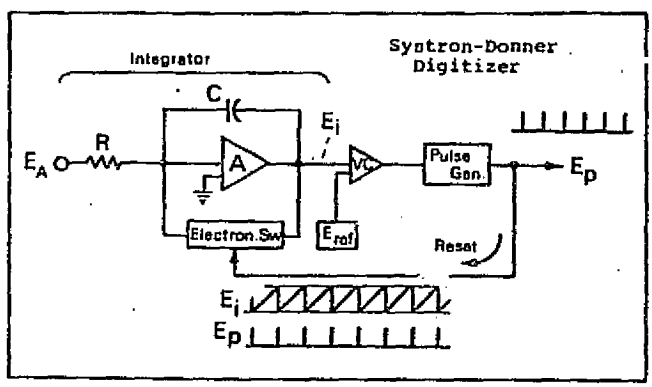

Figure 26. Digitizer block diagram.

block diagram of such a digitizer, illustrating the conversion of the acceleration signal E_A into a pulse train with a frequency directly proportional to the input acceleration.

The digitizer in Figure 26 is but one of several manufactured by Systron Donner to convert acceleration into digital form without degradation of the information from the precision guidance accelerometer. It operates by use of a precision analog integrator, which is reset to zero each time its output exceeds a reference value, producing an output pulse at each reset point. For maximum input, the reset rate is as high as 15,000/sec, providing a pulse train with a frequency directly proportional to the input

voltage from the accelerometer. Such a digitizer converts the ultra-precision analog output signal from the accelerometer to a like one of digital nature, so that all subsequent computations can be digital and hence fully independent of errors. The digitizer shown will thus preserve the basic high accuracy of the Model 4841 inertial guidance accelerometer and convert the data into the digital domain.

The Model 4841 accelerometer is space qualified and was designed to operate with a full-scale input force of 0.1 lb; test data show that it can readily measure to an accuracy of 0.5 parts in 10^7 or better. To accommodate the forces expected, the interface to the sensor must be designed to scale them down to 0.1 lb.

Systron Donner has indicated that it could provide a fully operational breadboard system to our specifications for about $25,000, with delivery in 90 to 120 days. The breadboard would consist of two packages, one containing the force transducer and the other, the electronics; each package has a volume of 75 cc and a weight of about 200 g. Two signal outputs are provided; one is a general-purpose analog signal (0 to 10 volts DC) for interface with a chart recorder or a filter, and the other is digital (TTL levels). The latter is derived from a voltage-to-frequency converter whose output (0 to 400 kHz full scale) is directly proportional to changes in applied force. The 0 to 400-kHz range will give a measurement accuracy of a few parts in 10^6, as desired. A block diagram of the package is shown in Figure 27.

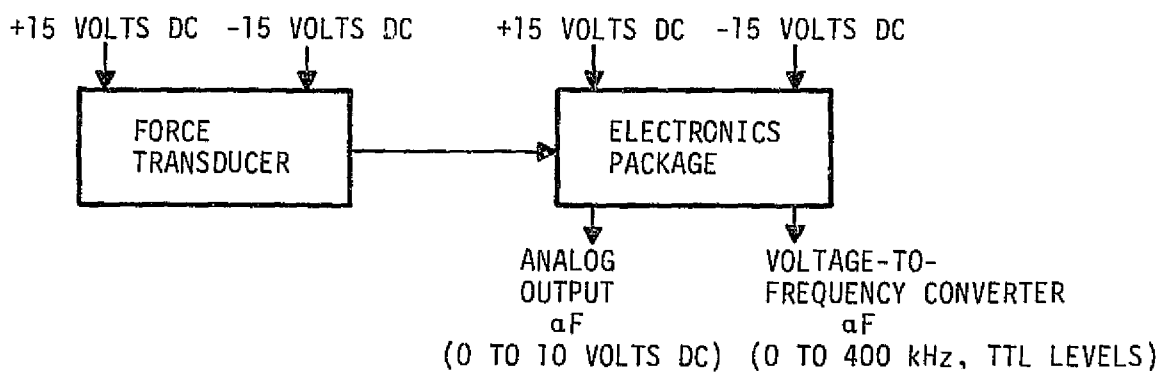

Figure 27. Block diagram of the servo accelerometer package.

7.1.2 Laser interferometer

If it is decided to measure the stretching of the tether, we would consider a laser interferometer system similar to the Hewlett Packard 5501A laser transducer, used in a plane mirror interferometer configuration. A block diagram of the basic measurement system is given in Figure 28, while Figure 29 shows the path of the plane mirror interferometer laser beam. The

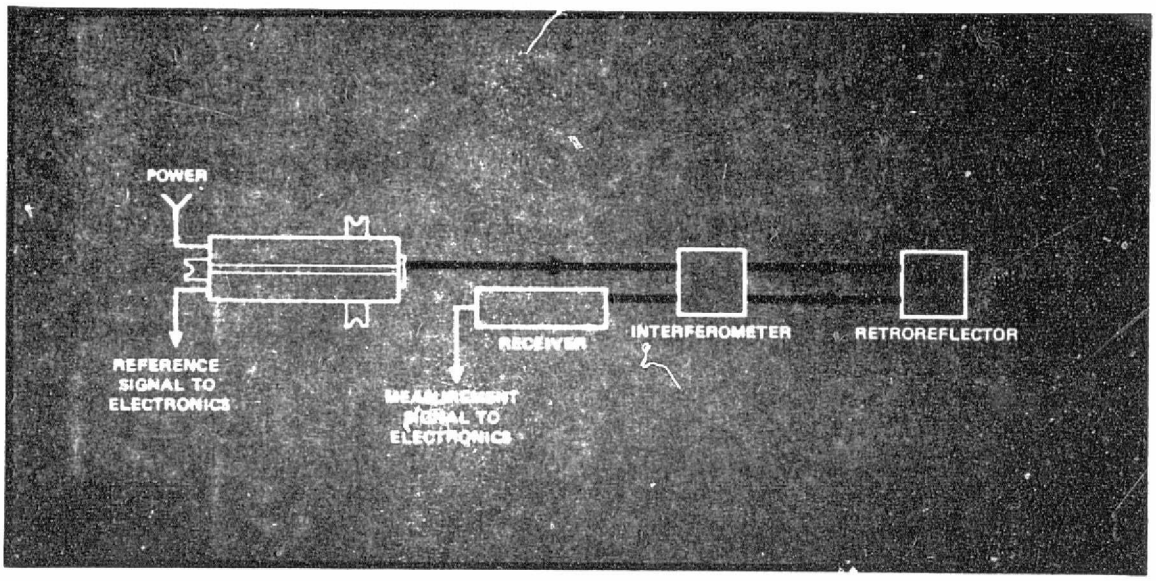

Figure 28. Basic measurement system.

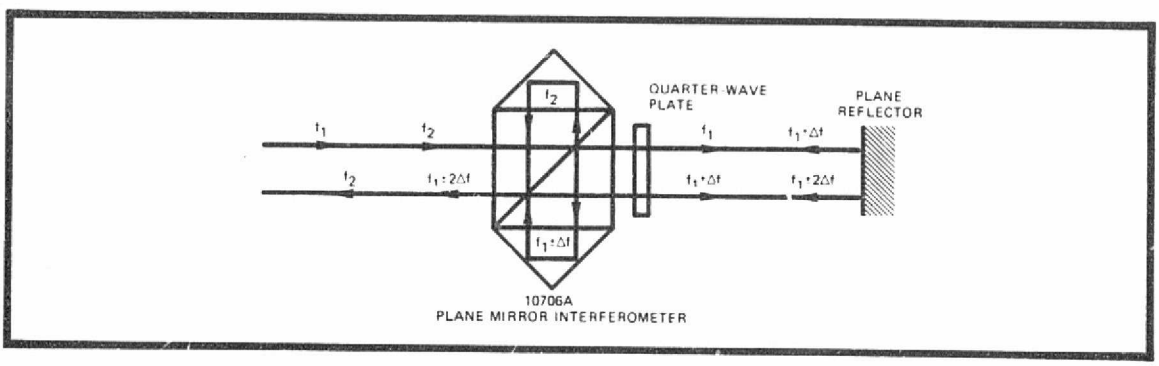

Figure 29. Path of the plane mirror interferometer laser beam.

following description and diagrams were taken from Hewlett Packard Application Note 197-2, Laser and Optics 5501A.

The beam entering the interferometer is split into f_1 and f_2, with f_2 returning to the receiver after retroreflection by the reference corner cube. As in a linear interferometer, f_1 is transmitted out to the plane retroreflector and reflected back on itself (Figure 29). The quarter-wave plate causes the polarization of the return frequency to be rotated through 90°, so that $f_1 \pm \Delta f$ is reflected out a second time and doppler-shifted again. The polarization of $f_1 \pm 2\Delta f$ is rotated again through 90° and transmitted back to the receiver. Resolution doubling is inherent because of the double doppler shift. Any tilting of the plane reflector relative to the beam axis results only in an offset of the return, not in a tilt, since tilting of the first reflected beam is exactly compensated by the second reflection.

A typical setup for a laboratory to measure a 1-cm full-scale displacement to 2 to 3 parts per million would cost approximately $20,000; this includes the laser, receiver, numeric display, and optical package.

7.1.3 Summary

At present, the measurement of tension in the tether appears to be a superior technique over the measurement of tether stretch. Thus, the servo accelerometer should be seriously considered as the prime candidate for the tension sensor on the Dumbbell experiment. Because of the accelerometer's sensitivity, we are optimistic that changes in the Dumbbell configuration, such as shortening the tether, can be accommodated without loss of measurement accuracy. Shortening the tether will increase the lifetime of the experiment. For example, for a full-scale input to the sensor of 0.1 lb, the length of the tether could be reduced from 1 km to ~100 to 200 m, and for 0.01 lb full scale, it could be 20 m long. In the case of the laser inter-

ferometer, a reduction in tether length would compromise the accuracy of the measurement because of the reduction in full-scale input.

Another advantage of the accelerometer is its compactness and minimum calibration requirements, in comparison with the interferometer, whose laser transmitter/receiver, interferometer, and reflector all require careful and stable alignment with each other.

However, we recommend that the final choice be made after both types of sensors have been thoroughly investigated against the background of the actual Dumbbell configuration during the feasibility stages of the experiment.

7.2 Manufacturing Feasibility of Tether

A study was undertaken to determine if a tether could be manufactured to satisfy the requirements previously stated within current technology, cost, and schedule constraints. Briefly stated, those requirements are as follows:

System risetime:	$\leq$ 10 sec
Thermal time constant:	$\geq$ 20 sec
Fractional tension noise:	$\leq 3 \quad 10^{-6}$
System area-to-mass ratio:	$\leq$ 0.02 cm^2/g
Cable test strength:	$\geq$ 1.5 kg
Average load:	$\approx$ 0.4 kg

One possible tether construction is shown in Figure 30. The tether has three main components, a central core, a bridal veil net, and an outer shield. The central core is composed of 5-μ strands of ULE tightly wound into a core measuring 1 to 2 mm in diameter. The exact central-core size will be determined later to match the system requirements such as end mass natural frequency. If required, the individual strands can be bonded by using a suitable binder of similar mechanical characteristics. The central

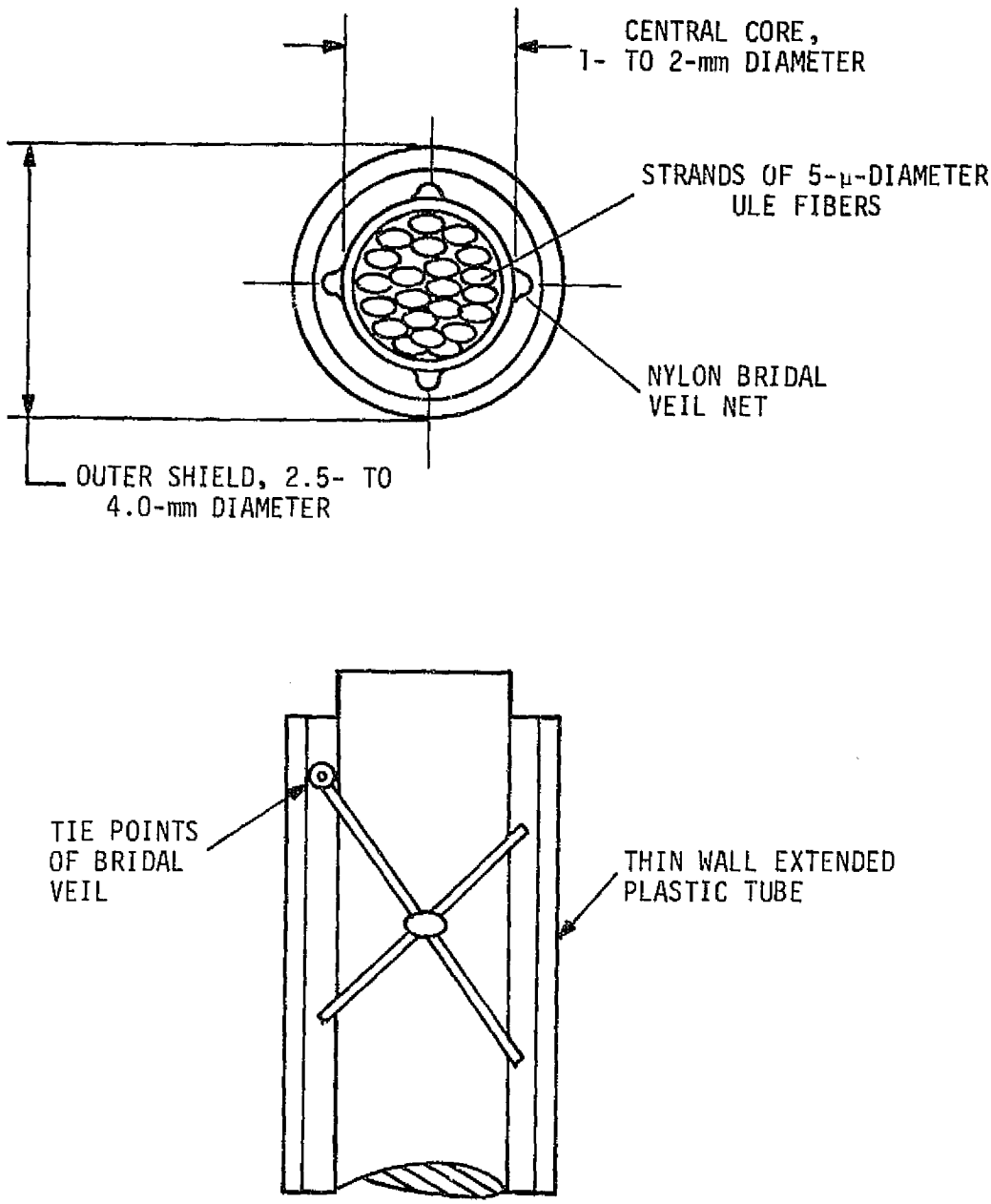

Figure 30. Tether construction.

core will then have a low-emissivity coating applied to its outer diameter to minimize radiative heat exchange. The coating will be done by a process similar to that of applying optical coatings to glass optical elements. Several candidate coatings exist (for example, aluminum, silver, and gold) that will yield an effective emissivity of between 0.03 to 0.05.

A bridal veil net will be applied over the central core to minimize the conductive heat transfer between the outer shield and the central core. It accomplishes this by employing a low-conductance material, such as nylon, and varying the number of strands, attachment points, spacing, and diameter of the strands. The exact design of the bridal veil will be deferred until several combinations can be tested to evaluate their effective thermal isolation, although it is evident that bridal veils can be fabricated to provide an effective means of limiting thermal conductance via point contact (at tie points) and high thermal impedance.

The outer shield is a loosely fitting extruded plastic tube. It acts as a protective covering for the tether during preflight handling and deployment. It also absorbs or reflects all the impinging thermal energy. It is decoupled from the central core such that its length and stiffness excursions do not impact gravity-gradient measurements. The shield is only thermally coupled to the central core via conduction through the bridal veil and radiation across the (vacuum) gap caused by their respective differences in diameter. Along the length of the outer shield, appropriate interruptions will be made such that the internal free volume of the tether will evacuate to the local ambient pressure within a reasonable period of time.

This cable design evolved after discussions with vendors currently involved in manufacture of optical communication cables. The tether cable described poses no significant technical problems in its manufacture, and several vendors have expressed an interest in participating in its construction. We thus feel sure that a tether with the required characteristics to perform the gravity-gradient measurements proposed is totally feasible at this time at a reasonable cost and that such a tether does not represent a major technological development program.

7.3 Damper Design

The use of dampers will be required to prevent tension noise from various natural oscillations of the system. The design of the damper will depend primarily on the frequency of the oscillation it has to damp and on the gravity-gradient acceleration at the place where the damper is located. The gravity-gradient acceleration can also be used as a restoring force for a damper. A basic requirement for the dampers is that their operation be smooth, so that tension noise is not introduced; a nutation damper consisting of a cavity partially filled with liquid could introduce noise as a result of splashing, for example. Dampers must be designed so that they do not stick and can move smoothly even at low velocity. One possible design consists of a mass suspended in a fluid by springs. Another possibility is a pendulum that takes advantage of the gravity gradient. A third configuration is the use of liquids with different densities in a cavity; this design could also take advantage of the gravity gradient by designing the system with a curved surface to that there would be a restoring force on the heavier liquid.

In the case of dampers for transverse wire oscillations, the weight of the damper must be less than the weight of the section of wire whose motion it is damping, so that it does not create a node. The damper must be accelerated, and there must be significant movement for the damper to be effective.

Dampers for low frequencies will probably be the most difficult to design, since they require that the ratio of the restoring force to the mass be very low. The most important periods to damp are those in the approximate range of 10 to 100 sec, as this is the most significant range for measuring gravity anomalies. The motions that have to be damped are the longitudinal and transverse oscillations of the wire and the rotational motions of the end mass, especially those rotations that change the angle between the wire and the end mass, resulting in tension noise.

8. CONCLUSIONS AND RECOMMENDATIONS

Three designs have been identified that appear to be capable of achieving the required sensitivity of 0.01 eu in making gravity-gradient measurements. The first consists of two end masses connected by a long wire. The most difficult problem to solve in this configuration is the tension noise due to drag-force variations; noise as a function of the system parameters is discussed in Section 3.4.6. Such a system would probably be limited to operation at higher altitudes or to times when atmospheric granularity is not severe. Inclusion of wind and and density measuring devices could allow the system to operate at lower altitudes and under higher noise conditions by identifying times of noisy data or by allowing corrections to be made to the data according to the expressions given in Section 3.4.6.

The second configuration is similar to the first but uses a large number of ballast masses along the wire to solve the problem of drag-force variations; the expression for drag-force noise is given in Section 3.4.8. An added benefit of this design is the wider bandwidth, since the fundamental period of the transverse oscillation of the system as a whole can be made long or even eliminated by proper design of the area-to-mass ratio along the system. The center of the system would probably be an advantageous place for the sensor, because the tension signal is largest at that point.

The third design, described in Section 3.4.9, is possible only with the high-sensitivity force transducer described in Section 7.1. The problem of drag-force variations is handled by use of a relatively short rod whose stiffness resists the bending effect of atmospheric drag. Since this third design appears very promising, we recommend further study of the tension measuring device on which it depends.

A tradeoff analysis will be necessary to choose among the three configurations considered and to decide on the best set of parameters for the design

selected. Depending on the approach taken, further study is also required of dampers suitable for the particular configuration. Since the exact nature of the atmospheric granularity is critical, particularly for the first configuration, further study of this area would be helpful. For the third design, additional mechanical and thermal analyses of the rod would be required, because the present studies did not include the effects of stiffness.

9. REFERENCES

Colombo, G., Arnold, D. A., Binsack, J. H., Gay, R. H., Grossi, M. D., Lautman, D. A., and Orringer, O., 1976. Dumbbell gravity-gradient sensor: A new application of orbiting long tethers. SAO Report in Geoastronomy No. 2, June.

Kalaghan, P. M., Arnold, D. A., Colombo, D., Grossi, M. D., Kirschner, L. R., and Orringer, O., 1978. Study of the dynamics of a tethered satellite system (Skyhook). Final Report, Contract NAS8-32199, March.

Kalaghan, P. M., and Colombo, G., 1978. Gravity gradient determination with tethered satellites. Presented at the UAH/NASA Workshop on the Uses of a Tethered Satellite System, Hunstville, Alabama, May.

Morris, H. D., 1976. A low cost precision inertial-grade accelerometer — The System-Donner Model 4841. Presented at the DGON Symposium on Gyro Technology, Braunschweig, Germany, March.

Morse, P. M., 1948. Vibration and Sound. McGraw-Hill Book Co., New York (see especially pp. 84 and 85).

Rice, C. J., and Sharp, L. R., 1977. Neutral atmospheric waves in the thermosphere and tropospheric weather systems. Report SAMSO-TR-77-98, Space and Missile Systems Organization, Air Force Systems Command, Los Angeles, May 10.